Biochemical Reaction Systems

From Elementary Chemical Reactions to Self-regulation of Biological Systems

Mads Kærn

University of Copenhagen
Department of Chemistry

This thesis has been submitted to partly fulfill the requirements for the Danish Cand. Scient degree in Chemistry from University of Copenhagen.

Graduate Studies has been carried out under supervision of

Lecturer, Professor Axel Hunding
Chemical Laboratory III
Department of Chemistry
University of Copenhagen

at the Center for Chaos and Turbulence Studies (CATS), Chemical Laboratory III, University of Copenhagen, Denmark, from September 1995 to July 1997.

Evaluation Committee:

Lecturer, Professor Axel Hunding
Chemical Laboratory III
Department of Chemistry
University of Copenhagen

Docent, Professor Erik Mosekilde
Department of Physics
Technical University of Denmark

Table of Contents

Preface

In this thesis, I will present the central focus of my graduate work at the Center for Chaos and Turbulence Studies (CATS), Chemical Laboratory III, University of Copenhagen, from September 1995 to July 1997. The objective of this thesis is the investigation of

- *the mathematical basis for the quasi-steady state approximation*
- *the instability generating mechanisms leading to sustained oscillation*
- *and the regulation of biological systems through sigmoidal dependencies*

The starting point is the classical mass action kinetic description for elementary chemical reactions and the most fundamental biochemical reaction scheme, the Michaelis-Menten reaction. After a brief introduction of chemical and biochemical kinetics, the quasi-steady state approximation (QSSA) is discussed. The QSSA is the most important and frequently applied method of simplifying kinetic equations and the QSSA, or its equivalent method in physics, the adiabatic elimination, is found in most models of physical, chemical, biological and economical nature. A detailed discussion of the mathematical basis of the QSSA is followed by an extension of the existing theory. This provides, combined with a short survey of principles from nonlinear dynamics, a solid foundation for investigations on nonlinear biological phenomena. The extended method for simplifying mass action kinetic rate equations is not trivial. To restrict the volume of the main text to a reasonable level, the detailed derivation of appropriate low dimensional systems has been collected in Appendix A and B.

The topics treated in the main body of this thesis are distributed among the following chapters:

- *Chapter 1. Biochemical Kinetics*
- *Chapter 2. The Quasi-steady State Approximation*
- *Chapter 3. Nonlinear Dynamics*

- *Chapter 4. Cooperativity and Allosteric Regulation*
- *Chapter 5. Oscillatory Oligomeric Enzymes*
- *Chapter 6. Coupled Oligomeric Enzymes*
- *Chapter 7. Kinetic Cooperativity*
- *Chapter 8. Cell Cycle Regulation*

I will summarize the most important results in Chapter 9 and present four abstracts from suggested publications in Appendix C.

After a brief survey of concepts and principles from nonlinear dynamics in Chapter 3, I turn to an introduction of the molecular bases of regulation in biological systems including an introduction to the concepts of cooperativity and allosteric regulation. In Chapter 5, a two-dimensional model of an autocatalytic dimeric enzyme reaction obtained through the QSSA has been claimed to be a prototypical mechanism leading to the emergence of sustained oscillatory behavior in biological systems. This reaction mechanism is reconsidered through the derivation of appropriate mathematical descriptions that take into account situations where the conditions for validity of two-dimensional model are violated. The dynamic behavior is investigated with emphasis on the dynamic effect of a slow allosteric transition. Other effects including high enzyme concentrations and slow association-dissociation rates of effector molecules are also included. A model comprised of two product activated allosteric dimeric enzymes placed in series has been used to investigate the emergence of complex dynamic phenomena, such as hard excitation, birhythmicity, chaos and bursting. In Chapter 6, the previously investigated model is extended to include a slow allosteric transition. The resulting four-dimensional model is used to investigate the effect of a slow allosteric transition on the emergence of chaotic, bursting and quasi-periodic oscillations.

In Chapter 7, a molecular mechanism based on Michaelis-Menten enzymes known to be capable of operating in a switch-like fashion is revisited. This mechanism may be central in the regulation of biological systems. The mechanism also allows for the emergence of sustained oscillatory behavior in a system composed of two opposing Michaelis-Menten enzymes that do not involve cooperativity in the traditional sense. It is suggested that the concept of cooperativity is extended to include apparent cooperativity arising from the kinetics of the reaction system. This change of perspective allows for measuring kinetic cooperativity in terms of Hill coefficients. In Chapter 8, I briefly review the cell cycle and propose an extension to an existing comprehensive model. The investigations on cell cycle regulation can be considered as a case study of a large biochemical reaction system and an illumination of the insight that can be achieved by combining mathematical tools with experimental knowledge.

Mads Kærn
August 7, 1997

CHAPTER 1

Biochemical Kinetics

The theoretical study of time-dependent behavior of chemical and biochemical reactions is based on a kinetic description of the interacting species through differential equations. The reactions considered here are all assumed to take place in homogeneous aqueous mixtures that are kept at a constant, uniformly distributed temperature. Usually, this assumption, which is valid in many chemical and biological systems (Heinrich & Schuster, 1996), implies that the change in concentrations $[X_1], \ldots, [X_n]$ of the species denoted $X_1, \ldots, X_n$ is uniquely defined by the *rate equations*

$$\begin{aligned} \frac{d}{dt}[X_1] &= F_1([X_1], \ldots, [X_n]) \\ &\vdots \\ \frac{d}{dt}[X_n] &= F_n([X_1], \ldots, [X_n]) \end{aligned} \tag{1.1}$$

The behavior in time will then be determined by the integral solution of Eqs. (1.1). Here, only autonomous systems are considered and the concentrations in Eqs. (1.1) do not depend explicitly on time. Therefore, the rate equations in Eqs. (1.1) constitutes a set of *autonomous ordinary differential equations* (AODE's).

1.1 Elementary Reactions

The rate functions defining the right hand sides of Eqs. (1.1) are typically derived from the *elementary reactions* of a plausible molecular reaction mechanism. An elementary chemical reaction represents collisions of reactants that may lead to the formation of products. Elementary reactions are by definition unidirectional and irreversible and the same species is not allowed to be both a reactant and a product. A general elementary reaction, where the reactants $X_1, \ldots, X_{m-1}$ are converted into products $X_m, \ldots, X_n$, can be written

$$s_1 X_1 + \ldots + s_{m-1} X_{m-1} \overset{k_f}{\rightarrow} s_m X_m + \ldots + s_n X_n \tag{1.2}$$

where k_f is a proportionality factor called the *rate constant*. The constants s_j $(j \in 1, \ldots, m)$ are called *stoichiometric coefficients*, which indicate the number of reactant molecules that collide in a single reaction event or how many product molecules are created by the reaction. The stoichiometric coefficient is, by definition, negative for a reactant and positive for a product and the sum of stoichiometric coefficients $s_1 + \ldots + s_{m-1}$ is called the *reaction order*. Usually, a elementary reaction with a reaction order exceeding two is taken to have negligible probability of occurrence.

1.2 The Law of Mass Action

When the elementary reactions of a plausible molecular mechanism have been identified one can derive the right hand sides of Eqs. (1.1) from the law of mass action. The law of mass action states that the rate of change in concentration of the product X_n in the elementary reaction described by Eq. (1.2) is

$$\frac{d}{dt}[X_n] = s_n k_f [X_1]^{s_1} \cdots [X_{m-1}]^{s_{m-1}}, \tag{1.3}$$

whereas the rate of change of the reactant $[X_1]$ in the same reaction is

$$\frac{d}{dt}[X_1] = -s_1 k_f [X_1]^{s_1} \cdots [X_{m-1}]^{s_{m-1}}. \tag{1.4}$$

The *rate of reaction* of an elementary reaction is defined by

$$v_f = \frac{1}{s_j}\frac{d}{dt}[X_j] = k_f [X_1]^{s_1} \ldots [X_{m-1}]^{m-1} \tag{1.5}$$

which allows one to write the rate of change of X_j as

$$\frac{d}{dt}[X_j] = s_j \frac{1}{s_j}\frac{d}{dt}[X_j] = s_j v_f, \qquad (j \in 1, \ldots, n), \tag{1.6}$$

1.3 Chemical Equilibrium

To any elementary reaction there will be a counter reaction defined by reversing the signs of the stoichiometric coefficients

$$s'_m X^m + \ldots + s'_n X^n \xrightarrow{k_b} s'_1 X_1 + \ldots + s'_{m-1} X_{m-1} \tag{1.7}$$

where k_b denotes the backward rate constant and $s'_j = -s_j$, $(j \in 1, \ldots, n)$. Similar to the forward rate of reaction, the counter reaction is associated with a backward rate of reaction given by

$$v_b = k_b [X_m]^{s_m} \ldots [X_n]^{s_n}. \tag{1.8}$$

Any chemical reaction can be regarded as reversible and there will to a given elementary reaction be defined a counter reaction. Taking the counter reaction into account the overall rate of a reversible reaction is

$$v = v_f - v_b = k_f [X_1]^{s_1} \ldots [X_{m-1}]^{s_{m-1}} - k_b [X_m]^{s_m} \ldots [X_n]^{s_n} = s_m (v_f - v_b). \tag{1.9}$$

When v is zero, the reaction has reached an equilibrium where $v_f = v_b$ and the *equilibrium constant*

$$K = \frac{k_f}{k_b} = \frac{[X_1]_{eq}^{s_1} \ldots [X_{m-1}]_{eq}^{s_{m-1}}}{[X_m]_{eq}^{s_m} \ldots [X_n]_{eq}^{s_n}}, \tag{1.10}$$

where the subscript eq indicates concentrations at equilibrium, can be obtained.

1.4 Multiple Elementary Reactions

When a chemical species is reactant or product in several elementary reactions the rate equation is given as a sum of the contributions from each elementary reaction. The rate equation for the concentration of a chemical species X_j that participates in l elementary reactions of a reaction system composed of n different chemical species can is written

$$\frac{d}{dt}[X_j] = \sum_l s_{jl} k_l \prod_i^n [X_i]^{|s_{il}|}, \tag{1.11}$$

where s_{il}, $(i \in 1, \ldots, n)$ is the stoichiometric coefficient of species X_i, $(i \in 1, \ldots, n)$ in reaction l and k_l is the rate constant associated with reaction l.

The stoichiometric coefficient s_{il} is defined to be zero if the species X_i is neither a reactant nor a product in the l'th elementary reaction.

A chemical reaction system composed of n different chemical species that react through m elementary reactions be written

$$\begin{aligned}\frac{d}{dt}[X_1] &= \sum_{l=1}^{m} s_{1l} k_l \prod_{i=1}^{n} [X_i]^{|s_{il}|} = \sum_{l=1}^{m} s_{1l} \mathrm{V}_l(\mathbf{X}) \\ &\vdots \\ \frac{d}{dt}[X_n] &= \sum_{l=1}^{m} s_{nl} k_l \prod_{i=1}^{n} [X_i]^{|s_{il}|} = \sum_{l=1}^{m} s_{nl} \mathrm{V}_l(\mathbf{X})\end{aligned} \tag{1.12}$$

where the definition of reaction rate has been employed. When defining the n dimensional concentration vector

$$\mathbf{X} = \begin{pmatrix} [X]_1 \\ \vdots \\ [X]_n \end{pmatrix}, \tag{1.13}$$

the m-dimensional *reaction vector*

$$\mathbf{V}(\mathbf{X}) = \begin{pmatrix} k_1 \prod_{i=1}^{n} [X_i]^{|s_{i1}|} \\ \vdots \\ k_m \prod_{i=1}^{n} [X_i]^{|s_{im}|} \end{pmatrix} = \begin{pmatrix} \mathrm{V}_1(\mathbf{X}) \\ \vdots \\ \mathrm{V}_\mathrm{m}(\mathbf{X}) \end{pmatrix}, \tag{1.14}$$

and the $m \times n$-dimensional *stoichiometric matrix*

$$\mathbf{N}' = \begin{pmatrix} s_{11} & \dots & s_{n1} \\ \vdots & & \vdots \\ s_{1m} & \dots & s_{nm} \end{pmatrix}, \tag{1.15}$$

the system in Eq. (1.12) can be written in the short form

$$\frac{d}{dt}\mathbf{X} = \mathbf{N}'\mathbf{V}(\mathbf{X}). \tag{1.16}$$

1.5 Conservation Relations

Elementary reactions in a closed chemical system obey a principle of detailed balance originating from the law of mass conservation. The principle of detailed balance imposes a number of *linear dependencies* between the rate equation for different species. In the elementary reaction described by Eq. (1.7) it is obvious that the change in the concentration of X_m is proportional to the change in concentration of X_1 as

$$\frac{d}{dt}[X_m] = s_m v_f = -\frac{s_m}{s_1}\frac{d}{dt}[X_1]. \tag{1.17}$$

That the rate equations are proportional implies that the *conservation relation*

$$[X_m](t) + [X_1](t) = [X_m](t^0) + [X_1](t^0) \tag{1.18}$$

holds, and the concentration of X_m can be calculated at all times if the initial conditions $[X_m](t^0)$, $[X_1](t^0)$ and the concentration of X_1 are known. A general reaction system described by Eq. (1.16) may contain similar relations, which are reflected as linear dependencies between the rows of the stoichiometric matrix. A reaction system is *linear dependent* if the stoichiometric matrix has linear dependent rows and is otherwise *linear independent*. A linear independent system is obtained from the linear dependent system by expressing one concentration for each linear dependency in accordance with the corresponding conservation relation. The $rank(\mathbf{N}')$ is the number of linear independent concentration variables whereas the number of eliminated concentrations is $n - rank(\mathbf{N}')$.

The stoichiometric matrix $\mathbf{N}'$ is equivalent with a matrix $\mathbf{N}$ of dimensionality $rank(\mathbf{N}')$ and is used to define the linear independent system containing the lowest number of concentrations required for a mathematical description of the reaction system. In the following, the linear independent reaction system

$$\boxed{\frac{d}{dt}\mathbf{X} = \mathbf{N}\mathbf{V}(\mathbf{X}),} \tag{1.19}$$

is called the *full set of AODE's* or simply the *full system.*

1.6 The Michaelis-Menten Reaction

The elementary principles introduced until now are exemplified by a mathematical description of the Michaelis-Menten reaction. In the Michaelis-Menten reaction scheme a substrate, denoted S, binds reversiblely to an enzyme E and forms the enzyme-substrate complex ES. The enzyme-substrate complex dissociates irreversibly into free product P and free enzyme (see e.g. Gutfreund, 1972; Atkins, 1992; Creighton, 1993). The reaction is composed of three elementary reactions

$$S + E \overset{k_{sf}}{\to} ES, \qquad ES \overset{k_{sb}}{\to} S + E, \qquad ES \overset{k_c}{\to} P + E, \tag{1.20}$$

and the initial conditions are normally

$$[S](t^0) = [S]^0, \qquad [E](t^0) = [E]^0, \qquad [ES](t^0) = 0, \qquad [P](t^0) = 0. \tag{1.21}$$

All elementary reactions are associated with a counter reaction that has to be considered. However, if the system is far from equilibrium the forward reaction rate may far exceed that of the backward reaction and neglecting the latter will still be a fairly good approximation.

Applying the law of mass action, one obtains the rate equations of the four species

$$\begin{aligned}
&\frac{d}{dt}[S] = k_{sb}[ES] - k_{sf}[S][E], \quad \frac{d}{dt}[E] = (k_{sb} + k_c)[ES] - k_{sf}[S][E], \\
&\frac{d}{dt}[P] = k_c[ES], \qquad \frac{d}{dt}[ES] = k_{sf}[S][E] - (k_{sb} + k_c)[ES],
\end{aligned} \tag{1.22}$$

which can be written in vector form

$$\frac{d}{dt}\mathbf{X}' = \mathbf{N}'\mathbf{V}(\mathbf{X}'), \tag{1.23}$$

where the concentration vector and rate vector are defined

$$\mathbf{X}' = \begin{pmatrix} [S] \\ [E] \\ [P] \\ [ES] \end{pmatrix}, \qquad \mathbf{V}(\mathbf{X}') = \begin{pmatrix} k_{sb}[ES] \\ k_{sf}[S][E] \\ k_c[ES] \end{pmatrix}, \tag{1.24}$$

and the stoichiometric matrix is

$$\mathbf{N}' = \begin{pmatrix} 1 & -1 & 0 \\ 1 & -1 & 1 \\ 0 & 0 & 1 \\ -1 & 1 & -1 \end{pmatrix}. \tag{1.25}$$

The rows of the stoichiometric matrix are not linear independent; adding row 1 and row 4 to row 3 followed by addition of row 4 to row 2 yields the matrix

$$\mathbf{N} = \begin{pmatrix} 1 & -1 & 0 \\ -1 & 1 & -1 \end{pmatrix}, \tag{1.26}$$

where row 2 and row 3 of zeros have been ignored. The row manipulations are equivalent to

$$\frac{d}{dt}[E] + \frac{d}{dt}[ES] = 0, \qquad \frac{d}{dt}[S] + \frac{d}{dt}[ES] + \frac{d}{dt}[P] = 0 \tag{1.27}$$

and the Michaelis-Menten reaction contains the conservation relations

$$[S] + [ES] + [P] = [S]^0, \qquad [E] + [ES] = [E]^0. \tag{1.28}$$

Replacing $[E]$ by $[E]^0 - [ES]$ and $[P]$ by $[S]^0 - [S] - [ES]$ the vector

$$\mathbf{X} = \begin{pmatrix} [S] \\ [ES] \end{pmatrix} \tag{1.29}$$

is sufficient to account for the concentrations of all the other species. The full set of AODE's is then

$$\frac{d}{dt}\mathbf{X} = \mathbf{N}\mathbf{V}(\mathbf{X}), \tag{1.30}$$

where

$$\mathbf{V}(\mathbf{X}) = \begin{pmatrix} k_{sb}[ES] \\ k_{sf}[S]([E]^0 - [ES]) \\ k_c[ES] \end{pmatrix}. \tag{1.31}$$

In standard dimensional form, the full description of the Michaelis-Menten reaction scheme is

$$\begin{aligned} \frac{d[S]}{dt} &= -k_{sf}[S]([E]^0 - [ES]) + (k_{sb} + k_c)[ES] - k_c[ES], \\ \frac{d[ES]}{dt} &= k_{sf}[S]([E]^0 - [ES]) - (k_{sb} + k_c)[ES], \end{aligned} \tag{1.32}$$

with initial conditions

$$[S](t^0) = [S]^0, \qquad [ES](t^0) = 0. \tag{1.33}$$

The concentrations of the eliminated concentrations $[E]$ and $[P]$ can always be found from the conservation relations and their initial concentration is omitted.

1.7 Non-ideal Environments

Mass action kinetics, in the formulation referred here, applies to homogeneous chemical systems but may be extended to heterogeneous environments by including spatial distribution and diffusion. There may be high thermally driven hydrodynamic fluctuations inside living cells (Mikhailov & Hess, 1995) that may have an important effect on the sub-cellular distribution of molecules. Such flows can be incorporated into the mass action description if a sufficiently high number of molecules is present at any time at any spatial location. In living cells, many reactions take place in compartments and organelles that are environments enclosed by a membrane. Proteins anchored in the membrane control the flux across the environment and mass action kinetics may in principle be used, although it would probably prove difficult in practice, to describe reactions involving flux across membranes incorporated as a diffusive process. The effect of active transport in and out of compartments can be captured by assuming that there exists distinct pools containing the same species distributed homogeneously across the environment (see e.g. Goldbeter, 1996).

The mass action kinetic description will, however, fail if the number of molecules is not sufficiently high to maintain a Maxwell distribution of velocities. If only a few molecules are present a model taking a stochastic distribution of velocities into account must be employed. Recent theoretical investigations of a low number of molecules confined to a small spatial volume suggest that such a system represents a *coherent molecular network* with strong temporal correlations (Hess & Mikhailov, 1995). Further studies of the molecular networks have shown that a system containing 100 auto-catalytic allosteric enzymes may undergo a transition from a state of uniformly distributed enzymatic activities to a state of coherent spiking (Hess & Mikhailov, 1996).

Many enzymes aggregate in clusters where the product of one enzymatic reaction is transfered directly to the active site of a subsequent enzyme. Such clusters are typically destroyed when investigated *in vitro* and detailed data on the structure and the kinetics of these clusters are not available. Theoretical models taking e.g. *molecular channeling* into account are emerging (see e.g. Heinrich & Schuster, 1996) and may be crucial for understanding the high efficiency of typical metabolic pathways. There is evidence that many biochemical reactions are restricted to one- and two-dimensional spaces such as membrane surfaces, trans-membrane channels and DNA strands. Recently, it has been suggested that experimental data generally should be fitted to "rate laws based on fractal kinetics" (Savageau, 1995) as such rate laws should represent the high organization and the dimensional restrictions better than the tradition interpretation of experimental data. Savageau suggests, based on the so-called *power law formalism* a kinetic description of the Michaelis-Menten reaction of the form

$$
\begin{aligned}
\frac{d[ES]}{dt} &= c_1[S]^{g_s}[E]^{g_e} - (c + c_2)[ES], \\
\frac{d[P]}{dt} &= c_2[ES]
\end{aligned}
\tag{1.34}
$$

(Savageau, 1995), where c, c_1 and c_2 are constants and g_s and g_e are called reaction orders. The values of g_s and g_e may in this formalism be non-integers. However, the power-law formalism is empirical and it has been stated that the power-law formalism is only acceptable when no kinetic details are available (Heinrich & Schuster, 1996).

It seems that no present comprehensive formulation can successfully combine spatial organization of living organisms, knowledge available on molecular mechanisms and mathematical tractability. With the rapid increase of computing power, mathematical tractability has been replaced somewhat with numerical tractability, but as long experimental biochemistry and genetics are qualitative and descriptive sciences, abstract and theoretical models will be the rule rather than the exception. New quantitative *in vivo* experimental methods are constantly developed but until more is known about the sub-cellular organization in particular, the homogeneous case and mass law kinetics is a reasonable place to start (Novak & Tyson, 1993b). Such abstract models may, although they all are simplistic, often reveal new insight into the self-regulation of biological systems.

CHAPTER 2

The Quasi-Steady State Approximation

The kinetic models of chemical and biochemical reaction systems quickly attain high dimensions as the number of constituting elementary reactions increases. Even though computational methods are available to investigate complicated and high dimensional reaction systems such numerical investigations typically do not provide for emergence of an extended conceptual basis. Most studies are therefore based on a simplified low dimensional model that captures the essential properties of the high dimensional description.

The most frequently employed simplification method, and undoubtedly the most fundamental in chemical kinetics, is the *quasi-steady state approximation* (QSSA). In a chemical reaction system composed of the reactions of the species $X_1, \ldots, X_n$, the standard implementation of the QSSA is to assume that the species X_n, which is indexed n for convenience, is in a *quasi-steady state* when the rate is approximately zero

$$\frac{d}{dt}[X_n] \approx 0, \tag{2.1}$$

(see e.g. Atkins, 1992; Esperson, 1995). When the rate equation is described by the function $F_n(X_1, \dots, X_n)$ the postulated steady state of X_n allows one to write

$$F_j(X_1, \dots, X_n) = 0, \tag{2.2}$$

which is then solved with respect to X_j. The solution of Eq. (2.2) with respect to $[X_n]$ is the algebraic function

$$\Phi_n([X_1], \dots, [X_{n-1}]), \tag{2.3}$$

that determines the approximate quasi-steady state concentration of X_n given $X_1, \dots, X_{n-1}$. The concentration of X_n is then replaced by the quasi-steady state value of X_n, Φ_n, and the rate equation for $[X_n]$ is omitted.

The QSSA is often implemented by postulating a quasi-steady state not based on kinetic or experimental considerations. The drawbacks of the standard implementation of the QSSA were illustrated by Edelson and Farrow (Farrow & Edelson, 1974) who compared the integral solution of a 50 variable photochemical propylene-$(NO)_x$ reaction model with a 29 variable model obtained by assuming quasi-steady states for 21 species. The investigation showed that the reduced system gave an integral solution that differed from the integral solution obtained from the full system. On this basis, the authors reject the standard QSSA as a reliable and precise method and suggest that the QSSA be replaced by a more sophisticated simplification approach. The QSSA may fail to make precise and quantitative predictions but can be used as a qualitative tool. If the QSSA is implemented through a detailed kinetic approach, the error made by the truncation will be minimized, and conditions where the low dimensional model is a good approximation will appear automatically.

2.1 Normalization of Rate Equations

The first step in a mathematical implementation of the QSSA is to transform the full set of AODE's in Eq. (1.19) into non-dimensional form through a process called *normalization*. The dimensional rate equations are normalized by defining dimensionless variables $x_1, \dots, x_n$ representing the concentrations $[X_1], \dots, [X_n]$ and a dimensionless time-scale τ. With standard units of concentration (mole/liter, M) and time (seconds, *sec.*) the dimensionless variables are defined

$$\tau = k, \qquad x_j = [X_j]/K_j, \qquad (j \in 1, \dots, n), \tag{2.4}$$

where k and K_j are constants with units of, respectively, $sec.^{-1}$ and *mole/liter*. The dimensionless rate equation for x_j is obtained from the rate equation for $[X_j]$ by the chain-rule

$$\frac{dx_j}{d\tau} = \frac{\partial x_j}{\partial [X_j]} \frac{\partial [X_j]}{\partial t} \frac{\partial t}{\partial \tau} = \frac{1}{K_j k} \frac{d}{dt}[X_j]. \tag{2.5}$$

The dimensionless rate equation is then rearranged so that a number of dimensionless parameters emerge. The normalization constants K_j and k in Eq. (2.5) can be chosen freely depending on what are intended of the dimensionless description. It is, however, good practice to try to minimize the number of dimensional parameters and to avoid extreme values of the dimensionless variables.

2.1.1 Dimensionless Reversible Reaction

Consider the reversible chemical reaction written in the general form

$$s_1 X_1 + \ldots + s_{m-1} X_{m-1} \underset{k_b}{\overset{k_f}{\rightleftarrows}} s_m X_m + \ldots + s_n X_n, \tag{2.6}$$

where s_j $(j \in 1, \ldots, n)$ denotes the stoichiometric coefficient of species X_j. The overall rate of reaction v is the difference between the forward and the backward rate of reaction

$$v = k_f \prod_{j=1}^{m-1} [X_j]^{s_j} - k_b \prod_{j=m}^{n} [X_j]^{s_j}. \tag{2.7}$$

Expressing the forward rate constant k_f using equilibrium constant $K_e = k_f/k_b$, one obtains

$$v = k_b \left[K_e \prod_{j=1}^{m-1} [X_j]^{s_j} - \prod_{j=m}^{n} [X_j]^{s_j} \right]. \tag{2.8}$$

The dimensionless overall rate of a reversible reaction ν is defined from the dimensional overall rate v through

$$\nu = \frac{v}{K_v k}, \tag{2.9}$$

where K_v is a normalization constant for the reaction rate and k an apparent first order rate constant. Expressing the overall rate of reaction in terms of the dimensionless variables $\mathbf{x} = x_1, \ldots, x_n$ representing the concentrations $[X_1], \ldots, [X_n]$, the dimensionless rate of reaction reads

$$\nu = \frac{k_b}{K_v k} \left[K_e \prod_{j=1}^{m-1} K_j^{s_j} x_j^{s_j} - \prod_{j=m}^{n} K_j^{s_j} x_j^{s_j} \right]. \tag{2.10}$$

Eq. (2.10) can be rearranged into

$$\nu = c_v \left[\rho \prod_{j=1}^{m-1} x_j^{s_j} - \prod_{j=m}^{n} x_j^{s_j} \right] = c_v f(x_1, \dots, x_n), \tag{2.11}$$

where

$$c_v = \frac{k_b}{K_v k} \prod_{j=m}^{n} K_j^{s_j}, \qquad \rho = K_e \prod_{j=1}^{m-1} K_j^{s_j} \prod_{j=m}^{n} K_j^{-s_j}. \tag{2.12}$$

The rate of change in the concentration of X_j, $(j \in 1, \dots, n)$, in the reversible reaction Eq. (2.6) may, in dimensionless form, then be written

$$\frac{dx_j}{d\tau} = \frac{s_j}{\varepsilon_v} f(x_1, \dots, x_n), \tag{2.13}$$

where

$$\varepsilon_v = \frac{K_j}{c_v K_v} = \frac{k}{k_b} K_j \prod_{j=m}^{n} K_j^{-s_j} \tag{2.14}$$

The parameter ε_v has a central role in the simplification of a mass action kinetic description of chemical and biochemical reaction systems. The value of ε_v is determined by the ratio k, i.e. the chosen normalization constant that eliminates the time-unit, to k_b which is a rate constant from the reaction. This ratio is multiplied by a ratio of normalization constants. If the ratio of normalization constants are of the order of unity and ratio k_b to k is low the ε_v is low, i.e. if $k_b \gg k$ implies $\varepsilon_v \to 0$. If, on the other hand, the ratio of k_b to k is of the order of unity, then $K_j \prod_{j=m}^{n} K_j^{-s_j} \to 0$ implies $\varepsilon_v \to 0$. Thus, the parameter ε_v may be small if there are large differences in either the rate of reaction, measured by k_b and k, or the chosen normalization constants. It is also noted the ε_v is associated with a specific reaction and the rate equation for every species involved in the reaction will contain a *rate term* proportional to ε_v.

2.1.2 Dimensionless Michaelis-Menten Reaction

The Michaelis-Menten reaction can be described by the dimensional rate equations

$$\begin{aligned} \frac{d[S]}{dt} &= -k_{sf}[S]([E]^0 - [ES]) + (k_{sb} + k_c)[ES] - k_c[ES], \\ \frac{d[ES]}{dt} &= k_{sf}[S]([E]^0 - [ES]) - (k_{sb} + k_c)[ES], \end{aligned} \tag{2.15}$$

with the initial conditions

$$[S](t^0) = [S]^0, \qquad [ES](t^0) = 0. \tag{2.16}$$

This description may be simplified by defining the Michaelis-Menten constant

$$K_m = \frac{k_{sb} + k_c}{k_{sf}}, \tag{2.17}$$

and normalizing using the dimensionless variables

$$\alpha = \frac{[S]}{K_m}, \qquad \gamma = \frac{[ES]}{e^0}, \qquad \tau = t k_{sf} e^0, \tag{2.18}$$

where e^0 is the total enzyme concentration.

The relation between the normalized and the original rate equations are

$$\frac{d\alpha}{d\tau} = \frac{d[S]/dt}{K_m k_{sf} e^0}, \quad \frac{d\gamma}{d\tau} = \frac{d[ES]/dt}{k_{sf}(e^0)^2}, \tag{2.19}$$

which is obtained from the chain-rule. The dimensionless rate equation for enzyme-substrate complex γ, is then

$$\begin{aligned} \frac{d\gamma}{d\tau} =& \frac{k_{sf} K_m}{k_{sf} e^0} \frac{[S]}{K_m} \left(1 - \frac{[ES]}{e^0}\right) - \frac{k_{sb} + k_c}{k_{sf} e^0} \left(\frac{[ES]}{\varepsilon^0}\right) \\ =& \frac{K_m}{e^0}(\alpha - \gamma(1 + \alpha)), \end{aligned} \tag{2.20}$$

whereas the dimensionless rate equation for the substrate, α, is

$$\begin{aligned} \frac{d\alpha}{d\tau} =& - \frac{k_{sb} + k_c}{K_m k_{sf} e^0} \left[\frac{[S]}{K_m} \left(1 - \frac{[ES]}{e^0}\right) - \frac{[ES]}{e^0}\right] - \frac{k_c}{K_m k_{sf}} \frac{[ES]}{e^0} \\ =& - \alpha + \gamma(1 + \alpha) - \frac{k_c}{k_{sb} + k_c}\gamma \end{aligned} \tag{2.21}$$

When defining the dimensionless parameters

$$\sigma = \frac{k_c}{k_{sb} + k_c}, \qquad \varepsilon = \frac{e_0}{K_m}, \tag{2.22}$$

the Michaelis-Menten reaction can be written in dimensionless form

$$\boxed{\begin{aligned} \frac{d\alpha}{d\tau} &= -\alpha + \gamma(1 + \alpha) - \sigma\gamma, \\ \frac{d\gamma}{d\tau} &= \frac{1}{\varepsilon}[\alpha - \gamma(1 + \alpha)], \end{aligned}} \tag{2.23}$$

with appropriate initial conditions

$$\alpha(\tau^0) = \frac{[S]^0}{K_m} = \alpha^0, \qquad \gamma(\tau^0) = \frac{[ES]^0}{e^0} = 0. \tag{2.24}$$

2.2 Singular Points

In the standard implementation of the QSSA, the quasi-steady state concentration of a species is obtained by solving the algebraic equation that emerges by nullifying the rate equation. In a chemical or biochemical reaction system those dimensionless rate equations are

$$\frac{d}{dt}\mathbf{x} = \mathbf{h}(\mathbf{x}), \tag{2.25}$$

where the n-dimensional vector $\mathbf{x}$ represents the dimensional concentrations represented by $[X_1], \ldots, [X_n]$ and $\mathbf{h}(\mathbf{x})$ is a n-dimensional vector containing the normalized dimensionless rate functions $h_1, \ldots, h_n$. The points $x_1^*, \ldots, x_n^* = \mathbf{x}^*$ for a differential equation Eq. (2.25) where

$$\frac{d}{dt}\mathbf{x}^S = 0 \Rightarrow \mathbf{h}(\mathbf{x}^*) = 0, \tag{2.26}$$

are in mathematical terminology called *singular points*. In a closed chemical system the singular point corresponds to an equilibrium, whereas a singular point in an open chemical system corresponds to a steady state. If Eq. (2.25) describes a subspace of a system composed of more than n species the singular point is a quasi-steady state in both open and closed systems. It is important to know if a singular point is stable or unstable to small changes in the values of $x_1^*, \ldots, x_n^*$. When a stable singular point experiences a small perturbation to the variables the disturbance will eventually die and the variables will return to the steady state. A small perturbation to an unstable singular point will, on the other hand, amplify, and the variables will never return to the steady state. If the singular point is neither stable nor unstable it is said to be neutral. The concentrations of chemical species in biological systems will always be fluctuating due to a naturally occuring noise. The state of a biological system will therefore will only be in an unstable singular point for a limited period of time unless there is a mechanism forcing the system to be close to the unstable state.

The stability of a singular point is to first approximation determined by the eigenvalues of the Jacobian matrix $\mathbf{J}(\mathbf{x})$ evaluated at the singular point. The

Jacobian matrix is, for the reaction system described by Eq. (2.25),

$$\mathbf{J}(\mathbf{x}) = \begin{pmatrix} \dfrac{\partial h_1(\mathbf{x})}{\partial x_1} & \cdots & \dfrac{\partial h_1(\mathbf{x})}{\partial x_n} \\ \vdots & & \vdots \\ \dfrac{\partial h_n(\mathbf{x})}{\partial x_1} & \cdots & \dfrac{\partial h_n(\mathbf{x})}{\partial x_n} \end{pmatrix} \tag{2.27}$$

and the stability determining eigenvalues is found by solving

$$det(\mathbf{J}(\mathbf{x}^*) - \lambda \mathbf{I}) = 0, \tag{2.28}$$

where $\mathbf{I}$ is the identity matrix. Eq. (2.28) yields an $n'th$ order polynomial in λ which can be quite difficult to solve analytically. In such a case, one can evaluate the eigenvalues by establishing the Ruth-Hurwitz conditions (see e.g. Murray, 1993; Heinrich & Schuster, 1996) or by using numerical methods. The stability of the singular points is determined by the real part of the eigenvalues. If all eigenvalues have negative real parts the singular point $\mathbf{x}^*$ is stable whereas it is unstable if one or more of the eigenvalues have positive real parts. The stability of singular points will be treated in more details in Chapter 3 but the above introduction is sufficient to for a formal discussion the quasi-steady state method.

2.3 Tihonov's Theorems

The mathematical basis of the QSSA in chemical and biochemical systems is two theorems called Tihonov's first and second theorem (Klonowski, 1983) which was derived by the Russian mathematician A. N. Tihonov (Tihonov, 1952). Due to the relatively simple formulation and the introduction of basic concepts, Tihonov's first theorem will be discussed first, even though it is a special case of the more general second theorem. It should be noted that the theorems apply equally well to systems of ordinary first order differential equations and not only to systems of AODE's as discussed here.

2.3.1 Tihonov's First Theorem

Consider the system of linearly independent AODE's

$$\frac{dx}{d\tau} = f(x,z), \qquad \varepsilon\frac{dz}{d\tau} = g(x,z), \tag{2.29}$$

with initial conditions

$$x(\tau^0) = x^0, \qquad z(\tau^0) = z^0, \tag{2.30}$$

called the *non-degenerate system* (see e.g. Tang & Othmer, 1995) or the full system. The dimensionless variables x, z, which may be vectors, represent concentrations of chemical species and the dimensionless functions $f(x, z)$ and $g(x, z)$, which may also be vectors, are derived from the law of mass action. The reader should, by the detailed normalization in sections 2.1.1 and 2.1.2, be convinced that the rate equations at least for some chemical and biochemical reaction systems can be written in the form appearing in Eq. (2.29) and that the parameter ε is a parameter associated with the rate of a chemical reaction. It is a requirement that the the integral solution of Eq. (2.29) is unique and that functions $f(x, z)$ and $g(x, z)$ are finite, smooth and continuous. These requirements are in most cases met when the rate equations are based on mass action kinetics.

In the limit $\varepsilon \to 0$ on the fast time-scale $\tau_\varepsilon = \tau/\varepsilon$ the AODE's read

$$\frac{dx}{d\tau_\varepsilon} = 0, \qquad \frac{dz}{d\tau_\varepsilon} = g(x, z), \tag{2.31}$$

with initial conditions

$$x(\tau_\varepsilon^0) = x^0, \qquad z(\tau_\varepsilon^0) = z^0. \tag{2.32}$$

On the time-scale τ_ε the "slow" variable x can be taken as a parameter as it has a zero rate of change on this time-scale. The *adjoined system* of Eq. (2.29) is defined

$$\frac{dz}{d\tau_\varepsilon} = g(x, z), \qquad z(\tau_\varepsilon^0) = z^0, \tag{2.33}$$

where x is parameterized. The singular point of the adjoined system is given by

$$g(x, z) = 0, \tag{2.34}$$

which can be solved with respect to z. The solution of Eq. (2.34) determines the quasi-steady state value z^* of z through the algebraic function

$$z^* = \phi(x). \tag{2.35}$$

If some initial conditions z^0 will tend to a the well defined quasi-steady state z^* after initiation of the system, i.e. if z^0 is under the influence of $z^* = \phi(x)$ and the singular solution of the adjoined system is uniquely defined and stable, the variable z may be considered to be in the steady state determined by $\phi(x)$ when after a critical time exceeding $\tau_c = |\varepsilon \ln(\varepsilon)|$ (Klonowski, 1983). When $\tau \gg \tau_c$ the full system in Eq. (2.29) reduces to the *degenerate system*

$$\frac{dx}{d\tau} = f(x, \phi(x)), \qquad z = \phi(x) \tag{2.36}$$

with initial conditions

$$x(\tau^0) = x^0, \qquad z(\tau^0) = \phi(x^0). \tag{2.37}$$

On the "slow" time-scale τ the "fast" variable z will be determined solely through $\phi(x)$ and z is said to "forget" its initial value (Klonowski, 1983).

The conditions for approximating the *non-degenerate* system in Eq. (2.29) by the degenerate system in Eq. (2.36) is summarized in

Tihonov's First Theorem. When $\varepsilon \to 0$ the solution to Eq. (2.29), with initial conditions $x(\tau^0) = x^0, z(\tau^0) = z^0$, tends to the solution of the degenerate system Eq. (2.36) if;

- the root $z = \phi(x)$ is a stable isolated singular point of the adjoined system;
- the initial values z^0 lie in the domain under influence of the root $z = \phi(x)$ for initial values x^0.

The degenerate system is, in singular perturbation theory, called the *outer solution* whereas the adjoined system is called the *inner solution* (Murray, 1993). The inner and the outer solutions describe, respectively, the dynamic behavior on the fast time-scale τ_ε and the slow time-scale τ. For intermediate time-scales, singular perturbation theory can be used to match the two solutions such that appropriate reduced descriptions exists on all time-scales. The singular perturbation approach becomes, however, quite complicated in large reaction systems and will not be considered here.

An important limitation to Tihonov's first as well as second theorem as applied to chemical and biochemical reaction systems arises from the parameterization of the "slow" variables x on the fast time-scale. To see why x needs to have a zero rate of change on the fast time-scale, let t_c be the relaxation time of z such that $\tau_c - \tau^0$ is the time it takes for z to change from z^0 to its steady state value. When x is not constant on the fast time-scale the values of x and z will after τ_c be

$$x(\tau_c) = x^0 + \int_{\tau^0}^{\tau_c} f(x(\tau), z(\tau))d\tau, \qquad z(\tau_c) = \phi(x(t_c)) \tag{2.38}$$

The latter equation cannot be found analytically unless the first equation can be solved analytically. This can not normally be done unless $x(\tau_c) = x^0$. In most reaction systems, the "slow" and the "fast" species react with each other and their rate equations will contain cross terms. The QSSA can only be applied when the establishment of steady states of the "fast" variables leaves the "slow" variables unchanged.

2.3.2 The Michaelis-Menten Rate Law

The Michaelis-Menten reaction is in dimensionless form described by

$$\frac{d\alpha}{d\tau} = -\alpha + \gamma(1+\alpha) - \sigma\gamma, \qquad \varepsilon\frac{d\gamma}{d\tau} = \alpha - \gamma(1+\alpha) \tag{2.39}$$

with the initial conditions

$$\alpha(\tau^0) = \alpha^0, \qquad \gamma(\tau^0) = 0. \tag{2.40}$$

This system is in a form where Tihonov's first theorem applies when $\varepsilon \to 0$. It is noted that the rate equation for α can be written

$$\frac{d\alpha}{d\tau} = -\varepsilon\frac{d\gamma}{d\tau} - \sigma\gamma, \tag{2.41}$$

which shows the rate equation of α is not independent of a change in γ. Fortunately, the first term of Eq. (2.41) is negligible when ε is small but this may not be the case when one chooses another normalization. Setting $\tau_\varepsilon = \tau/\varepsilon$ the system is described by

$$\frac{d\alpha}{d\tau_\varepsilon} = -\varepsilon^2\frac{d\gamma}{d\tau} - \varepsilon\sigma\gamma, \qquad \frac{d\gamma}{d\tau_\varepsilon} = \alpha - \gamma(1+\alpha) \tag{2.42}$$

with initial conditions

$$\alpha(\tau_\varepsilon^0) = \alpha^0, \qquad \gamma(\tau_\varepsilon^0) = 0, \tag{2.43}$$

on the fast time-scale τ_ε. When $\varepsilon \to 0$ the rate equation of α nullifies and the adjoined system is given by

$$\frac{d\gamma}{d\tau_\varepsilon} = \alpha - \gamma(1+\alpha), \qquad \gamma(\tau_\varepsilon^0) = 0, \tag{2.44}$$

where α can be treated as a constant. The singular solution of the adjoined system is given by

$$\alpha - \gamma(1+\alpha) = 0 \tag{2.45}$$

which, solved with respect to γ, yields the steady state value of enzyme-substrate complex

$$\gamma^* = \frac{\alpha}{1+\alpha}. \tag{2.46}$$

The singular point of the adjoined system is easily shown to be stable and it is uniquely defined by the value of α.

Now consider the adjoint system on the slow time-scale τ

$$\frac{d\gamma}{d\tau} = \frac{1}{\varepsilon}[\alpha - \gamma(1+\alpha)]. \tag{2.47}$$

When the initial values are $\alpha(\tau^0) = \alpha^0$ and $\gamma(\tau^0) = 0$ the initial rate of change in γ will be α/ε. As the singular point of the adjoined system is stable and any initial values of α and γ is under the influence of the singular point, γ will approach the quasi-steady state value γ^* with a rate that approaches infinity as $\varepsilon \to 0$. When the quasi-steady state is reached, $d\gamma/d\tau = 0$ and any change in α will immediately be followed by the establishment of a new steady state in γ given by Eq. (2.46).

Inserting the quasi-steady state value γ^* into the non-degenerate system, the degenerate system is obtained be ignoring the rate equation for γ

$$\frac{d\alpha}{d\tau} = -\frac{\sigma\alpha}{1+\alpha}, \qquad \alpha(\tau^0) = \alpha^0, \tag{2.48}$$

which in dimensional from yields the well-known Michaelis-Menten rate law

$$\frac{d}{dt}[S] = -\frac{k_c e^0 [S]}{K_m + [S]}. \tag{2.49}$$

The smallness of ε ensures the validity of the QSSA in the Michaelis-Menten reaction. In dimensional from the condition reads $e^0 << K_m$ in agreement with a recent report (de la Selva *et al.*, 1996). Using the initial substrate concentration instead of the Michaelis-Menten constant to normalize the substrate concentration, the condition $e^0 << s^0$ can be derived (Heineken *et al.*, 1967; Klonowski, 1983; Murray, 1993). This choice of normalization is, however, not very convenient when investigating long term behavior. Another method for establishing applicability conditions for the QSSA is based on time-scale estimations. Using this approach, the conditions for employing the QSSA in the Michaelis-Menten reaction is $e^0 << s^0 + K_m$ (Segel & Slemrod, 1989). This is complemented by the recently reported conditions $e^0 + s^0 >> k_c/k_{sb}$ and $k_{sb} >> k_c$ (Borghans *et al.*, 1996) obtained through time-scale estimation combined with a variable transformation. Whereas the time-scale estimation method seems to establish precise conditions for the applicability of the QSSA, the method of normalization is directly applicable even to very complicated reaction systems where characteristic time-scales may not be directly accessible.

2.3.3 Tihonov's Second Theorem

Tihonov's second theorem pertains to systems of ordinary first order differential equations containing several small parameters in the derivatives. Consider the set of linear independent AODE's given by

$$\begin{aligned}\frac{dx}{d\tau} &= f(x, z_j),\\ \varepsilon_j \frac{dz_1}{d\tau} &= g_1(x, z_j), \qquad j \in 1, \dots, m\end{aligned} \tag{2.50}$$

with initial conditions

$$x(\tau^0) = x^0, \qquad z_j(\tau^0) = z_j^0, \qquad j \in 1, \dots, m. \tag{2.51}$$

Again, the dimensionless variables $x, z_1, \dots, z_m$, which may be vectors, represent concentrations, whereas the dimensionless functions $f, g_1, \dots, g_m$ describe the reaction rates of the constituting reversible and Michaelis-Menten reactions.

When $\varepsilon_m \to 0$ such that $\varepsilon_m/\varepsilon_j \to 0$ for constant ε_j $(j \in 1, \dots, m-1)$, the *adjoined system of first order* is

$$\frac{dz_m}{d\tau_m} = g_m(x, z_1, \dots, z_m), \qquad z_m(\tau^0) = z_m^0, \tag{2.52}$$

where $\tau_m = \tau/\varepsilon_m$ and $x, z_1, \dots, z_{m-1}$ can be taken as parameters. The steady state function z_m^* of z_m is found as the singular solution to the adjoined system of first order $g_m(x, z_1, \dots, z_m) = 0$ as an algebraic function

$$z_m^* = \phi_m(x, z_1, \dots, z_{m-1}). \tag{2.53}$$

The *degenerate system of first order* is given by

$$\begin{aligned}\frac{dx}{d\tau} &= f(x, z_1, \dots, z_{m-1}, z_m^*),\\ \varepsilon_j \frac{dz_1}{d\tau} &= g_1(x, z_1, \dots, z_{m-1}, z_m^*), \qquad j \in (1, \dots, m-1)\end{aligned} \tag{2.54}$$

with initial conditions

$$x(\tau^0) = x^0, \qquad z_j(\tau^0) = z_j^0, \qquad (j \in 1, \dots, m-1), \tag{2.55}$$

if the singular point of the adjoined system of first order is stable.

When $\varepsilon_{m-1} \to 0$ such that $\varepsilon_{m-1}/\varepsilon_j \to 0$ $(j \in 1, \dots, m-2)$, the quasi-steady state value of z_{m-1}^* of z_{m-1} can be found from the singular point of the adjoined system of second order, which determines the behavior of the non-degenerate system at the time-scale τ_{m-1}. If the singular point of the adjoined system of second order is stable, the *degenerate system of second order* is obtained from the degenerate system of first order by replacing z_{m-1} with z_{m-1}^* in the same way that the degenerate system of first order is obtained from the non-degenerate system. The degenerate system of second order contains $m-2$ small parameters $\varepsilon_1, \ldots, \varepsilon_{m-2}$ and the variables $x, z_1, \ldots, z_{m-2}$. Analogously, one obtains the degenerate system of k'th order by in turn setting $e_m, \ldots, e_k$ to zero and replacing $z_m, \ldots, z_k$ by their steady state values $\phi_m, \ldots, \phi_k$. The conditions for the degenerate system of k'th order to be a valid approximation to the non-degenerate system is summarized in

Tihonov's Second Theorem. Let $j \in k, \ldots, m-1$, $m < n$. When $\varepsilon_j \to 0$ such that $\varepsilon_j/\varepsilon_i \to 0$ $(i \in 1, \ldots, j-1)$, the solution to Eqs. (2.50), with initial conditions $x(\tau^0) = x^0, z_j(\tau^0) = z_j^0$, tends to the solution of the degenerate system of j'th order if:

- the roots $z_j^* = \phi_j$ are stable, isolated, singular point of the adjoint system of $j'th$ order;

- the initial values z_j^0 lie in the domain under the influence of the root $z_j^* = \phi_j$ for initial values $x^0, z_i^0 i \in (1, \ldots, j-1)$.

2.4 Complex Reaction Systems

Tihonov's theorems require that the fast variables z_j in Eq. (2.50) are associated with a single small parameter ε_j. If the chemical species, whose concentration are represented by z_j, are reactants or products in multiple reactions the rate equation for z_j is of the form

$$\frac{dz_j}{d\tau} = \sum_{l=1}^{m} \frac{s_{j,l}}{\varepsilon_l} g_{j,l}(x, z_1, \ldots, z_n), \tag{2.56}$$

where the summation is over the *sub-reactions* of z_j that each contributes with a rate term given by Eq. (2.13).

When $\varepsilon_m \to 0$ such that $\varepsilon_m/\varepsilon_j \to 0$ $(j \in 1, \ldots, m-1)$, the rate equation of z_j on the time-scale $\tau_m = \tau/\varepsilon_m$ will be given by

$$\frac{dz_j}{d\tau_m} = s_{m,j} g_{m,j}(x, z_1, \ldots, z_n). \tag{2.57}$$

The singular point of Eq. (2.57) may, however, not be uniquely defined if another species in the system, say z_i, is a reactant or a product in the same reaction as

z_j, as well as in other reactions whose rate term are nullified on the time-scale τ_m. In that case, the rate equation of z_i on the time-scale τ_m reads

$$\frac{dz_i}{d\tau_m} = s_{m,i} q_{i,j} g_{m,j}(x, z_1, \ldots, z_n), \tag{2.58}$$

where $q_{i,j}$ is a non-zero proportionality factor reflecting the different normalization of z_i and z_j. The algebraic equation

$$g_{m,j}(x, z_1, \ldots, z_n) = 0 \tag{2.59}$$

may be solved with respect to z_j but the solution z_j^* will be a function of the indeterminable variable z_i. The mathematical description of a reaction system where species are reactants or products in several entangled reactions can not be simplified using Tihonov's theorems and will here be called *complex reaction systems*. The complex reactions systems considered here will be limited to those that can be written

$$\begin{aligned}
\frac{dx}{d\tau} &= f(x, z_1, \ldots, z_n) \\
\frac{dz_1}{d\tau} &= \frac{s_{1,1}}{\varepsilon_1} g_{1,1}(x, z_1, \ldots, z_n) + \ldots + \frac{s_{1,m}}{\varepsilon_m} g_{1,m}(x, z_1, \ldots, z_n) \\
&\vdots \\
\frac{dz_n}{d\tau} &= \frac{s_{n,1}}{\varepsilon_1} g_{n,1}(x, z_1, \ldots, z_n) + \ldots + \frac{s_{n,m}}{\varepsilon_m} g_{n,m}(x, z_1, \ldots, z_n)
\end{aligned} \tag{2.60}$$

with initial conditions

$$x(\tau^0) = x^0, \qquad z_j(\tau^0) = z_j^0, \qquad (j \in 1, \ldots, n). \tag{2.61}$$

2.4.1 Standard Simplification Method

The standard method of simplifying a complex reactions system as described in Eq. (2.60) is to assume that all sub-reactions of $z_1, \ldots, z_n$ have identical characteristic time-scales, i.e. $\varepsilon = \varepsilon_1 = \ldots = \varepsilon_m$ (see e.g. Klonowski, 1983). The full system in Eq. (2.60) may then be written

$$\begin{aligned}
\varepsilon \frac{dz_1}{d\tau} &= s_{1,1} g_{1,1}(x, z_1, \ldots, z_n) + \ldots + s_{1,m} g_{1,m}(x, z_1, \ldots, z_n), \\
&\vdots \\
\varepsilon \frac{dz_n}{d\tau} &= s_{n,1} g_{n,1}(x, z_1, \ldots, z_n) + \ldots + s_{n,m} g_{n,m}(x, z_1, \ldots, z_n),
\end{aligned} \tag{2.62}$$

with initial conditions

$$x(\tau^0) = x^0, \qquad z_j(\tau^0) = z_j^0, \quad (j \in 1, \dots, n), \tag{2.63}$$

where Tihonov's first theorem applies. The quasi-steady state values $\Phi(x) = \phi_1(x), \dots, \phi_m(x)$ of $z_1, \dots, z_n$ are in general found from singular points of Eq. (2.62) by solving the algebraic equations

$$\sum_{j=1}^{n} s_{i,j} g_{i,j}(x, z_1, \dots, z_n) = 0, \quad (i \in 1, \dots, m), \tag{2.64}$$

but most often only the solutions of the more simple equations

$$g_{i,j}(x, z_1, \dots, z_n) = 0, \quad (j \in 1, \dots, m), \quad (i \in 1, \dots, n), \tag{2.65}$$

are considered. It will shortly become clear why solving Eq. (2.65) instead of solving the more general Eq. (2.64) is reasonable. If $\varepsilon \to 0$ and the conditions of Tihonov's first theorem are met, the full system can be approximated by the degenerate system

$$\frac{dx}{d\tau} = f(x, \phi_1(x), \dots, \phi_m(x)), \qquad x(\tau^0) = 0. \tag{2.66}$$

2.4.2 Extending Tihonov's Theorems

The standard method of assuming identical characteristic time-scales fails in situations where one or more of the parameters ε_j in Eq. (2.60) is not small. Consider the system in Eq. (2.60) where ε_j, $(j \in 1, \dots, m)$ are distinct, and let $\varepsilon_m \to 0$ such that $\varepsilon_m/\varepsilon_j \to 0$ $(j \in 1, \dots, m-1)$. On the time-scale τ_m, Eq. (2.60) reads

$$\begin{aligned}
\frac{dx}{d\tau_m} &= 0, \\
\frac{dz_1}{d\tau_m} &= s_{1,m} g_{1,m}(x, z_1, \dots, z_n), \\
&\vdots \\
\frac{dz_n}{d\tau_m} &= s_{n,m} g_{n,m}(x, z_1, \dots, z_n),
\end{aligned} \tag{2.67}$$

with initial conditions

$$x(\tau_m^0) = x^0, \qquad z_j(\tau^0) = z_j^0, \qquad (j \in 1, \dots, n). \tag{2.68}$$

When the stoichiometric coefficients $s_{i,m}$ $(i \in 1, \dots, l-1)$ are zero, i.e. when species z_i $(i \in 1, \dots, l-1)$ are neither reactants nor products in the reactions associated with ε_m, Eq. (2.67) reduces to

$$\begin{aligned} \frac{dz_l}{d\tau_m} &= s_{l,m} g_{l,m}(x, z_1, \dots, z_n), \\ &\vdots \\ \frac{dz_n}{d\tau_m} &= s_{n,m} g_{n,m}(x, z_1, \dots, z_n), \end{aligned} \tag{2.69}$$

with initial conditions

$$z_j(\tau^0) = z_j^0, \qquad j \in (l, \dots, n), \tag{2.70}$$

where $x, z_1, \dots, z_{l-1}$ can be taken as parameters as their rate equations nullify on the time-scale τ_m.

In the singular solution of Eq. (2.69) one obtains the algebraic equations

$$g_{i,m}(x, z_1, \dots, z_n) = 0, \qquad i \in (l, \dots, n). \tag{2.71}$$

When the equations (2.71) contain k linear dependencies one can express the variables z_i, $i \in (l+k+1, \dots, n)$ as functions of $x, z_1, \dots, z_{l+k}$

$$z_i = \phi_i(x, z_1, \dots, z_{l+k}), \qquad i \in (l+k+1, \dots, n), \tag{2.72}$$

which represent the quasi-steady state values of z_i, $i \in (l+k+1, \dots, n)$. The k linear dependencies in equations (2.71) imply that the rate Eqs. (2.69) contain k conservation relations

$$\eta_j(z_l, \dots, z_n) = 0, \qquad (j \in 1, \dots, k), \tag{2.73}$$

which can be solved with respect to z_i, $i \in (l, \dots, l+k)$. The solutions

$$\vartheta_i(z_{l+k+1}, \dots, z_n), \qquad i \in (1, \dots, k), \tag{2.74}$$

replace $z_l, \dots, z_l + k$ in Eq. (2.69), which then reduces to the adjoined system of first order

$$\begin{aligned} \frac{dz_{l+k+1}}{d\tau_m} &= s_{l+k+1,m} g_{l+k+1,m}(x, z_1, \dots, z_n), \\ &\vdots \\ \frac{dz_n}{d\tau_m} &= s_{n,m} g_{n,m}(x, z_1, \dots, z_n), \end{aligned} \tag{2.75}$$

with initial conditions

$$x(\tau^0) = x^0, \quad z_i(\tau^0) = z_i^0, \qquad j \in (l, \dots, n). \tag{2.76}$$

The variables $x, z_1, \dots, z_l$ can be parameterized and the variables $z_l, \dots, z_{l+k}$ are algebraic functions of $z_{l+k+1}, \dots, z_n$.

If the singular solution of the adjoined system of first order is stable and the initial conditions are under the influence of the singular point, the degenerate system of first order is

$$\begin{aligned}
\frac{dx}{d\tau} &= f(x, z_1, \dots, z_n) \\
\frac{dz_1}{d\tau} &= \frac{s_{1,1}}{\varepsilon_1} g_{1,1}(x, z_1, \dots, z_n) + \dots + \frac{s_{1,m-1}}{\varepsilon_{m-1}} g_{1,m-1}(x, z_1, \dots, z_n) \\
&\vdots \\
\frac{dz_{l+k}}{d\tau} &= \frac{s_{l+k,1}}{\varepsilon_1} g_{l+k,1}(x, z_1, \dots, z_n) + \dots + \frac{s_{l+k,m-1}}{\varepsilon_{m-1}} g_{l+k,m-1}(x, z_1, \dots, z_n)
\end{aligned} \tag{2.77}$$

with initial conditions

$$x(\tau^0) = x^0, \qquad z_j(\tau^0) = z_j^0, \qquad (j \in 1, \dots, l+k) \tag{2.78}$$

and

$$z_i = \phi_i(x, z_1, \dots, z_{l+k}), \qquad i \in (l+k+1, \dots, n). \tag{2.79}$$

The degenerate system of first order has the same structure as the non-degenerate system but with a lower dimensionality. The method just described can be re-applied to the degenerate system of first order and if the singular solution to the adjoined system of second order is stable, one can obtain a degenerate system of second order that has a lower dimensionality than the degenerate system of first order. If all ε_i $(i \in 1, \dots, m)$ approaches zero and the singular solutions of the $i'th$ $(i \in 1, \dots, m)$ adjoined systems are stable, the degenerate system of $m'th$ order is given by

$$\frac{dx}{d\tau} = f(x, \phi_1(x), \dots, \phi_m(x)), \qquad x(\tau^0) = 0. \tag{2.80}$$

where the functions $\phi_1(x), \dots, \phi_m(x)$ are found from the algebraic functions

$$g_{i,j}(x, z_1, \dots, z_n) = 0, \quad (i \in 1, \dots, n), \quad (j \in 1, \dots, m), \tag{2.81}$$

which coincides with the algebraic solutions that are solved when using the standard method described in section 2.4.1. The method presented here is an improvement on the standard method, as it is possible to obtain a reduced set of

AODE's when species participate in multiple reactions with distinct time-scales. It seems plausible that a mathematical proof of the extended method, which will be applied in detail later, may be obtained based on Tihonov's theorems, but this is beyond the scope of the present text.

The extended method for simplification of mass action kinetic rate equations is relevant when one or more of the parameters ε_j $(1 \in 1, \ldots, m)$ appearing in Eqs. (2.60) are not small. In the case where all the parameters are small the extended method reduces to the standard simplification method. The implementation of extended method is in Appendix A and Appendix B exemplified through detailed derivations of simplified models of, respectively, a case of ligand binding to a Michaelis-Menten enzyme and a open auto-catalytic reaction scheme.

CHAPTER 3

Nonlinear Dynamics

In this chapter, a short survey of the mathematical field of nonlinear dynamics will be made to provide the basis for the discussions in the chapters to follow. It is at this point important to stretch that the survey of concepts and principles is to be considered from an applied perspective. The level of mathematical detail is kept at a minimum and it may be argued the some central concepts are lacking. This chapter provides the *vocabulary* for the mathematical level found appropriate in the treatment of the dynamic behavior of biochemical systems. A much deeper discussion of nonlinear dynamics can be found elsewhere (Thompson & Stewart, 1986; Seydel, 1988; Hale & Kocak, 1991; Perko, 1996).

The reaction systems or *dynamic systems* considered herein are all continuous in time and described by the linear independent AODE's

$$\frac{d}{dt}\mathbf{x} = \mathbf{f}(\mathbf{x}), \tag{3.1}$$

where $\mathbf{f}$ is a vector field defined by the chemical reactions described in Chapter 1 and Chapter 2. The study of dynamic systems is mainly a study of *flows* of some variables which can represent anything that changes in finite steps or continuously in time. The flow of an n-dimensional dynamic system is a mapping $\phi : \mathbf{R}^n \to \mathbf{R}^n$ such that applying ϕ on $\mathbf{x}(t)$ brings the system forward in time, i.e. $\phi(\mathbf{x}(t)) = \mathbf{x}(t+\epsilon)$, $\epsilon > 0$. The mapping represents a difference equation but, will, in the limit of $\epsilon \to 0$, be described by the differential Eq. (3.1). The *phase plane* of a dynamic system is the space of the mapping, i.e. $\mathbf{R}^n$, and a *phase plane trajectory* is the curve $\boldsymbol{\phi}(\mathbf{x}^0, t)$ in phase space with parameterized time and is defined uniquely by the initial conditions $\mathbf{x}^0$. Usually, phase trajectories will tend to a confined subspace of the phase space called an *attractor* of the system. An attractor may be of non-integer dimension, i.e. an *strange attractor*, but will typically be a point, a line or a surface. The *basin of attraction* of an attractor is defined by the set of initial conditions producing phase trajectories converging to the attractor.

3.1 Phase Plane Analysis

Consider a dynamic system described by the two AODE's

$$\begin{aligned} \frac{dx_1}{dt} &= f(x_1, x_2), \\ \frac{dx_2}{dt} &= g(x_1, x_2), \end{aligned} \tag{3.2}$$

which, given initial conditions

$$x_1(t^0) = x_1^0, \qquad x_2(t^0) = x_2^0, \tag{3.3}$$

have a uniquely defined solution $x_1(t), x_2(t)$ for any $t > 0$. As discussed in Chapter 1 the solutions x_1^*, x_2^* of Eq. (3.2) that satisfy

$$f(x_1^*, x_2^*) = g(x_1^*, x_2^*) = 0, \tag{3.4}$$

are called singular points or steady states. The two-dimensional dynamic system in Eq. (3.2) can, in the vicinity of a singular point, when the singular point is chosen as the origin of the reference system, be approximated by the linear system

$$\begin{aligned} \frac{dx_1}{dt} &= ax_1 + bx_2, \\ \frac{dx_2}{dt} &= cx_1 + dx_2, \end{aligned} \tag{3.5}$$

where the constants a, b, c, d are the elements of the Jacobian matrix

$$\mathbf{J} = \begin{pmatrix} \frac{\partial f}{\partial x_1} & \frac{\partial f}{\partial x_2} \\ \frac{\partial g}{\partial x_1} & \frac{\partial g}{\partial x_2} \end{pmatrix} = \begin{pmatrix} a & b \\ c & d \end{pmatrix}. \tag{3.6}$$

The integral solution of Eq. (3.5) is

$$\begin{pmatrix} x_1(t) \\ x_2(t) \end{pmatrix} = c_1 \mathbf{v_1} \exp[\lambda_1 t] + c_2 \mathbf{v_2} \exp[\lambda_2 t], \tag{3.7}$$

where c_1, c_2 are arbitrary constants and $\mathbf{v_1}$, $\mathbf{v_2}$ are eigenvectors of the Jacobian matrix associated with the eigenvalues λ_1, λ_2. The stability of a steady state is determined by the real parts $Re\lambda_i$ of the eigenvalues. When real parts of the eigenvalues are negative, the steady state is asymptotically stable and any small perturbation will die out as the system returns to x_1^*, x_2^*. The subspace spanned by the eigenvectors associated with eigenvalue with negative real parts is called a stable manifold. The subspace spanned by the eigenvector with positive eigenvalues is called an unstable manifold of the steady state. The subspace spanned by the eigenvectors with eigenvalues that have a zero real parts is called the *center manifold.*

The two eigenvalues λ_1, λ_2 of the Jacobian matrix or a two-dimensional system are determined by

$$det \begin{bmatrix} a-\lambda & b \\ c & c-\lambda \end{bmatrix} = (a-\lambda)(c-\lambda) - bc = \lambda^2 - Tr(\mathbf{J})\lambda + det(\mathbf{J}) \Rightarrow$$

$$\lambda_1, \lambda_2 = \frac{1}{2} Tr(\mathbf{J}) \pm \frac{1}{2}\sqrt{Tr(\mathbf{J})^2 - 4det(\mathbf{J})} \tag{3.8}$$

where $Tr(\mathbf{J})$ and $det(\mathbf{J})$ denote the trace and the determinant of the Jacobian matrix. The different combinations of eigenvalues λ_1, λ_2 lead to different dynamic behavior in the vicinity of a steady state. These are listed below

Catalogue of Steady States

(I) λ_1, λ_2 real and distinct, i.e. $4det(\mathbf{J}) < Tr(\mathbf{J})^2$:

(a) λ_1 and λ_2 have the same sign. The steady state is called a node and may be either unstable or stable whether the eigenvalues are positive or negative. If the eigenvalues are larger than zero the solutions x_1, x_2 of Eq. (3.5) will move away from the steady state as time evolves whereas x, y will tend exponentially to the steady state if the eigenvalues are negative reals.

(b) λ_1 and λ_2 have different signs. In the direction of the eigenvector associated with the positive eigenvalue the system will escape from the steady state whereas the steady state will be an attractor of the system in the direction of the eigenvector associated with the negative eigenvalue. This steady state is called a saddle and is always unstable.

(II) λ_1, λ_2 complex, i.e. $4det(\mathbf{J}) > Tr(\mathbf{J})^2$: Solutions to Eq. (3.5) involve the term $\exp[Re(\lambda)t]\exp[\pm iIm(\lambda)t]$ implying an oscillatory integral solution.

(a) When $Tr(\mathbf{J}) < 0$ the steady state will be stable and the solutions of Eq. (3.5) will follow a damped oscillatory path toward the steady state which is called a stable spiral.
(b) The steady state where $Tr(\mathbf{J}) = 0$ is called a center and its stability is neutral. After a small perturbation the system will tend neither to or from the steady state but settles in a periodic orbit. Such periodic orbits, which are called *Lotka-Volterra type oscillations* are not stable to small perturbations and is not of interest here.
(c) When $Tr(\mathbf{J}) > 0$ the steady state is unstable and the solutions of Eq. (3.5) will tend away from the steady state following an oscillating trajectory with increasing amplitude. This steady state is called an unstable spiral.

(III) λ_1, λ_2 identical. i.e. $4det(\mathbf{J}) = Tr(\mathbf{J}))^2$: The Jacobian matrix has typically only one eigenvector and the steady state is called either a type II node or a star dependent on the form of the solution.

The phase plane trajectories in the vicinity of steady states are distinct and the identity of a steady state can readily be found by examination of the *phase plane portrait*. The flow around steady states or *phase plane singularities* is depicted in Fig. (3.1) for different combinations of the trace and the determinant of the Jacobian matrix in a two-dimensional system. The categorization used in two-dimensional systems is also used in systems of higher dimensionality. In higher dimensional systems the steady states have to be evaluated by calculation of the eigenvalues and not by evaluation of the trace and the determinant of the Jacobian matrix. Analytic stability analysis may be performed by establishing

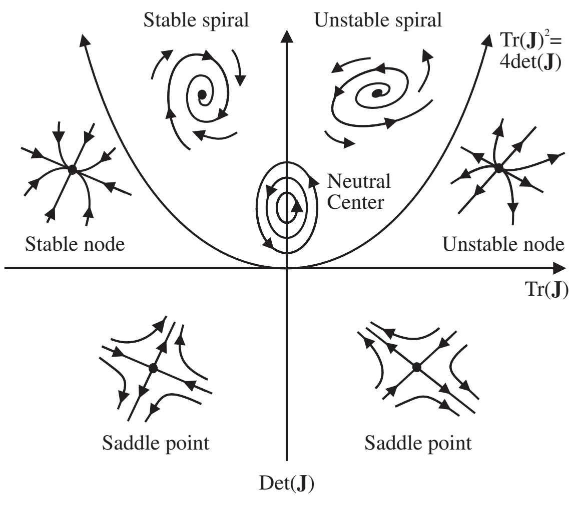

Fig. 3.1: Phase plane portraits of common steady state solutions. The dynamic behavior close to steady states can be approximated by a linear system given by the Jacobian matrix. In a two-dimensional system, the trace and the determinant of the Jacobian matrix determines the properties of the steady state; if $det(\mathbf{J}) < 0$ the steady state will be an unstable saddle and if $det(\mathbf{J}) > 0$ the steady state is a node, a spiral or a center. The spiral and the center steady states emerge when $Tr(\mathbf{J})^2 < 4det(\mathbf{J})$ and the latter only when $Tr(\mathbf{J}) = 0$. The spiral is stable if $Tr(\mathbf{J}) < 0$ and unstable if $Tr(\mathbf{J}) > 0$. If $det(\mathbf{J}) > 0$ and the steady state is neither a spiral nor a center, it is a node. A node is stable if $Tr(\mathbf{J}) < 0$ and unstable if $Tr(\mathbf{J}) > 0$.

the Ruth-Hurwitz conditions (see e.g. Murray, 1993; Heinrich & Schuster, 1996) but it is quite common that the eigenvalues can only be found numerically as the inequalities obtained from the Hurwitz matrix can be quite complicated.

3.2 Periodic Solutions

When a system has settled in a steady state the condition $\mathbf{x}(t) = \mathbf{x}(t+\epsilon)$ is met for all $\epsilon > 0$. When an integral solution is not a steady state solution but meets $\mathbf{x}(t) = \mathbf{x}(t+kT)$ where T is a finite constant called the period and k is an positive integer, the solution is a periodic solution. If the phase trajectory $\boldsymbol{\phi}(\mathbf{x}^*)$ is a closed curve in phase space it is called a *limit cycle*. In a two dimensional system, the Poincaré-Bendixson theorem gives the condition for the existence of a limit cycle:

Poincaré-Bendixson Theorem: If, and only if, a trajectory remains for $t^0 \leqslant t < \infty$ within a finite region D of the phase plane without approaching a steady state this trajectory is a periodic trajectory or tends to such a trajectory for $t \to 0$.

A limit cycle may be either stable or unstable to small perturbations depending on whether the perturbation dies out or amplifies. Suppose that a point $\mathbf{x}^*$ lies on a limit cycle such that $\mathbf{x}^*(t) = \mathbf{x}^*(t+T)$ and a small perturbation $\mathbf{d}$ is applied to the system such that $\mathbf{x}^*$ changes to $\mathbf{y} = \mathbf{x}^* + \mathbf{d}$. The perturbed solution will progress through a phase trajectory $\phi(\mathbf{y}, t)$ with a distance to the limit cycle $\boldsymbol{\phi}(\mathbf{x}^*, t)$ given by

$$\|\mathbf{d}(t)\| = \|\phi(\mathbf{y}, t) - \phi(\mathbf{x}^*, t)\|. \tag{3.9}$$

After one period T the distance from the perturbed trajectory to the limit cycle is the norm of the vector

$$\mathbf{d}(T) = \phi(\mathbf{y}, T) - \mathbf{x}^*. \tag{3.10}$$

If the distance between the trajectory and the limit cycle decreases, $\phi(\mathbf{y}, t)$ will typically converge toward $\phi(\mathbf{x}^*, t)$ and the limit cycle is stable. An unstable limit cycle will repel the trajectory $\phi(\mathbf{y}, t)$ and the distance in phase space will increase.

The *Poincaré section* of an n-dimensional system is defined by the plane Ω with a dimensionality of $n-1$ such the $\Omega \times \phi(x^*, t) = 0$, i.e. the limit cycle intersects Ω transversally. The *Poincaré map* or the *first return map* is defined as the mapping $\mathbf{P} : \Omega \to \Omega$ that brings a point $\mathbf{y} \in \Omega$ to the point $\mathbf{P}(\mathbf{y}) \in \Omega$ by $\mathbf{P}(\mathbf{y}) = \phi(\mathbf{y}, T')$ where T' is the *return time*. The *Poincaré map* is illustrated schematically in Fig. (3.2). It is obvious that $\mathbf{P}(\mathbf{x}^*) = \mathbf{x}^*$ and that $T' \to T$ for $\mathbf{d} \to 0$. Thus, $\mathbf{x}^*$ is a *fixed point* of the map (or difference equation) $\mathbf{x}_{k+1} = \mathbf{P}(\mathbf{x}_k)$ whose stability is determined by the norm of the eigenvalues of the linearization of $\mathbf{P}$ in Ω around $\mathbf{x}^*$. It can by shown that the $n-1$ eigenvalues obtained by a such linearization in Ω are also eigenvalues of the *monodromy* matrix

$$\mathbf{M} = \frac{\partial \phi(\mathbf{x}^*, T)}{\partial \mathbf{x}} \tag{3.11}$$

obtained by a first order expansion of Eq. (3.10) around $\mathbf{x}^*$

$$\mathbf{d}(T) = \frac{\partial \phi(\mathbf{x}^*, T)}{\partial \mathbf{x}}. \tag{3.12}$$

The monodromy matrix has n eigenvalues, of which $n-1$ determines the stability of $\mathbf{x}^*$ in the subspace spanned by Ω and the remaining always have a value of unity corresponding to a perturbation along the limit cycle. The eigenvalues of the monodromy matrix are called *Floquet multipliers*. The latter eigenvalue is associated with the eigenvector of the flow along the limit cycle and is not considered when evaluating the stability of the limit cycle. The stability of a fixed point in a difference equation is in general determined by the norm of the eigenvalues of the linearized system. The fixed point is stable if all eigenvalues have a norm less than unity and unstable if at least one eigenvalue has a norm greater than unity. Thus, a limit cycle is stable if all eigenvalues of the monodromy matrix, except one that is always unity, have a norm less than unity and unstable if at least one eigenvalue has a norm greater than unity.

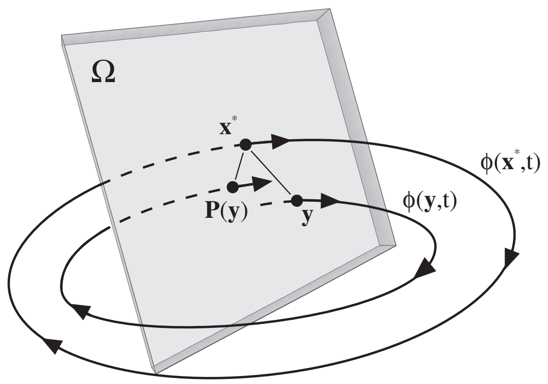

Fig. 3.2: Graphical illustration of the Poincaré section Ω and the return map. The point $\mathbf{x}^*$ lies on a limit cycle with a period of T. The limit cycle is in the phase plane given by the trajectory $\phi(\mathbf{x}^*, t)$ and thus $\phi(\mathbf{x}^*, t+T) = \phi(\mathbf{x}^*, t)$. The trajectory passing through a point y close to $\mathbf{x}^*$ also passes through the point $\mathbf{P}(\mathbf{y}) = \phi(\mathbf{y}, T)$. All trajectories intersect Ω transversally and Ω is spanned by the vectors $\mathbf{d}(\mathbf{y}, 0)$ and $\mathbf{d}(\mathbf{y}, T)$. As the norm of $\mathbf{d}(\mathbf{y}, T)$ is less than the norm of $\mathbf{d}(\mathbf{y}, 0)$ the depicted limit cycle is stable.

3.3 Bifurcations of Steady States

In linear systems, a *bifurcation* can be defined as the reversing of stability of the singular point. This is usually achieved by changing a parameter μ, the *bifurcation parameter*, through a *critical point* μ_c. If the following criteria for a single eigenvalue λ are met for the bifurcation parameter

$$Re(\lambda)|_{\mu_c=0} = 0, \qquad \frac{dRe(\lambda)}{d\mu_c}|_{\mu_c} \neq 0 \tag{3.13}$$

then the value of μ_c is called the *bifurcation point*. When a bifurcation parameter passes through a bifurcation point the structure of the vector field close to the steady state is changed and the flow around the steady state is altered. When the altered flow around the steady state cause changes to the qualitative features of the system the bifurcation is here said to change the *dynamic behavior* of the system. A change in dynamic behavior is for example a change from convergence to a steady state solution to convergence to a limit cycle solution or the emergence of new steady state solutions. The center manifold theorem (Perko, 1996) implies that the change in dynamics can be restricted to the center manifold spanned by the eigenvectors whose eigenvalues cause the bifurcation. This is very useful as bifurcations then can be classified in accordance with the number of eigenvalues reversing stability in the bifurcation independently of the actual dimension of the dynamic system.

The bifurcation point is usually single valued and any small change to the bifurcation parameter will cause the bifurcation point to vanish. This can be referred to as *structural instability* of the vector field. All bifurcations are structurally unstable but may have different *co-dimensions*. When a vector field is structurally unstable to a single bifurcation parameter the bifurcation is said to be of co-dimension one, if to parameters needs to have a unique value the bifurcation is said to be co-dimension two and vice versa. The effect of a co-dimension one bifurcation can be depicted in one-dimensional *bifurcation diagram* illuminating the dependency between a *bifurcation variable* x and a bifurcation parameter μ. This usually involves *steady state branches*, i.e. the steady state value of x^* for a given value of μ, and an illustration of *periodic branches*. Usually, the maximum value of x in the limit cycle is used to outline the periodic solution but other local frequently used as well. The stability of the solution, whether it is steady state or periodic branch, is typically illustrated by full lines and broken lines when the solution is, respectively, stable and unstable. A bifurcation points will then typically, but not in general, be located where a broken line replaces a full line or vice versa. A two-dimensional bifurcation diagram is used to depict the location of co-dimension one, which will appear as lines, or co-dimension two bifurcation points, which will appear as points, in the parameter space spanned by two bifurcation parameters. The steady state value of a bifurcation variable is sometimes included to produce a three-dimensional representation.

3.3.1 The Saddle-node Bifurcation

The bifurcation discussed in Eq. (3.13) where a single eigenvalue passes the imaginary axis in the complex plane and becomes positive or vice versa is called a *saddle-node* or *fold* bifurcation. In the bifurcation diagram of a saddle-node bifurcation, the saddle and the node coexist and approach each other as the bifurcation parameter approaches the bifurcation point. At the critical value of the bifurcation parameter, i.e. at the bifurcation point, the two steady states collide and are annihilated. The saddle-node steady state, generated when the saddle and the node collide, exists only for a single value of the bifurcation parameter. Such behavior will here be called structural instability as any small change in the bifurcation parameter will move the system away from the bifurcation point.. The saddle-node may either vanish completely or be replaced by two steady states, i.e. the saddle and the node, as depicted in Fig. (3.3).

3.3.2 The Cusp Bifurcation

In a cusp bifurcation, a node changes stability and in the process two new steady states emerge. The topology changes from a single steady state to three coexisting steady states. The generated steady states are typically stable nodes whose basin of attraction is separated by a saddle, and the system will be *bistable*. The cusp bifurcation is a co-dimension two bifurcation which mean that the bifurcation do not exist when a second bifurcation parameters is slightly changed. With a small change in the second bifurcation parameter the cusp is destroyed and is replaced by a saddle-node bifurcation in the first bifurcation parameter. A three dimensional representation of the two-dimensional bifurcation diagram of the cusp looks like a folded sheet where the folds of the sheet are saddle-node bifurcation. This structure is also depicted in Fig. (3.3).

3.3.3 The Hopf Bifurcation

Whereas the saddle-node is associated with a single eigenvalue passing zero the Hopf bifurcation occurs when two complex conjugated eigenvalues pass the real axis in the complex plane. In a two-dimensional system, the bifurcation point is determined by $Tr(\mathbf{J}) = 0$ when $det > 0$ and a spiral reverses its stability. The change in stability involves a limit cycle and the Hopf bifurcation is the most important bifurcation related to the emergence of sustained periodic behavior. In the *super-critical* Hopf bifurcation, a steady state solution becomes unstable and a stable limit cycle is born. The limit cycle emerges in the close vicinity of the steady state and shows low amplitude oscillations. The period and amplitude of the periodic solution can, in the neighborhood of the super-critical Hopf bifurcation point, be calculated from the eigenvalues of the Jacobian matrix. This is one of the few cases where a global structure (the limit cycle) can be described by a local calculation (the steady state). In a *sub-critical* Hopf bifurcation, an unstable limit cycle emerges as two eigenvalues crosses the imaginary axis and a stable spiral bifurcate to an unstable saddle. An unstable limit cycle is born in the bifurcation and will typically be the boundary of the basin of attraction of the spiral. The super- and sub-critical Hopf bifurcations are depicted in Fig. (3.3).

3.3.4 The Bogdanov-Takens Bifurcation

In a saddle-node bifurcation of a two-dimensional system, the determinant of the Jacobian matrix is zero. Suppose, that a two-dimensional system has a saddle-node bifurcation in one bifurcation parameter and that the variation of a second parameter in a range does not pass a cusp bifurcation. It is possible to obtain a situation where both the trace and the determinant of the Jacobian matrix is zero and where variation of the second parameter causes both eigenvalues to pass the imaginary axis and become positive. This co-dimension two bifurcation is called the *Bogdanov-Takens bifurcation* and can be interpreted as a collision of

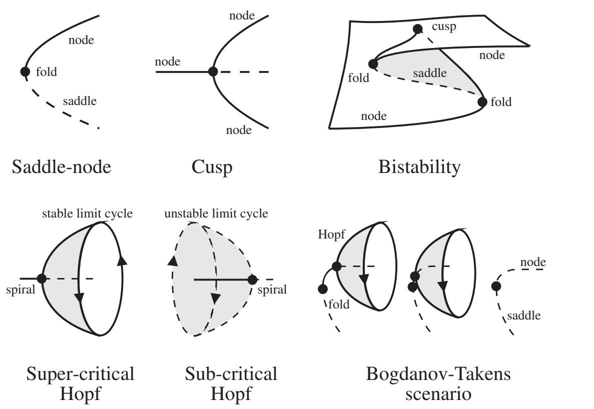

Fig. 3.3: Graphic catalogue of steady state bifurcations. The saddle-node and the cusp bifurcations are depicted in one-dimensional bifurcation diagrams whereas the emergence of bistability is depicted in a three dimensional representation of a two-dimensional bifurcation diagram. The Hopf bifurcations are drawn in a three dimensional representation of a one-dimensional bifurcation diagram to illustrate the birth of the limit cycle in the phase plane. The Bogdanov-Taken scenario illustrates the destruction of a Hopf bifurcation through three one-dimensional bifurcation diagrams at three different values of a second bifurcation parameter. The black dots indicate the location of bifurcation points.

a saddle-node and a Hopf bifurcation, which destroys the Hopf bifurcation. On the other hand, the Bogdanov-Takens bifurcation can be viewed as the birth of a Hopf bifurcation from a saddle-node bifurcation. The destruction (or birth) of a super-critical Hopf bifurcation through a Bogdanov-Takens bifurcation is depicted schematically in Fig. (3.3).

3.4 Bifurcations of Limit Cycles

Whereas the linear stability of steady states change when the eigenvalues of the Jacobian matrix passes the imaginary axis of the complex plane the stability of limit cycles is associated the stability of the fixed point of the Poincaré map. An bifurcation of a periodic solution occur when the fixed point of the Poincaré map changes stability. This corresponds to one or more of the Floquet multipliers leaving the unit circle of the complex plane.

3.4.1 The Saddle-node Bifurcation

The saddle-node bifurcation of a limit cycle occurs when a single eigenvalue of the monodromy matrix passes $+1$ from inside the complex unit circle or vice versa. Similar to with the saddle-node bifurcation of a steady state, the saddle-node bifurcation usually generates a pair of periodic solutions. Typically, one of the limit cycles is stable whereas the other is unstable. The saddle-node bifurcation or fold of periodic solutions is frequently observed together with a sub-critical Hopf bifurcation where an unstable limit cycle collides with a stable spiral causing the spiral to become unstable and destroying the limit cycle. The typical partnership between a saddle-node bifurcation of periodic solutions and a sub-critical Hopf bifurcation is depicted in Fig. (3.4). Usually, a stable steady state coexists with a stable limit cycle. The latter is generated at a saddle-node bifurcation of periodic solutions together with an unstable limit cycle that separates the basins of attraction of the two stable attractors. This has been coined *hard excitation* as the flow changes to a high amplitude limit cycle from a stable steady state upon a small change in a bifurcation parameter.

The saddle-node bifurcation may also generate multiple coexisting limit cycles similar to the multiple steady states generated through a cusp bifurcation. Coexistence of two stable periodic solutions has been termed *birhythmicity* as the systems have two possible stable attractors with different periods of oscillation.

3.4.2 The Period Doubling Bifurcation

When a single eigenvalue of the monodromy matrix passes through -1 the system undergoes a *period doubling bifurcation*. In a period doubling bifurcation, a limit cycle solution reverses its stability and a new limit cycle appears in its immediate neighborhood. The new limit cycle has a period that is twice the period of the original limit cycle as it has to traverse the Poincaré section before returning to the point in the section where it originated. This is illustrated in Fig. (3.4). The first maxima in a variable on a limit cycle generated through a period doubling bifurcation is typically slightly higher than the maxima of the original limit cycle. The second maxima is slightly less, whereas the third maxima has the same value as the first. The limit cycle is hence said to be of period two. The differences in maxima gives the period doubling bifurcation its characteristic portrait when drawing the bifurcation diagram using local maxima as depicted in Fig. (3.4). The period two limit cycle may undergo another period doubling and a period four limit cycle is generated as the period two limit cycle looses its stability. The generation of subsequent period 8,16,32, etc. limit cycles is the well-known period doubling route to chaos. Traditionally, the bifurcation diagram of a period doubling sequence contains the local maxima of the bifurcation parameter. as drawn in Fig. (3.4) together with the two-dimensional phase plane portrait of a stable period two limit cycle and the unstable period one limit cycle.

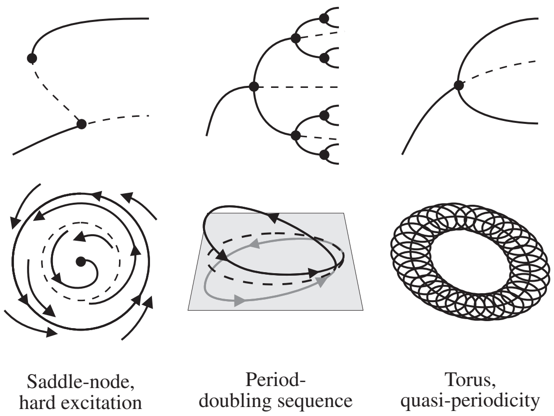

Fig. 3.4: Common bifurcation diagrams and phase plane portraits of limit cycles. The saddle-node bifurcation is illustrated along with its common partner, the sub-critical Hopf bifurcation. The period doubling sequence is drawn traditionally by plotting all local maxima in the bifurcation variable during a period. The phase plane portrait contains the unstable period one (broken line) and the stable period two (full line). The gray line indicates that the solution is below the plane of the period one limit cycle. The torus bifurcation generates a low amplitude limit cycle within a higher amplitude limit cycle.

3.4.3 The Torus Bifurcation

A torus emerges as the fixed point of the Poincaré section becomes unstable with a pair of complex conjugated eigenvalues leaving the unit circle. The stable fixed point is replaced by a stable limit cycle in the Poincaré section which initially has a negligible amplitude that increases when the distance to the bifurcation point increases. Due to the resemblance with the Hopf bifurcation, the torus bifurcation has also been termed the *secondary Hopf bifurcation.* A torus bifurcation may, as the Hopf bifurcation, be either super- or sub-critical and the generated torus may be either periodic or quasi-periodic if a single trajectory eventually fill the entire surface of the torus. The bifurcation diagram of super-critical torus bifurcation is depicted in Fig. (3.4) where the global maxima and minima of a bifurcation variable in the Poincaré intersection is used to outline the location of the torus. A typical phase plane portrait is also presented.

3.4.4 The Homoclinic Bifurcation

Whereas the previously discussed bifurcations have been associated with eigenvalues of linearized systems in the neighborhood of steady states or fixed points it is possible to observe *global bifurcations* that cannot be revealed by an examination of local properties. One such is the *homoclinic bifurcation* which, for example, can result in the appearance of a stable limit cycle from a saddle. Before the homoclinic bifurcation, the unstable manifold of the saddle forms *heteroclinic connections* to nearby steady states. When the bifurcation parameter is in the bifurcation point the heteroclinic connection is replaced by a homoclinic connection such that the unstable manifold is also a stable manifold of the steady state. The homoclinic connection is a closed trajectory in phase space and the *homoclinic orbit* is thus a closed trajectory. However, motion along the homoclinic connection will never be able to pass the saddle, so the homoclinic orbit has an infinite period. The homoclinic bifurcation is typically found in the neighborhood of saddle-node bifurcations and a sub-critical Hopf bifurcation. In fact, a homoclinic bifurcation is guaranteed in the neighborhood of a Bogdanov-Takens bifurcation (Thompson & Stewart, 1986). This fact is not evident from Fig. (3.3) which is only to illustrate the destruction of the Hopf bifurcation.

CHAPTER 4

Cooperative Binding and Allosteric Regulation

Cooperative binding and *allosteric regulation* are two very central concepts in the theory of regulation of biological systems. The term cooperative binding is assigned to biochemical reactions where the binding of one molecule affects the binding of subsequent molecules whereas allosteric regulation, in its original definition, is the process where the activity of an enzyme is mediated by an effector with a structure different from the structure of substrates and products of the reaction catalyzed by the enzyme (Monod *et al.*, 1963). The two distinct phenomena have been entangled and the interaction between binding sites, whether they involve *isosteric* or *allosteric* molecules, is in general referred to as *allostery* (see e.g. Creighton, 1993).

4.1 Allosteric Regulation

The concept of allosteric regulation was introduced as a plausible mechanism for regulation of biological activity by effectors that do not interact with the substrates or products of the reaction (Monod *et al.*, 1963). An allosteric effector binds to a site distinct from the active site and causes an *allosteric transition* in the enzyme. The most simple example of allosteric regulation is provided by the binding of a ligand L to a Michaelis-Menten enzyme following the reaction scheme illustrated below.

$$\begin{array}{ccccc} S+E+L & \underset{k_{sb}}{\overset{k_{sf}}{\rightleftharpoons}} & C_1+L & \xrightarrow{k_c} & E+P+L \\ k_{lf}\downarrow\uparrow k_{lb} & & k'_{lf}\downarrow\uparrow k'_{lb} & & \\ S+EL & \underset{k'_{sb}}{\overset{k'_{sf}}{\rightleftharpoons}} & C_2 & \xrightarrow{k'_c} & EL+P \end{array}$$

The substrate S can combine with either the free enzyme E or with the enzyme-ligand complex EL, and produce either an enzyme-substrate complex C_1, or an enzyme-substrate-ligand complex C_2. The complexes C_1 and C_2 then dissociate irreversibly into product and free enzyme, or enzyme-ligand complex. When the ligand binds to the effector site the enzyme may undergo a structural change that alters the active site. The allosteric transition may typically involve e.g. the movement of polypeptide chains which is detectable using e.g. X-ray or NMR methods. The reaction scheme also applies to biochemical reactions that do not involve an allosteric transition, such as competitive inhibition, which takes place in the active site. The cases where the ligand binding do introduce an allosteric transition includes non-competitive inhibition and activation. Non-competitive inhibition occurs when the catalytic constant k'_c of the enzyme-substrate-ligand complex is lower than the catalytic constant k_c for the enzyme-substrate complex. Activation occurs if $k'_c > k_c$ but may also be mediated indirectly by the removal of a bounded inhibitor.

In Appendix A, it is shown that the reaction rate of a Michaelis-Menten enzyme subject to binding of a ligand is given by Eq. (4.1) if appropriate conditions are met (see Appendix A).

$$v = \frac{k_c e^0 \left(1 + \frac{k'_c}{k_c}\frac{[L]}{K'_l}\right)[S]}{K_m\left(1 + \frac{[L]}{K_l}\right) + [S]\left(1 + \frac{[L]}{K'_l}\right)} \tag{4.1}$$

In Eq. (4.1) the total enzyme concentration is denoted by e^0, K_m denotes the Michaelis-Menten constant when no ligand is present, and K_l and K'_l are the dissociation constants of ligand from, respectively, the enzyme-substrate complex E and enzyme-substrate-ligand complex C_2. The rate Eq. (4.1) is of first order in both substrate and ligand, and the rate equation will be hyperbolic obeying an appearent Michaelis-Menten rate law.

4.2 Cooperative Binding

The most simple biochemical example of cooperative binding is provided by an enzyme E composed of two identical monomeric subunits, each having one active site for substrate S and no other binding sites. The binding of substrate to the first active site affects the binding of substrate to the second active site which is reflected in the differences in the catalytic efficiency. Consider the reaction scheme

$$\begin{aligned} S + E &\underset{k_{b1}}{\overset{k_{f1}}{\rightleftarrows}} C_1 \overset{k_{c1}}{\rightarrow} P + E \\ S + C_1 &\underset{k_{b2}}{\overset{k_{f2}}{\rightleftarrows}} C_2 \overset{k_{c2}}{\rightarrow} P + C_1 \end{aligned} \tag{4.2}$$

where C_1, C_2 denotes enzyme-substrate complexes with, respectively, one and two substrate molecules bound. P is the product of the irreversible reaction. The mass action kinetic equations describing the evolution of each species are

$$\begin{aligned} \frac{d}{dt}[S] &= -k_{f1}[S][E] + k_{b1}[C_1] - k_{f2}[S][C_1] + k_{b2}[C_2], \\ \frac{d}{dt}[E] &= -k_{f1}[S][E] + (k_{b1} + k_{c1})[C_1], \\ \frac{d}{dt}[C_1] &= k_{f1}[S][E] - (k_{b1} + k_{c1})[C_1] - k_{f2}[S][C_1] + (k_{b2} + k_{c2})[C_2], \\ \frac{d}{dt}[C_2] &= k_{f2}[S][C_1] - (k_{b2} + k_{c2})[C_2], \\ \frac{d}{dt}[P] &= k_{c1}[C_1] + k_{c2}[C_2], \end{aligned} \tag{4.3}$$

with appropriate initial conditions

$$[S](t^0) = [S]^0, \quad [E](t^0) = e^0, \quad [C_1](t^0) = 0, \quad [C_2](t^0) = 0, \quad [P](t^0) = 0. \tag{4.4}$$

It is immediately observed that total enzyme and total substrate is conserved

$$e^0 = [E] + [C_1] + [C_2], \qquad [S]^0 = [S] + [C_1] + [C_2] + [P], \tag{4.5}$$

and only three of the rates of Eqs. (4.3) needs to be considered. The reaction system can be normalized by defining two distinct Michaelis-Menten constants

$$K_{m1} = \frac{k_{b1} + k_{c1}}{k_{f1}}, \qquad K_{m2} = \frac{k_{b2} + k_{c2}}{k_{f2}}, \tag{4.6}$$

and the dimensionless variables

$$\alpha = \frac{[S]}{K_{m2}}, \quad \gamma_1 = \frac{[C_1]}{e^0}, \quad \gamma_2 = \frac{[C_2]}{e^0}, \quad \tau = k_{f2} e^0 t. \tag{4.7}$$

The dimensionless rate equations

$$\begin{aligned} \frac{d\alpha}{d\tau} &= \rho(\gamma_1 - q\alpha(1 - \gamma_1 - \gamma_2)) + \gamma_2 - \alpha\gamma_1 - \sigma(\delta\gamma_1 + \gamma_2) \\ \varepsilon\frac{d\gamma_1}{d\tau} &= q\alpha(1 - \gamma_1 - \gamma_2) - \gamma_1 + \gamma_2 - \alpha\gamma_1 \\ \varepsilon\frac{d\gamma_2}{d\tau} &= \alpha\gamma_1 - \gamma_2 \end{aligned} \tag{4.8}$$

emerge upon normalization of Eq. (4.3) along with the dimensionless parameters

$$\varepsilon = \frac{e^0}{K_{m2}}, \quad \rho = \frac{k_{b2} + k_{c2}}{k_{b1} + k_{c1}}, \quad q = \frac{K_{m2}}{K_{m1}}, \quad \delta = \frac{k_{c1}}{k_{c2}}, \quad \sigma = \frac{k_{c2}}{k_{b2} + k_{c2}}. \tag{4.9}$$

Eq. (4.8) can readily be shown to meet the conditions for Tihonov's first theorem, when ε is vanishing and the quasi-steady state values γ_1 and γ_2 are obtained by solving the algebraic equations

$$\begin{gathered} \alpha(1 - \gamma_1 - \gamma_2) - \gamma_1 = 0, \qquad \alpha\gamma_1 - \gamma_2 = 0 \Rightarrow \\ \gamma_1 = \frac{\gamma_2}{\alpha}, \qquad \gamma_2 = \frac{q\alpha^2}{1 + q\alpha(1 + \alpha)}. \end{gathered} \tag{4.10}$$

Inserting the quasi-steady state values from Eq. (4.10) into Eq. (4.8), one obtains the rate equation

$$\frac{d\alpha}{d\tau} = -q\sigma\frac{\delta\alpha + \alpha^2}{1 + q\alpha(1 + \alpha)}, \tag{4.11}$$

which is an appropiatte description of the system when $\varepsilon \to 0$. Eq. (4.11) can be further simplified when assuming that $\delta = 0$ and $\alpha \gg 1$. With these assumptions Eq. (4.11) reads

$$\frac{d\alpha}{d\tau} = \frac{-q\sigma\alpha^2}{1 + q\alpha^2}, \tag{4.12}$$

which in dimensional form is

$$\frac{v}{v_{max}} = \frac{[S]^2}{K + [S]^2}, \tag{4.13}$$

where v and v_{max} denote, respectively, the rate of reaction and the maximum velocity of the enzyme. The constant K is defined by $K = K_{m1}K_{m2}$.

Eq. (4.11) is the *Hill rate law* with a *Hill coefficient* of two. The general Hill rate law is written

$$\frac{v}{v_{max}} = \frac{[S]^{n_h}}{K + [S]^{n_h}}, \tag{4.14}$$

where, n_h denotes the Hill coefficient. The rate law corresponds either to the rate law of a reaction where n_h substrate molecules simultaneously bind to the enzyme or to a reaction similar to the reaction leading to the rate equation in Eq. (4.11) with appropriate assumptions about the parameters. It is the standard to interpret experimentally obtained biochemical data through a *Hill plot*. In a Hill plot, experimentally measured rates of reactions, usually in the range $0.1v_{max}$ to $0.9v_{max}$ (Neet, 1995), are fitted to the linear expression

$$\ln\left(\frac{v}{v_{max} - v}\right) = n_h \ln[S] - \ln K, \tag{4.15}$$

and the Hill coefficient n_h is determined by estimating the slope of the fitted curve. For a Michaelis-Menten enzyme the Hill coefficient equals one. A slope less than one is referred to a *negative cooperativity* as the binding of one substrate molecule inhibits the binding of subsequent substrate molecules. When the Hill constant is higher than unity the binding of the first substrate molecule eases the binding of the following which is called *positive cooperativity*. The Hill coefficient is the most common means of evaluating and comparing cooperativity and offers the most immediate, conceptual meaning to practicing biochemists (Neet, 1995). Measuring the Hill coefficient allows the practicing biochemist, when the Hill coefficient is higher than one, to conclude that the value of n_h is less than the actual number of subunits and provides, if the number of subunits is known in advance, a measure of the strength of interactions between subunits. In the case of negative cooperativity the Hill coefficient is not related to the number of subunits in the enzyme (Neet, 1995).

Although the Hill coefficient was introduced as an emperic relation between a substrate and the rate of reaction, the Hill rate law has found many other application in theoretical studies of biological regulation (see e.g. Murray, 1993; Hunding & Engelhart, 1995; Goldbeter, 1996). In some models, the Hill rate law is used although the system is not of molecular origin (see e.g. Mackey, 1978) and a phenomena of sigmodal dependency is sometimes refered to as cooperativity although the underlying kinetic scheme does not involve cooperativity between subunits.

4.3 Allosteric Enzymes

Measuring the Hill coefficient does not tell a lot about the mechanisms of an enzyme reaction. The assumptions $k_{c1} = 0$ and $[S] >> K_{m1}$ which may link the second-order Hill rate law to a molecular mechanism are unrealistic, and so is a simultaneous binding of multiple substrates. A relatively simple molecular model that may explain the appearance of sigmoidal dependencies was presented by Monod, Wyman and Changeux in the mid-sixties (Monod *et al.*, 1965). The model was followed by a more detailed model a year later (Koshland *et al.*, 1966) and finally Eigen presented a comprehensive model (Eigen, 1968). These models are today accepted as accurate descriptions of enzymes composed of multiple interacting subunits. The proposed molecular mechanisms has been accepted to the extent that the name *allosteric* is typically used as a reference to oligomeric enzymes, i.e. enzymes containing multiple identical subunits (Monod *et al.*, 1963), although the activity of monomeric enzymes may also be regulated through allosteric effects. Moreover, the subunits of oligomeric enzymes can be independent(see e.g. Smolen, 1995) and an oligomeric enzyme is not necessarily allosteric. To avoid confusion, enzymes containing multiple identical subunits are here said to be oligomeric whereas enzymes regulated through binding of a molecule at a site on the enzyme that is distinct from the active site are called allosteric.

4.4 Oligomeric Allosteric Enzymes

The model suggested by Monod *et al.*, is the most frequently applied, probably due to the relatively simple formulation of the theory. In the MWC model, an enzyme is composed of n subunits which usually are identical. The spatial arrangement of atoms in a subunits allows the enzyme to exist in either a T-form (tensed) or an R-form (relaxed) which have different catalytic activities. When the subunits of both forms are assumed identical the overall structure of the enzyme will always contain at least one symmetry axis. The allosteric transition from the T to the R-form, or vice versa, is a concerted "all-or-none" structural change where all subunits simultaneously change shape resulting in a changed structure of the active site and hence an altered catalytic activity. In the more detailed model proposed by Koshland (Koshland *et al.*, 1966) the allosteric transition is not conserted and the binding of an effector only affects neighbooring subunits. This model was complemented by Eigen (Eigen, 1968) who consider all statistically possible combinations of of binding to tensed and relaxed subunits. The latter is undoubtfully the most comphrensive, but also the most complex and impracticable, model of allosteric oligomeric enzymes.

The derivation of the MWC model (Monod *et al.*, 1965) is treated in detail elsewhere (see e.g. Gutfreund, 1972; Kurganov, 1981; Neet, 1995) and it can be shown, by truncation of the mass action kinetic rate equations through the QSSA, that the rate of reaction catalyzed by an enzyme obeying MWC theory can be written in the form

$$\frac{v}{v_{max}} = \frac{Lc\alpha(1+c\alpha)^{n-1} + \alpha(1+\alpha)^{n-1}}{L(1+c\alpha)^n + (1+\alpha)^n} \tag{4.16}$$

where α is the substrate concentration divided by the dissociation or Michaelis-Menten constant of the $R - form$, c is the ratio of affinity for substrate of the T-form and the R-form. L denotes the equilibrium constant of the allosteric transition. When assuming that the T-form cannot bind substrate, one can neglect the terms involving c and the rate law reads

$$\frac{v}{v_{max}} = \frac{\alpha(1+\alpha)^{n-1}}{L + (1+\alpha)^n} \tag{4.17}$$

According to the MWC-theory, the effect of allosteric effectors is through a favoring of either the T-form (inhibition) or the R-form (activation). This is taken into account by replacing the allosteric constant L in Eq. (4.16) by an apparent allosteric constant L' defined by

$$L' = L\frac{(1+\gamma)^n}{(1+\beta)^n} \tag{4.18}$$

where γ represents a dimensionless concentration of an allosteric inhibitor that binds to the T-form, and β represents a dimensionless concentration of an allosteric activator that binds to the R-form. The concentrations of γ and β are made dimensionless by division with the dissociation constants for, respectively, inhibitor from the T-form and activator from the R-form.

The rate of reaction will therefore, in the absence of an allosteric inhibitor, be given by

$$\frac{v}{v_{max}} = \frac{\alpha(1+\alpha)^{n-1}(1+\beta)^n}{L+(1+\alpha)^n(1+\beta)^n} \tag{4.19}$$

in the case of R-exclusive binding. This expression is derived in details for an product activated allosteric enzyme in Appendix B. When either the allosteric constant L or the apparent allosteric constant $L' = L/(1+\beta)^n$ is negligible, the enzyme operates as a Michaelis-Menten enzyme obeying the rate law

$$\frac{v}{v_{max}} = \frac{\alpha}{1+\alpha}. \tag{4.20}$$

This shows that the rate function of an MWC enzyme is hyperbolic when L is low or when the concentration of activator is high. When the concentration of substrate is high such that $\alpha \gg 1$ the reaction rate in Eq. (4.19) is equivalent to a Hill type expression

$$\frac{v}{v_{max}} = \frac{\alpha^n(1+\beta)^n}{L+\alpha^n(1+\beta)^n} = \frac{\alpha^n}{K+\alpha^n}, \qquad K = \frac{L}{(1+\beta)^n}, \tag{4.21}$$

showing that an enzyme obeying MWC theory may give straight lines in a Hill plot having slopes higher than unity.

CHAPTER 5

Oscillatory Oligomeric Enzymes

A simple biochemical reaction scheme that allows for the emergence of sustained oscillatory behavior is provided by an open reaction catalyzed by an allosteric oligomeric enzyme, where the reaction product P acts as an allosteric activator. In this scheme, the substrate, denoted by S, flows into the system at a constant rate v_{in} whereas the rate of product removal is proportional to an apparent first order rate constant k_{out}. The overall reaction scheme is illustrated schematically by

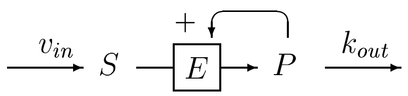

where E symbolizes the oligomeric allosteric enzyme. For simplicity, it is assumed that the allosteric enzyme obeys the R-exclusive MWC-theory (Monod *et al.*, 1965) and that the reaction is effectively mono-substrate and irreversible. With these assumptions, the chemical reactions of a dimeric allosteric enzyme will be limited to those shown in Fig. (5.1). When the reactions obey the law of mass action, the binding of substrate to the active site and of the product to the allosteric site is associated with the second-order rate constants k_{sf} and k_{pf}. The dissociation reactions of the enzyme-substrate complex into free enzyme and either substrate or product, are associated, respectively, with the first-order rate constants k_{sb} and k_c, whereas the rate of product dissociation from the allosteric site is proportional to the first-order constant k_{pb}. The allosteric transition is associated with the first-order rate constant k_{tb} for the conformational change taking place at the transition from active R-form to inactive state T-form and k_{tf} for reversed transition. The ratio of k_{tb} to k_{tf} defines the allosteric constant L.

5.1 Reduced Mathematical Description

When the law of mass action is applied to the elementary reactions illustrated schematically in Fig. (5.1) a system of 11 independent AODE's emerges. The full mathematical description can be truncated to appropriately low dimensional models describing different kinetic cases using the extended method discussed in Chapter 3. The derivation of low dimensional approximations is discussed in detail in Appendix B. The reaction system in Fig. (5.1) may be considered as being composed of three sub-reactions; an allosteric transition, a Michaelis-

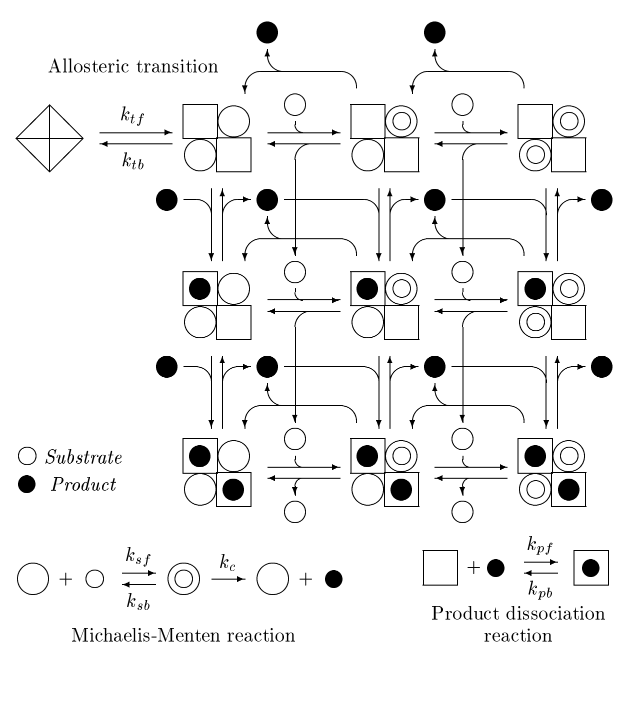

Fig. 5.1: Elementary Reactions of a dimeric product activated allosteric enzyme described by the R-exclusive concerted MWC-model. The enzyme exists in an inactive T-conformation (diamond) and in an active R-conformation. The latter contains two active sites (circles) and two allosteric sites (squares). The elementary reactions comprise three sub-reactions and the rate constants in the system are defined in the labeled illustrations of the sub-reactions. The sub-reactions are identified as a Michaelis-Menten reaction, a product dissociation reaction and an allosteric transition. The exclusive binding of product to the R-conformation comprises an auto-catalytic feedback loop which, when the system is open to the surroundings, allows for the emergence of sustained oscillatory behavior.

Menten reaction and a reversible product dissociation reaction. In Appendix B it is shown that the three sub-reactions are associated with the parameters

$$\varepsilon = \frac{k_{out}}{k_{tb}}, \qquad \varepsilon_1 = \frac{k_{out}}{k_{sb} + k_c}, \qquad \varepsilon_2 = \frac{k_{out}}{k_{pb}}, \tag{5.1}$$

for, respectively, the allosteric transition, the Michaelis-Menten reaction and the product dissociation reaction. When the total enzyme concentration, measured through the parameter $\epsilon = e^0/K_m$, where e^0 is the total enzyme concentration and K_m is the Michaelis-Menten constant, and $\varepsilon, \varepsilon_1, \varepsilon_2$ approach zero, it can be shown that the product activated allosteric reaction can be described by the two rate equations

$$\begin{aligned} \frac{d\alpha}{d\tau} &= \nu - \frac{2\sigma\alpha(\alpha+1)(\beta+1)^2}{L + (\alpha+1)^2(\beta+1)^2}, \\ \frac{d\beta}{d\tau} &= \frac{2q\sigma\alpha(\alpha+1)(\beta+1)^2}{L + (\alpha+1)^2(\beta+1)^2} - \beta, \end{aligned} \tag{5.2}$$

where α and β represent the concentrations of substrate and product divided by, respectively, the Michaelis-Menten and the product dissociation constant K_p. The time-scale has been made dimensionless by defining dimensionless time $\tau = tk_{out}$ and the dimensionless parameters ν, σ, q are defined by

$$\nu = \frac{v_{in}}{K_m k_{out}}, \qquad \sigma = \frac{k_c e_0}{K_m k_{out}}, \qquad q = \frac{K_p}{K_m}. \tag{5.3}$$

The system in Eq. (5.2) has been used to study the emergence of sustained oscillatory behavior in the glycolysis (see Goldbeter, 1996, for survey) where the enzyme phosphofructokinase is activated by its own product adenosine diphosphaste (ADP) or the more potent activator adenosine 5'-monophosphate (AMP), and has been shown to obey MWC-theory (Schirmer & Evans, 1990). The existence of sustained periodic behavior has been shown mathematically (Erle *et al.*, 1979), and it has been reported that the system has only one periodic solution for a given set of parameter values (Segel & Goldbeter, 1994). Segel and Goldbeter report that fulfillment of the condition

$$\nu\sqrt{\frac{q\sigma}{L}} << 1 \tag{5.4}$$

ensures the emergence of relaxation type oscillations (Segel & Goldbeter, 1994) in the truncated model in Eq. (5.2). The condition in Eq. (5.4) is however not sufficient as the rate equations in Eqs. (5.2) are based on truncation through the QSSA which is not justified by fulfillment of Eq. (5.4). Eq. (5.2) is an appropriate asymptotic approximation to the full mass action description, if the total enzyme concentration is sufficient low and ε, ε_1 and ε_2 are close to zero. These conditions, which are derived in Appendix B, are not guaranteed to be met *in vivo* and it is therefore of fundamental importance to investigate the dynamic effect of their violation.

5.2 Slow Allosteric Transition

It is well known to the biochemist that allosteric enzymes, and some monomeric enzymes (Cornish-Bowden & Cárdenes, 1987), may show "hysteresis" or "hysteric" behavior. The term "hysteresis" in this context refers to the experimental situation where the enzyme shows a nonlinear time dependent rate of product formation under conditions which normally produce a linear reaction rate. It is thus different from the definition used in nonlinear dynamics where hysteresis is the passage though a saddle-node bifurcation in a bistable system. Hysteric behavior of enzymes can be introduced by a slow allosteric transition where the time-scale of the transition is comparable to the time-scale of measurement and the catalytic event (Kurganov, 1981). In such a case, the rate of reaction is measured experimentally in a "boundary layer", a term taken from fluid dynamics (Murray, 1993), where the different enzyme species are not in a quasi-steady state. Kurganov (Kurganov, 1981) lists 75 allosteric enzymes known to have a slow transition and there is no reason to believe that the list has not expanded since then, as more elaborated experimental techniques have been introduced.

In the following sections the dynamic effect of a slow allosteric transition in an oscillatory allosteric enzyme is investigated. The time-scales for the Michaelis-Menten reaction and the product dissociation reaction, measured by, respectively, ε_1 and ε_2 are considered to be fast, i.e. $\varepsilon_1 \to 0$ and $\varepsilon_2 \to 0$. In that case, the three dimensional model in Eqs. (5.5) is a valid description of the reaction system if the enzyme concentration is sufficiently low as discussed in Appendix B,

$$\begin{aligned}
\frac{d\alpha}{d\tau} &= \nu - \frac{2\sigma\gamma\alpha}{\alpha+1}, \\
\frac{d\beta}{d\tau} &= \frac{2q\sigma\gamma\alpha}{\alpha+1} - \beta, \\
\varepsilon\frac{d\gamma}{d\tau} &= \frac{1}{L} - \gamma\left[\frac{(\alpha+1)^2(\beta+1)^2+L}{L(\alpha+1)^2(\beta+1)^2}\right],
\end{aligned} \tag{5.5}$$

where γ represents the total amount of enzyme in the active R-form divided by the total enzyme concentration e^0. The dynamic effect of a slow product dissociation reaction and a slow Michaelis-Menten reaction is investigated at the end of the chapter where also the effect of a high enzyme concentration will be studied.

5.2.1 Effect of a Slow Transition on Oscillations

When the allosteric transition is slow (i.e. moderate ε) the limit cycle solution predicted by the two-dimensional model, obtained in the limit $\varepsilon \to 0$, is altered. This is shown in Fig. (5.2) for $\nu = 1.0$, $\sigma = 10$, $q = 10$ and $L = 5.0 \cdot 10^6$. In the two-dimensional model, the limit cycle has a well defined location in the α, β phase plane and qualitative information about the periodic solution can be obtained directly by drawing the α and β *nullclines*. The α and β nullclines are defined in the α, β plane as the set α, β for which $d\alpha/d\tau = 0$ and $d\beta/d\tau = 0$ respectively. In Fig. (5.2), the α and β nullclines are drawn with broken lines. The β nullcline is N-shaped starting close to (0,0) with the left branch partly hidden by the heavy line and the right branch located rightmost in Fig. (5.2). The turning points (saddle-node bifurcations) of the β nullcline (marked with circles) indicate the existence of two threshold values in α. Between the two turning points, the β nullcline is repulsive so that phase trajectories close to the β nullcline leads away from it. The intersection of the nullclines is at $\alpha = 46.2$, $\beta = 10.0$ and the steady state solution (i.e. $d\alpha/d\tau = d\beta/d\tau = 0$) is located where the β nullcline is repulsive, indicating that the steady state solution is an unstable saddle. The left and the right branch of the nullclines located on each side of the turning points are attractive, and any trajectory close to one of these tends to get closer to the nullcline when time evolves. The α nullcline goes asymptotically towards the lines $\beta = 0$ and $\alpha = 0$ for low and high levels of β respectively. The α nullcline has no turning points and is always attractive. The α and β nullclines separate the phase space into four regions with different effects on the α, β-phase plane trajectory of the limit cycle. These regions are labeled A, B, C, and D. In region A, α tends to increase and β tends to decrease. In region B both α and β are increasing. In region C α is decreasing whereas β is increasing, and in D both are decreasing. The stable periodic solution (heavy line in Fig. (5.2)) passes all four regions and the behavior of the solution changes as it traverses the nullclines.

Following the limit cycle predicted by the two-dimensional model (heavy line) through the phase plane, one can explore the difference in behavior in the different region of the phase space. Starting in A, where the periodic and the α nullcline intersect (intersection between heavy and the lower broken line in Fig. (5.2)), the attractive left branch of the β nullcline causes the level of β to decrease rapidly and the β nullcline is traversed with only a small further change in β. Thus, the periodic solution has a nearly horizontal transition through region A. In region B, the periodic solution almost coincides with the nearly vertical β nullcline and α increases with only a slight increase in β. When α passes the threshold value at $\alpha = 78.8$, the periodic solution is attracted to the rightmost branch of the β nullcline. This yields a sharp increase in the level of β and the periodic solution traverses the α nullcline as it enters region C. In an ideal relaxation oscillator, the trajectory in region C would be horizontal and the α nullcline would influence this region very little. With the present choice of parameter values, the periodic solution is forced downward in α bringing the level of β down and making the horizontal transition less sharp than in an ideal relaxation oscillator. In region D, an ideal relaxation oscillator would follow the β nullcline downward until the turning point of the β nullcline where a horizontal transition to the left branch of the β nullcline would occur. Here, the α, β-phase plane trajectory of the limit cycle traverses the rightmost part of the β nullcline and the periodic solution enters region D, and it is observed that the periodic solution is located below the β nullcline. It seems possible that the periodic solution is forced downwards from the β nullcline due to attraction to the α nullcline. The decrease in β in region D is rather sharp and coincides with the behavior of a relaxation oscillator. When β has decreased sufficiently, the phase plane trajectory closes the limit cycle as the heavy line passes the α nullcline and enters region A.

The regions A, B, C and D in the phase plane plot in Fig. (5.2) correspond to different catalytic modes of the enzyme. In region A the reaction product (proportional to β) is rapidly removed without any significant uptake of substrate

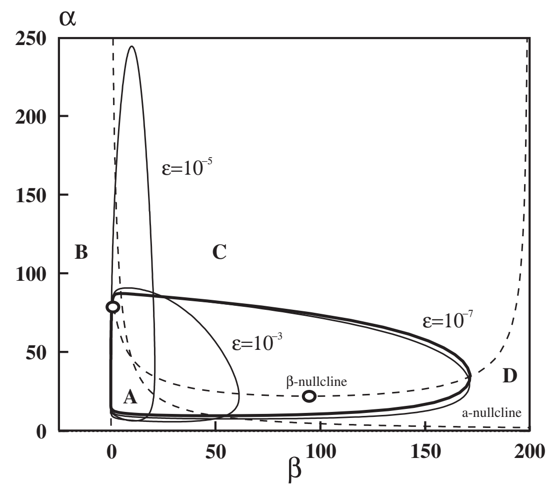

Fig. 5.2: Trajectories in the α, β phase plane for various time-scales of the allosteric transition when $\nu = 1.0$, $\sigma = 10$, $q = 10$ and $L = 5.0 \cdot 10^6$. The heavy line outlines the phase plane trajectory obtained from the two-dimensional model Eq. (5.2). When the allosteric transition is fast ($\varepsilon < 10^{-7}$) the phase trajectory of the three dimensional model coincides with that of the two-dimensional model. When the value of ε is lowered to 10^{-5} the amplitude in β is lowered but the amplitude in α is virtually unchanged. Below $\varepsilon = 10^{-5}$ the amplitude in α increases dramatically and the amplitude in β continues to decrease toward the steady state located at the intersection of the nullclines (broken lines)

(proportional to α). In region B, the system is depleted of product and the catalytic activity is correspondingly low as most of the enzyme is in the inactive conformation. In this region, free substrate accumulates and the catalytic activity increases slowly. At the turning point, the enzyme possesses a catalytic activity to increase the level of α and the auto-catalytic feedback loop is triggered. The result is a sharp increase in free product and entry into region C. The high level of free substrate that builds up in region B is slowly depleted in region C where the catalytic activity of the enzyme is at its highest. The depletion of free substrate eventually causes a passage into region D where free product is removed. In region D, the catalytic activity is still high enough to cause a further decrease in the level of free substrate.

When the allosteric transition is slow (i.e. non-zero ε) the location of the periodic solution in the α, β phase may indeed be very different from what is predicted by the two-dimensional model. When $\varepsilon = 10^{-7}$ the location of the periodic solution is shifted slightly toward the α nullcline but the solution is still very close to that of the two-dimensional model (heavy line in Fig. (5.2)). Slowing down the allosteric transition to $\varepsilon = 10^{-5}$, the amplitude in β has decreased significantly to about one third of the amplitude observed when $\varepsilon = 10^{-7}$. This indicates that the horizontal transition toward the right branch of the β nullcline in region C is being inhibited by the increase of ε. At the same time the amplitude in α is slightly increased, as its maximum value increases and its minimum value decreases. The same behavior is observed when the allosteric transition is made still slower, $\varepsilon = 10^{-3}$. The amplitude increases for α and decreases for β, and a quite dramatic 2.5 fold increase in the maximum value of α is observed. This effect is probably due to an increased threshold value in α as discussed below.

The bifurcation diagram in Fig. (5.3) with ε as a bifurcation supports the conclusions made from the phase plane analysis. The diagram presented in Fig. (5.3) contains the maximum values of the three variables α, β and γ during oscillations together with the period of the stable periodic solution (heavy lines). For clarity, the variables have been rescaled to unity so that the left hand scale corresponds to $\alpha/10^3$, $\beta/200$ and γ. The period is indicated on the right hand scale in units $\tau/10^3$. The broken line indicates that the periodic solution is unstable. The steady state values of α, β and γ, which are independent of ε, are indicated by the horizontal lines. The steady state value is drawn with full lines when stable and with broken lines when unstable.

From the bifurcation diagram, it is confirmed that the oscillation does not change significantly when ε is below 10^{-7}. This value of ε corresponds to the validity limit of the two-dimensional model in Eq. (5.2). When ε raises above 10^{-7}, it is observed, as in Fig. (5.2), that the maximum value of β decreases. The decrease in β is closely correlated with a lowered amplitude of total active enzyme

γ, indicating that a slow allosteric transition favors the inactive conformation of the enzyme. When the allosteric transition is fast, more than 90% of the enzyme is in the active conformation when the catalytic activity is at its highest. When allosteric transition is slowed down, more of the enzyme rests in the inactive state. The amplitude in β decreases correspondingly as the maximum rate of product formation decreases. This behavior corresponds to the inhibition of the horizontal transition in region C of Fig. (5.2).

The decrease in β and γ starts at about $\varepsilon = 10^{-7}$ and continues to about $\varepsilon = 10^{-4}$ where the decrease levels off. During this decrease, the period of oscillation changes from about 90 to about 200 (in dimensionless units τ). The change in period, due to the lowered amplitudes of β and γ, is small compared to the change in period observed above $\varepsilon = 10^{-4}$. The maximum values of β and γ are very low at $\varepsilon = 10^{-4}$ and the oscillation evolves closely around the unstable steady state as shown in Fig. (5.2). The repulsive effect of the β nullcline makes a further decrease in the maximum values of β and γ impossible. Instead, a dramatic increase in α is observed. As ε is increased above 10^{-4}, more and more free substrate (increasing α) is required to achieve the catalytic activity needed to switch from region B to C in Fig. (5.2). Due to the constant inflow of substrate, it therefore takes longer and longer before the shift from the mode of substrate uptake in region B to the product producing mode in region C occurs. In this way, the period increases from a value of about 200 to a maximum value 3500

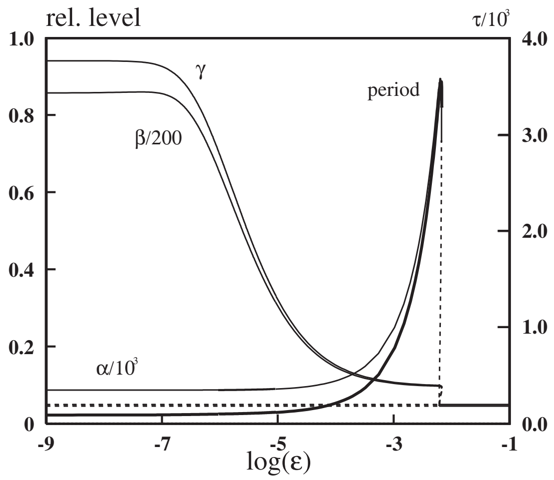

Fig. 5.3: Bifurcation diagram with ε as bifurcation parameter. Parameter values are given in Fig. (5.2). Thin and heavy lines indicate the maximum value of, respectively, α and β during oscillations and the steady state values. Broken lines indicate that the solution is unstable. As ε is increased above 10^{-7} the maximum value of β during oscillations decreases. The maximum value of α increases dramatically when $\varepsilon > 10^{-3}$ whereas the decrease in the maximum value in β levels out. At $\varepsilon = 6.8 \cdot 10^{-3}$ the periodic solution looses its stability before through a saddle-node bifurcation before it is destroyed through a sub-critical Hopf bifurcation at $\varepsilon = 9.4 \cdot 10^{-3}$. The presence of a sub-critical Hopf bifurcation implies that a stable limit cycle and a stable steady state coexists. The range in ε where this occur is however insignificant.

and the maximum value of α increases from 110 to about 900 as ε changes from 10^{-4} to $6.4 \cdot 10^{-3}$. When ε exceeds $6.4 \cdot 10^{-3}$, the period and the maximum value of α start to decrease until the periodic solution looses its stability through a fold at $\varepsilon = 6.7 \cdot 10^{-3}$. The periodic solution is now destroyed through a sub-critical Hopf bifurcation at $\varepsilon = 6.2 \cdot 10^{-3}$ where the steady state solution becomes stable.

The value of ε has no effect on the location of the steady state (horizontal lines in Fig. (5.3)), but it has indeed an effect on the shape and stability of the periodic solution and the stability of the steady state. The behavior found in Fig. (5.3) was not unexpected. The high value of the allosteric constant ($L = 5.0 \cdot 10^6$) strongly favors the inactive conformation and it seems reasonable that a slow allosteric transition (i.e. a relative large value of ε) will make it more difficult to attain the high amplitude oscillations seen when the allosteric transition is fast ($\varepsilon < 10^{-7}$). Recall that for small values of ε more than 90% of the enzyme is in the active conformation at its highest. The reason for the strong correlation between the amplitudes in β and γ is obvious from the fact that β is the auto-catalytic agent, and the feedback loop is weakened through a slowed allosteric transition. The change in both β and γ levels off as the periodic solution is forced closer and closer to the unstable steady state solution. At about $\varepsilon = 10^{-4}$ there is a change, although smooth, in the effect of a slow allosteric transition, from a decrease in the β and γ amplitudes to a dramatic increase in the amplitude of α. This change arises because the enzyme is difficult to activate and therefore very high levels of free substrate accumulate before the amount of active enzyme, measured by γ, reaches a level where the conversion rate is greater than the inflow rate.

5.2.2 Slow Transition-induced Instability

In the previous section, it was shown that a slow allosteric transition inhibits the ability of the system to oscillate as the amount of active enzyme, measured by γ, does not reach the same high levels as when the allosteric transition is fast (see Fig. (5.3)). The auto-catalytic feedback loop is weakened as the allosteric transition is slowed down (increasing ε) and ultimately, the steady state solution is stabilized through a sub-critical Hopf bifurcation.

A slow allosteric transition, i.e. non-zero value of ε, may have an unexpected effect in regions where the two-dimensional model in Eqs. (5.2) predict a stable steady state solution. This is shown in Fig. (5.4) where the time dependent behavior of α and β in the three-dimensional model Eq. (5.5) is shown. The flow parameter $\nu = 7.5$ is chosen in a region where the two-dimensional model does not show sustained oscillations, but tends to a stable steady state solution. The other parameters are as in Fig. (5.2). When the allosteric transition is fast, the three-dimensional model Eqs. (5.5) predict a stable steady state as illustrated for

$\varepsilon = 10^{-8}$ in Fig. (5.4) (heavy lines). Integration, with initial values of the three variables α, β and γ being zero, yields damped oscillations that converge toward a stable steady state. When the allosteric transition is slowed down such that $\varepsilon = 10^{-6}$ the dynamic mode changes. Instead of damped oscillations, one observes sustained oscillations. This indicates that an increased value of ε destabilizes the steady state solution and limit cycle becomes stable.

The instability induced by a slow allosteric transition is investigated further in Fig. (5.5) where a two-dimensional bifurcation diagram in ε, ν parameter space is presented. The parameters are as in Fig. (5.2). In Fig. (5.4) the steady state solution passes through a Hopf bifurcation as ε passes from 10^{-8} to 10^{-6} and the attractor changes from being a steady state to a periodic solution. The location of the Hopf bifurcation in the ε, ν parameter space is traced out in the two-dimensional bifurcation diagram in Fig. (5.5). The Hopf bifurcation curve outlines the boundaries where the periodic solution is created (or destroyed) and the region enclosed by the Hopf bifurcation curve (heavy line) outlines the region of sustained oscillatory behavior. In the region outside the Hopf bifurcation curve the steady state solution is stable. When $\varepsilon = 0$, i.e. the two-dimensional model in Eq. (5.2) is an appropriate description, the system shows sustained oscillatory behavior in a window in ν ranging from 0.10 to 6.06 and the horizontal line marked ν_{2D} marks the latter bifurcation value. When $\varepsilon = 10^{-9}$ the Hopf bifurcation curve is very close to the bifurcation value predicted by the two-dimensional model and coincides, as expected, with ν_{2D} in the limit $\varepsilon \to 0$. It is noted that the bifurcation for $\varepsilon = 10^{-9}$ is slightly higher than ν_{2D}, and the bifurcation value of ν decreases asymptotically toward the limit value at $\varepsilon = 0$. It is not surprising that the

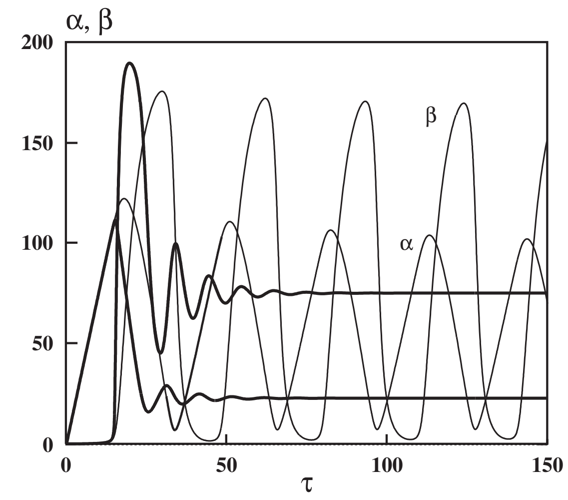

Fig. 5.4: Time-dependent behavior of α and β when the allosteric transition is slow. Parameters are as in Fig. (5.2) except $\nu = 7.5$. When $\varepsilon = 10^{-8}$ (heavy lines), the three-dimensional model Eq. (5.5) predicts a stable steady state. When the allosteric transition rate is slowed down such that $\varepsilon = 10^{-6}$ the three dimensional model predicts that the system evolves toward a stable periodic solution. A finite rate of the allosteric transition may thus change the dynamic behavior from steady state to sustained oscillations and introduce oscillatory behavior where the two-dimensional QSSA model in Eq. (5.2) predicts a steady state.

Hopf bifurcation curve approaches the bifurcation value ν_{2D} observed in the two-dimensional model asymptotically as $\varepsilon \to 0$, as the two-dimensional model Eq. (5.2) is an asymptotic approximation to the three dimensional model Eq. (5.5) (see Appendix B). It is however rather unexpected that the Hopf bifurcation curve approaches ν_{2D} from above. The two-dimensional model thus *underestimates* the maximum bifurcation value of ν when the allosteric transition occurs at a finite but fast time-scale.

When ε is increased above 10^{-9} in Fig. (5.5), the distance between the Hopf bifurcation curve and ν_{2D} increases until the maximum bifurcation value at 8.02 for $\varepsilon = 1.9 \cdot 10^{-6}$ (labeled ν_{max} in Fig. (5.5)). The lower bifurcation value of ν does not change significantly when ε increases, and the slowed allosteric transition may thus increase the width of the oscillatory window in ν by up to 32% as compared to the width predicted by the two-dimensional model. As ε is increased above $1.9 \cdot 10^{-6}$ the oscillatory window in ν contracts, and at $\varepsilon = 2.1 \cdot 10^{-5}$ (marked ε_{crit} in Fig. (5.5)) the bifurcation values in ν coincide in the two models. At values of ε above ε_{crit} the window continues to contract and the width of the oscillatory domain is vanishing as $\varepsilon \to 1$. The limiting value of ε where no oscillations are observed for any value of ν is located out of scale in Fig. (5.5) at $\varepsilon = 0.2$.

Figure (5.5) shows that a slow allosteric transition may have a dual effect on the width of the oscillatory window in ν, whether the value is above or below the critical value ε_{crit} of ε, where the bifurcation values in ν coincide in the two and

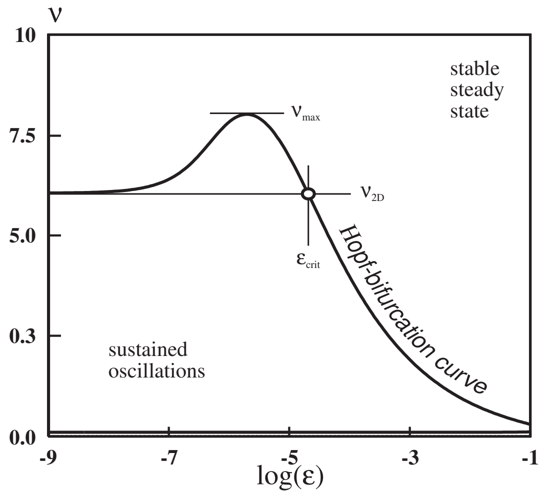

Fig. 5.5: Two-dimensional steady state bifurcation diagram in ν, ε. Parameters are as in Fig. (5.4). The Hopf bifurcation curve (ε_H, ν_H) in (ε, ν) parameter space encloses a region of sustained oscillations. The vertical lines labeled ν_{max} and ν_{2D} corresponds to the maximum bifurcation value observed in the three- and the two- dimensional model respectively. The intersection between the ν_{2D} line and the Hopf bifurcation curve labeled ε_{crit} correspond to the point where the two- and three-dimensional models have the same value of ν_H. When $\varepsilon < \varepsilon_{crit}$, the value of ν_H approaches ν_{2D} asymptotically as $\varepsilon \to 0$, indicating that the two-dimensional QSSA model in Eq. (5.2) underestimates the maximum bifurcation value in ν. When $\varepsilon > \varepsilon_{crit}$, the value of ν_H decreases rapidly indicating that the QSSA model overestimates the bifurcation value in this region.

the three-dimensional models. For ε above the critical value, the quasi-steady state approximation (i.e. the two-dimensional model) overestimates the window in ν, but when ε is less than the critical value, the QSSA underestimates the ability of the system to oscillate. This might indicate a physiological function of the experimentally observed slowed allosteric transitions. If it is beneficial for a biological system regulated by an allosteric system to have sustained oscillatory behavior in its metabolites, an optimization of the rate of the allosteric transition can make the oscillatory window in ν broader. The oscillatory mode will be more stable to perturbations in the inflow rate of substrate and in the rate of product removal, as well as fluctuations in the other dimensionless parameters.

5.2.3 Birhythmicity

Prior investigations (see Segel & Goldbeter, 1994) have only been able to detect a single periodic solution in the two-dimensional model for a given set of parameters. Coexistence of two periodic solutions, the phenomena coined birhythmicity (see e.g. Goldbeter, 1996) and Chapter 3, has been thought to occur only in more complex models such as two auto-catalytic enzymes placed in series (Decroly & Goldbeter, 1982) and Chapter 6 herein. In Fig. (5.6) it is shown that birhythmicity may indeed be present in the simple system described by Eq. (5.5) when the allosteric transition is not in the limit $\varepsilon \to 0$. Fig. (5.6) shows the bifurcation diagram of the three-dimensional model with ε as a bifurcation parameter. The parameters are the same as in Fig. (5.5) and the variables have been rescaled to unity such that the left hand scale indicates $\alpha/200$, $\beta/200$ and γ. In Fig. (5.6)

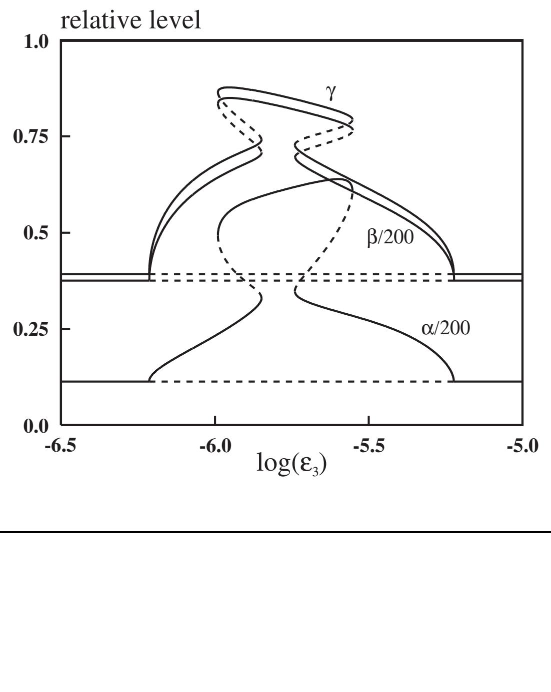

Fig. 5.6: Bifurcation diagram with ε as bifurcation parameter showing the bifurcations of the steady state solution and the limit cycle. Heavy lines shows either the maximum relative values of α, β or γ during oscillation or the steady state level. Broken lines indicates that the periodic or steady state solution is unstable. The steady state changes stability at $\varepsilon = 5.6 \cdot 10^{-6}$ and $6.1 \cdot 10^{-7}$ through Hopf bifurcations. Within the Hopf bifurcations the periodic solution changes stability four times through four saddle-node bifurcations that allows for two coexisting stable limit cycles within limited boundaries of ε.

the horizontal lines indicate the steady state values of α, β and γ respectively. Broken lines indicate that the steady state solution is unstable. The steady state becomes unstable and a periodic solution exists between two super-critical Hopf bifurcations at, respectively, $\varepsilon = 6.1 \cdot 10^{-7}$ and $\varepsilon = 5.6 \cdot 10^{-6}$. It is observed that the periodic solution changes stability four times through saddle-node bifurcation at, respectively, $\varepsilon = 1.0 \cdot 10^{-6}$, $1.4 \cdot 10^{-6}$, $1.8 \cdot 10^{-6}$ and $\varepsilon = 2.8 \cdot 10^{-6}$. The regions where the periodic solution is unstable is indicated by broken lines. This shows that two stable periodic solutions coexist from $\varepsilon = 1.0 \cdot 10^{-6}$ to $1.4 \cdot 10^{-6}$, and again from $1.8 \cdot 10^{-6}$ to $2.8 \cdot 10^{-6}$.

In Fig. (5.7) the coexisting periodic solutions for $\varepsilon = 2.0 \cdot 10^{-6}$ are outlined in the α, β phase plane together with the α and β nullclines and the phase plane trajectory predicted by the two-dimensional model. The steady state solution, located at the intersection of the nullclines, is stable for $\varepsilon = 0$ and the phase trajectory of the two-dimensional model is a spiraling convergence toward the steady state solution. When $\varepsilon = 2.0 \cdot 10^{-6}$, two stable periodic solutions (labeled LC_1 and LC_2 in Fig. (5.7)) evolve around the steady state solution, which, for this rate of the allosteric transition, is unstable. The two periodic solutions differ in both amplitude and period (not shown). The LC_1 periodic solution is a small amplitude, rapid oscillation with a period of 28.0, whereas the LC_2 periodic solution is a high amplitude slow oscillation with a period of 40.6. It is interesting to observe that birhythmicity can occur in the simple enzyme model. Not only is a slow allosteric transition able to enhance the nonlinearity of the system (see the previous section) it also introduces dynamic behavior previously believed to rely

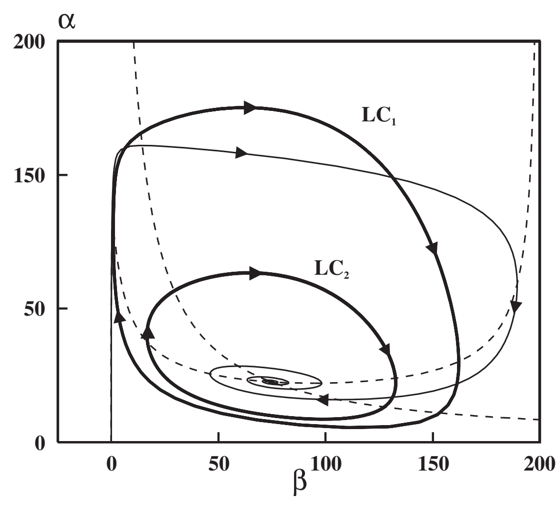

Fig. 5.7: Phase plot of location of two coexisting stable limit cycles in the α, β phase space. Parameters are as in Fig. (5.4). The two coexisting stable periodic solutions, labeled LC_1 and LC_2, obtained for $\varepsilon = 2.0 \cdot 10^{-6}$ (heavy lines) are compared with the dynamic behavior of the two-dimensional QSSA model Eq. (5.2) derived assuming a fast allosteric transition. The two-dimensional model predicts a phase trajectory (thin line) that spirals toward a stable steady state located at the intersection of the nullclines (broken lines). In the three dimensional model Eq. (5.5) the stable steady state is unstable and the system shows potential for birhythmicity.

on more complicated mechanisms involving at least one additional enzyme (see Goldbeter, 1996).

5.3 Other Violations of the QSSA

The investigation of the dynamic effect of a slow allosteric transition was motivated by the experimental evidence available (Kurganov, 1981). The three dimensional model derived in Appendix B to account for a slow allosteric transition requires that the parameters ε_1 and ε_2 associated with, respectively, the Michaelis-Menten and the product dissociation reactions as well as the enzyme concentration represented through the parameter ϵ, are small. The parameters ϵ and ε_1 are not independent and $\epsilon \to 0$ implies that $\varepsilon_1 \to 0$. The extended simplification method presented in Chapter 3 provides for derivation of appropriate reduced descriptions in the case where the allosteric transition is fast and one of the other QSSA conditions are violated. These models are also derived in Appendix B.

5.3.1 Slow Product Dissociation

When ε and ϵ are close to zero it can be shown that the system

$$\begin{aligned}
\frac{d\alpha}{d\tau} &= \nu - 2\sigma\alpha(\alpha+1)\frac{L(r_{01}+r_{02})+1}{L+(\alpha+1)^2},\\
\frac{d\beta}{d\tau} &= 2q\sigma\alpha(\alpha+1)\frac{L(r_{01}+r_{02})+1}{L+(\alpha+1)^2} - \beta\\
&\quad + q\frac{\epsilon}{\varepsilon_2}\left[(\beta+1)(\alpha+1)^2(r_{01}+2r_{02}) - 2\beta(\alpha+1)^2\frac{L(r_{01}+r_{02})+1}{L+(\alpha+1)^2}\right],\\
\frac{dr_{01}}{d\tau} &= \frac{1}{\varepsilon_2}\left[2r_{02} - r_{01} + \beta\left(2\frac{L(r_{01}+r_{02})+1}{L+(\alpha+1)^2} - 3r_{01} - 2r_{20}\right)\right],\\
\frac{dr_{02}}{d\tau} &= \frac{1}{\varepsilon_2}(\beta r_{01} - 2r_{02}).
\end{aligned} \tag{5.6}$$

is an appropriate reduced description of the 11 mass action kinetic equation obtained from the elementary reactions in Fig. (5.1). When the allosteric transition and the enzyme concentration is sufficiently low, one can obtain the two-dimensional bifurcation diagram presented in Fig. (5.8) where the parameters are as in Fig. (5.5)

Similar to the bifurcation diagram obtained for a slow allosteric transition, the vertical line labeled ν_{2D} in Fig. (5.8) marks the maximum bifurcation value of

ν obtained in the two-dimensional model in Eq. (5.2). The effect of a moderate value of ε_2 is not identical with the effect of a moderate value of ε, and there is a significant difference between the two-dimensional bifurcation diagrams Fig. (5.8) and Fig. (5.5). In Fig. (5.5) the bifurcation curve approaches the bifurcation ν_{2D} asymptotically from *above* as $\varepsilon \to 0$. This leads to an expansion of the oscillatory window in ν for finite values of ε below a critical value ε_{crit}. In Fig. (5.8) the Hopf bifurcation curve in ν, ε_2 approaches ν_{2D} asymptotically from *below* as $\varepsilon_2 \to 0$ and ν_{2D} represents the maximum bifurcation of ν at any value of ε_2. An expansion in the width of the oscillatory window by an slow product dissociation reaction is not observed. The vertical line labeled ε_{crit} in Fig. (5.8) represents the maximum value of ε_2 where there is no significant difference between the bifurcation values in ν obtained from the four dimensional model Eq. (5.6), and the low reduced model in Eq. (5.2). When $\varepsilon_2 > \varepsilon_{crit}$ the window of sustained oscillations contracts and finally vanishes.

5.3.2 High Enzyme Concentration

The truncation through the QSSA requires that the enzyme concentration is low so that the substrate α and the product β have a zero rate of change on the time-scales associated with the fast reactions supposed to be eliminated. Low enzyme concentrations are not guaranteed *in vivo* and the total concentration of an enzyme may in fact be quite high inside cells (Srivastava & Bernard, 1987). It is therefore important to investigate how the oscillations observed in the QSSA

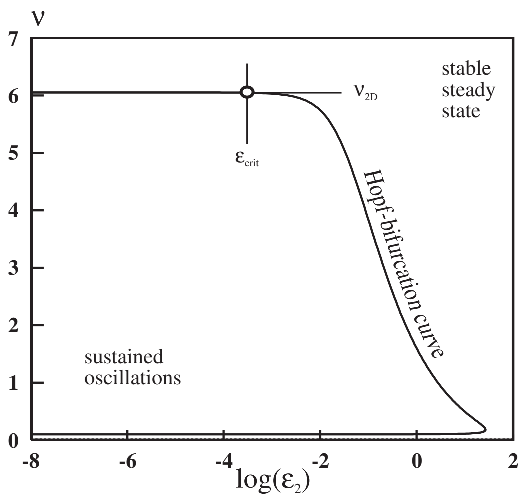

Fig. 5.8: Two-dimensional steady state bifurcation diagram in ν and ε_2. The Hopf bifurcation curve outlines the location of Hopf bifurcations and encloses a region where the four-dimensional model in Eq. (5.6) shows sustained oscillatory behavior. The allosteric transition and the Michaelis-Menten reaction are assumed to be fast equilibrating (i.e. ϵ, $\varepsilon \to 0$). The other parameters are identical with those of Fig. (5.5). The point ε_{crit} marks a critical value of ε_2. When $\varepsilon_2 < \varepsilon_{crit}$ no significant difference between the two-dimensional QSSA model in Eq. (5.2) and the model in Eq. (5.6) can be observed, but when $\varepsilon_2 > \varepsilon_{crit}$ the slow product dissociation reaction inhibits the ability of the system to oscillate.

models are altered when the enzyme concentration is increased. With the choice of dimensionless variables used in Appendix B, it is not possible to simplify the full system significantly using the QSSA without assuming that the total enzyme concentration is low. The dynamic effect of high values of ϵ is therefore investigated directly on the normalized 11 mass action kinetic rate equations written in Tab. (B.1) in Appendix B.

The effect of high enzyme concentrations, taken a constant maximum velocity (i.e. a constant value of σ), is investigated in Fig. (5.9) through analysis of the α, β phase space. The phase plane trajectories obtained from the full model written in Tab. (B.1) in Appendix B are plotted for different values of ϵ. The parameters are the same as in Fig. (5.2) except that ε_1, ε_2 and ε are set to 10^{-8}. The heavy curve in Fig. (5.9) outlines the stable periodic solution obtained from the full model setting $\epsilon = 10^{-6}$. This solution coincides with the periodic solution obtained from the reduced model in Eq. (5.2) (compare with Fig. (5.3)). The periodic solution obtained for $\epsilon = 1.0$ is located very near to the heavy lined limit cycle solution, indicating that ϵ is not required to be close to zero for the QSSA model to be valid. The parameter ϵ is defined as the ratio e^0/K_m of total enzyme concentration to the Michaelis-Menten constant, and the high total enzyme concentration does not alter the behavior of the limit cycle solution significantly as long $e^0 \leq K_m$. The coincidence with the QSSA condition in the Michaelis-Menten reaction scheme (see Chapter 3) is noted. The stable periodic solutions obtained for $\epsilon = 10^1$, $\epsilon = 10^2$ and $\epsilon = 10^3$ are drawn with thin lines in

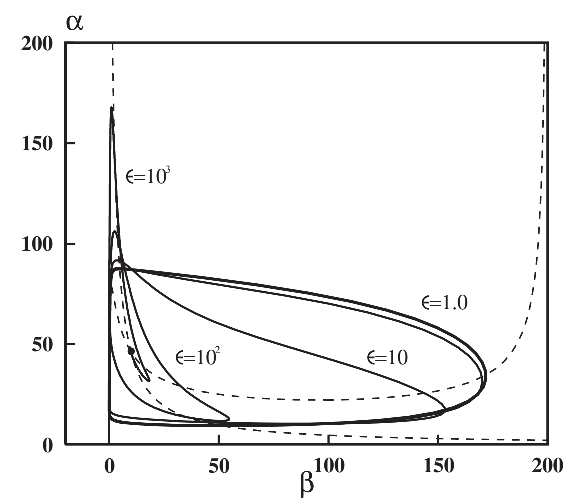

Fig. 5.9: Effect of high enzyme concentration on oscillations of the full model. Parameters are as in Fig. (5.3) with $\varepsilon_1 = \varepsilon_2 = \varepsilon = 10^{-8}$. The heavy line outlines the periodic solution obtained from the reduced model Eq. (5.2) whereas the thin lines outline the periodic solutions of the full model for, respectively, $\epsilon = 1.0$, $\epsilon = 10^1$, $\epsilon = 10^2$ and $\epsilon = 10^3$. Even when $\epsilon = 1.0$ the reduced model (obtained assuming $\epsilon \to 0$) is an appropriate approximation to the full model written in Tab. (B.1) in Appendix B as the phase trajectories predicted by these to models nearly coincide. When $\epsilon = 10^4$ the steady state solution is stable and phase space trajectory spirals toward the steady state point at the intersection of the nullclines (broken lines).

Fig. (5.9) and it is observed that the amplitude in β decreases and the amplitude in α increases as ϵ is increased. For $\epsilon = 10^4$ the phase trajectory converges to the steady state point located at the intersection of the nullclines (broken lines). This indicates that the steady state is stable and that the system probably has passed a Hopf bifurcation.

The full model does not lose the ability to oscillate even when the enzyme concentration is high. When the ratio $\epsilon = e^0/K_m$ is not low, the stringent mathematical derivation of reduced models in Appendix B fails formally. In the derivations of the truncated models it is assumed $\epsilon \to 0$ and $q\epsilon \to 0$ to ensure that α and β have a zero rate of change on the time-scales of the fast reactions. The above investigations shows that this requirement may be relaxed and that the error, made by treating α and β as slow variables when they are not, is not significant as long as the total enzyme concentration is small compared to the Michaelis-Menten constant ($e^0 \leq K_m$). A high enzyme concentration has an inhibitory effect on the ability to oscillate and the model, in the derivation considered here, will fail to make even qualitative predictions. To model systems containing high enzyme concentrations, it is necessary to make a variable transformation before simplifying the system as discussed in Appendix B and performed in practice in Chapter 7. It should be noted, however, that some enzymes, including phosphofructokinase (Aragón & Sols, 1991), show concentration dependent activities arising from increased oligorimization at increased concentrations (Kurganov *et al.*, 1976). It is therefore important that the molecular mechanism used to define the constituting elementary reactions are based on *in vivo* measurements as *in vitro* experiments may cause oligomeric enzymes to dissociate. The above investigations do not take protein-protein interactions into account, but they show that the mathematical condition of low enzyme concentration may be relaxed.

5.3.3 Slow Michaelis-Menten Reaction

It was shown in the previous section that the total enzyme concentration does not influence the dynamic behavior significantly as long as $\epsilon \leq 1$. That the low enzyme condition can be relaxed allows for the investigation of a slow Michaelis-Menten reaction as the small parameter ε_1 associated with the Michaelis-Menten reaction is restricted to values lower than ϵ. When $\varepsilon, \varepsilon_2 \to 0$ and the value of $q\epsilon$ is low, one can, as shown in Appendix B, obtain the reduced model in Eqs. (5.7).

$$
\begin{aligned}
\frac{d\alpha}{d\tau} &= \nu-\sigma(\beta+1)^2(r_{10}+2r_{20}) \\
&\quad+\frac{\epsilon}{\varepsilon_1}\left[(\alpha+1)(\beta+1)^2(r_{10}+2r_{20})-2\alpha(\beta+1)^2\frac{L(r_{10}+r_{20})+1}{L+(\beta+1)^2}\right], \\
\frac{d\beta}{d\tau} &= q\sigma(\beta+1)^2(r_{10}+2r_{20})-\beta, \qquad (5.7)\\
\frac{dr_{10}}{d\tau} &= \frac{1}{\varepsilon_1}\left[2r_{20}-r_{10}+\alpha\left(2\frac{L(r_{10}+r_{20})+1}{L+(\beta+1)^2}-3r_{10}-2r_{20}\right)\right], \\
\frac{dr_{20}}{d\tau} &= \frac{1}{\varepsilon_1}(\alpha r_{10}-2r_{20}).
\end{aligned}
$$

The two-dimensional bifurcation diagram presented in Fig. (5.10) confirms that the low dimensional model in Eq. (5.7) is an appropriate approximation to the full system of normalized mass action kinetic equations. In Fig. (5.10) the location of the Hopf bifurcation points in ν, ε_1 parameter space is outlined as predicted by the reduced model in Eq. (5.7) and the full system in table B.1 in Appendix B. In the latter $\epsilon = 0.1$, $\varepsilon_2 = 10^{-8}$ and $\varepsilon = 10^{-8}$ whereas, $\sigma = 10$, $q = 10$ and $L = 5.0 \cdot 10^6$ in both. The predictions are drawn with full and broken

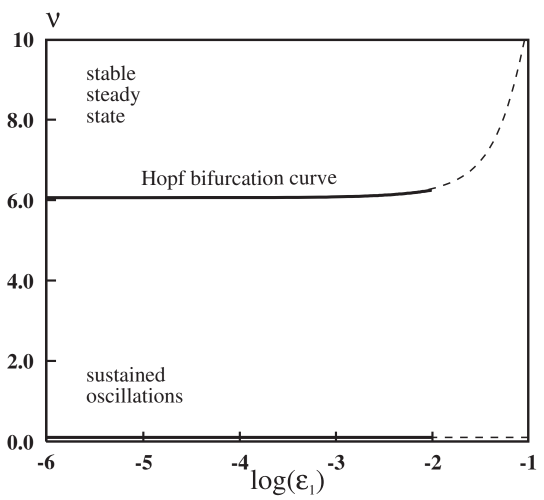

Fig. 5.10: Comparison of the bifurcation diagrams in ν, ε_1 predicted by the full 11 dimensional mass kinetic model and the reduced model Eq. (5.7). In the full model, $\epsilon = 0.1$ and $\varepsilon = 10^{-8}$ whereas the other parameters are as in Fig. (5.5) where appropriate. The Hopf bifurcations predicted by the full model is drawn with full lines and the maximum value of ε_1 is limited by $\varepsilon_1 \leq \epsilon/\sigma = 10^{-2}$. The Hopf bifurcations predicted by the simplified model are drawn with broken lines and ε_1 is not limited as the reduced model does not take ϵ into consideration. The two curves are almost coinciding indicating that the condition $\epsilon \to 0$ may be relaxed. The width of the window in ν where the system oscillates expands slightly when ε_1 approach 10^{-2}. The expansion continues in the reduced model as $\varepsilon_1 > 10^{-2}$ but this range is not accessible due to the restrictions on the value of ε_1.

lines for the full and simplified model, respectively. As $\epsilon = 0.1$ in the full model, the maximum value of ε_1 is 10^{-2} (see caption of Fig. (5.10)).

5.3.4 Combined Effects

It has previously been shown that variation of ε_2 when $\epsilon, \varepsilon \rightarrow 0$has only an inhibitory effect on the ability of the system to oscillate. It has also been shown that the enzyme concentration through ϵ has little effect as long $e^0 < K_m$, Fig. (5.9), and that a slow Michaelis-Menten reaction has a small expanding effect on the width of the oscillatory window in ν when the enzyme concentration is high ($\epsilon = 10^{-1}$), Fig. (5.10). However, investigation of the full 11 dimensional model written in table B.1 in Appendix B shows that the combination of a high enzyme concentration, a slow Michaelis-Menten reaction and a slow product dissociation reactions may have the same dynamic effect as shown in Fig. (5.5) for a slow allosteric transition.

In Fig. (5.11), a three-dimensional bifurcation diagram in $\varepsilon_1, \varepsilon_2, \nu$ parameter space is presented. The surfaces are predicted by the full 11-dimensional model in table B.1 with the same parameters as investigated previously except that $\varepsilon = 10^{-8}$ and $\epsilon = 10^{-1}$. Below the two-dimensional Hopf bifurcation surface the steady state and the system will show sustained oscillatory behavior until a lower Hopf bifurcation (see e.g. Fig. (5.5)) is reached. To preserve the clarity of the figure, the minimum Hopf bifurcation surface in ν has been omitted.

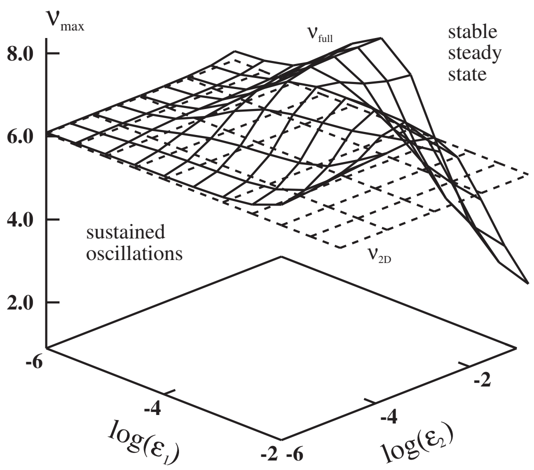

Fig. 5.11: Three-dimensional bifurcation diagram in $\epsilon, \varepsilon_1, \varepsilon_2$ predicted by the full 11 dimensional mass action kinetic equations. The parameters are the same as in Fig. (5.5) except that $\epsilon = 0.1$ and $\varepsilon = 10^{-8}$. The surface drawn with full lines outlines the location of Hopf bifurcations and encloses a volume of where the steady state solution is unstable. The lower boundary of this volume has been omitted for clarity. The surface drawn with broken lines outlines the bifurcation value of ν predicted when $\varepsilon_1 = \varepsilon_2 = 10^{-8}$. The right combinations of ε_1 and ε_2 may either expand or contract the width of the oscillatory window in ν as observed in Fig. (5.5) for a slow allosteric transition.

The surface outlined with broken lines represents the maximum bifurcation value in ν as predicted by the full model when $\varepsilon_1, \varepsilon_2 = 10^{-8}$ and corresponds to the maximum bifurcation value in ν observed in the two-dimensional model in Eq. (5.2). The prediction that variation of ε_2 gives an increased ability to show sustained oscillatory behavior made from Fig. (5.8) does not hold. Even for $\varepsilon_1 = 10^{-8}$, a slight increase in the maximum bifurcation value of ν is observed when ε_2 is varied. Secondly, the right combinations of high ε_1 and ε_2 may either expand or contract the window in ν, where the system shows sustained oscillatory behavior. This behavior is similar to the behavior induced by a slow allosteric transition in Fig. (5.5). The ability to producing sustained oscillatory behavior requires the right correlation between ε_1 and ε_2 indicating that the ability to oscillate may be further enhanced by variation of ε together with the right combination of ε_1 and ε_2. The investigation of varying ε, ε_1 and ε_2 simultaneously, which is not shown here, showed that increasing the value of ε, which is 10^{-8} in Fig. (5.11), does not cause a further increase in the maximum bifurcation value in ν. In fact, increasing ε overrules the effect observed by increased ε_1 and ε_2 indicating that the effects are not cumulative.

CHAPTER 6

Coupled Oligomeric Enzymes

In a reaction scheme where two auto-catalytic oligomeric allosteric enzymes are placed in series, a wide range of different complex behaviors can emerge when truncating the number of rate equations using the QSSA. In the last chapter, it was shown that a slow allosteric transition especially may have a significant influence on the simple oscillatory behavior of a single enzyme reaction. Here, the effect of a slow allosteric transition on the different modes of complex dynamic behavior observed in the truncated model of a coupled oligomeric enzyme reaction scheme is investigated. In schematic form the coupled enzyme reactions scheme can be depicted

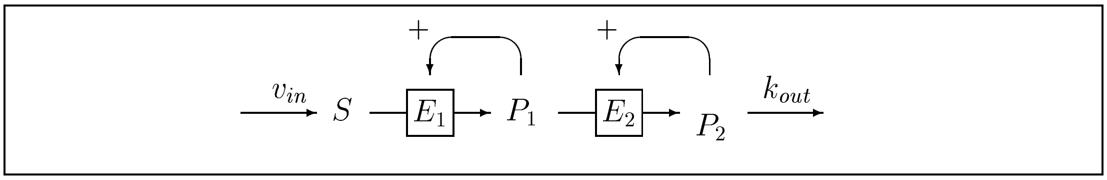

where E_1 and E_2 represent the first and the second enzyme and P_1 and P_2 represent the product of, respectively, the first and second enzyme reactions. The substrate of the first enzyme S flows into the system at a constant rate v_in and the product of the second enzyme reaction P_2 is removed from the system with an apparent first order rate constant k_{out}. Both enzymes are assumed to be dimeric and to obey the R-exclusive MWC-theory discussed in Chapter 4.

6.1 The Goldbeter Model

The coupled allosteric enzyme reaction scheme has been studied intensively for applications to the emergence of complex dynamic behavior in biological systems (Decroly & Goldbeter, 1982, 1985, 1987; Holden & Erneux, 1993). The reaction scheme has, for example, been used to argue for the existence of complex behavior in glycolysis (see Goldbeter, 1996) even before chaos was actually found experimentally (Nielsen *et al.*, 1997). The mass action kinetic description of the coupled enzyme reaction contains a total of 21 variables and each enzyme can exist in nine different binding states (see Chapter 5). The standard QSSA method can be employed and the 21 rate equations can be truncated to only three rate equations for the dimensionless variables

$$\alpha = \frac{[S]}{K_{m1}}, \qquad \beta_1 = \frac{[P_1]}{K_{P1}}, \qquad \beta_2 = \frac{[P_2]}{K_{P2}}, \tag{6.1}$$

where K_{m1} is the Michaelis-Menten constant of E_1 and K_{P1}, K_{P2} denotes, respectively, the dissociation constants of P_1 and P_2 from the allosteric sites of E_1 and E_2. The truncation employed in the original publications (Decroly & Goldbeter, 1982, 1985) is similar to the two-dimensional description of the mono-enzyme reaction scheme in Chapter 5 except that the time-unit is not eliminated. With only the concentrations eliminated the coupled enzyme reaction is described by

$$\begin{aligned} \frac{d\alpha}{dt} &= \frac{v_{in}}{K_{m1}} - \sigma_1'\Phi(\alpha, \beta_1), \\ \frac{d\beta_1}{dt} &= q_1\sigma_1'\Phi(\alpha, \beta_1) - \sigma_2'\Theta(\beta_1, \beta_2), \\ \frac{d\beta_2}{dt} &= q_2\sigma_2'\Theta(\beta_1, \beta_2) - k_{out}\beta_2, \end{aligned} \tag{6.2}$$

where $\Phi(\alpha, \beta_1)$ and $\Theta(\beta_1, \beta_2)$ are defined by

$$\begin{aligned} \Phi(\alpha, \beta_1) &= \frac{\alpha(\alpha+1)(\beta_1+1)^2}{L_1 + (\alpha+1)^2(\beta_1+1)^2}, \\ \Theta(\beta_1, \beta_2) &= \frac{\beta_1(\delta\beta_1+1)(\beta_2+1)^2}{L_2 + (\delta\beta_1+1)^2(\beta_2+1)^2}. \end{aligned} \tag{6.3}$$

The equations in Eqs. (6.3) are identical to those obtained from R-exclusive MWC-theory and describe the degree of substrate saturation (i.e. the relative amount of substrate bound to active sites (Monod *et al.*, 1965)). The parameters σ'_2 and σ'_2, with units of $sec.^{-1}$, represent the maximum velocities V_1 and V_2 of, respectively, the first and the second enzyme divided by their Michaelis-Menten constants K_{m1} and K_{m2}. The other dimensionless parameters are defined; $q_1 = K_{m1}/K_{P1}$; $q_2 = K_{P1}/K_{P2}$ and $\delta = K_{P1}/K_{m1}$. Moreover, L_1 and L_2 denote the allosteric constants for E_1 and E_2 respectively.

The system has been found, when assuming quasi-steady state, to exert a wide range of nonlinear phenomena. In the prior investigations (Decroly & Goldbeter, 1982, 1985, 1987) the preferred bifurcation variable has been the apparent first order rate constant k_{out} for product removal. The different dynamic modes found at varied values of k_{out} are summarized in Tab. (6.1) which is reproduced from Decroly & Goldbeter (1982). It is noted that chaotic behavior is found for $k_{out} = 2.0$ when the other parameters are as defined in the figure legend.

6.2 Extended Model

The QSSA truncation of the mathematical description of system composed of a single auto-catalytic oligomeric allosteric enzyme is discussed in detail in Appendix B. A similar method can be applied to reduce the 21 rate equations describing the coupled system considered herein. The extended method presented in Chapter 2 allows for establishing the conditions where the three dimensional model in Eq. (6.2) is valid and for the derivation of reduced models when one or more of the

Parameter range, sec^{-1}	Observed behavior
$k_{out} \leq 0.972$	One limit cycle
$1.584 < k_{out} \leq 1.82$	Two limit cycles (birhythmicity)
$1.82 < k_{out} \leq 1.974$	One limit cycle
$1.974 < k_{out} \leq 1.99$	Two limit cycles, one of which undergoes a sequence of period doubling leading to chaos
$1.99 < k_{out} \leq 2.034$	Aperiodic oscillations (chaos)
$2.034 < k_{out} \leq 12.8$	Complex periodic oscillations (including bursting)
$k_{out} > 12.8$	One limit cycle

Tab. 6.1: Dynamic behavior of two instability-generating allosteric enzymes in series at varied k_{out} (reproduced from Decroly & Goldbeter, 1982). The parameter values are, with the definitions employed here, $\nu_{in} = 0.45$ sec^{-1}, $L_1 = 5.0 \cdot 10^8$, $L_2 = 100$, $\sigma'_1 = \sigma'_2 = 10$ sec^{-1}, $q_1 = 50$, $q_2 = 0.02$ and $\delta = 0.0$.

QSSA conditions are violated. The conditions for the truncation of the 21 variable system are analogous to those that validate the QSSA in the model considered in Chapter 5, i.e. sufficiently low concentrations of the enzymes, fast allosteric transitions and fast Michaelis-Menten and product dissociation reactions. When the parameter ε, which is associated with the rate of the allosteric transition of the first enzyme, is not small, the model in Eq. (6.2) will be invalid. To take account for a slow allosteric transition in E_1 a variable γ, representing the relative amount of the first enzyme that is in the active state, is defined by

$$\gamma = \frac{1}{e_1^0} \sum_{ij=0}^{2} r_{ij}, \tag{6.4}$$

where e_1^0 is the total enzyme concentration of E_1, and r_{ij} is the nine different binding states of the active enzyme (see Chapter 5). Instead of describing the first enzyme reaction using the saturation function $\Phi(\alpha, \beta_1)$ defined in Eq. (6.3) a description similar to that used in the previous chapter is invoked, and the first enzyme reaction will be described using α, β_1 and γ. In the following, the dimensionless variables in Eq. (6.1) are unchanged but the new dimensionless parameters

$$\nu = \frac{v_{in}}{K_m k_{out}}, \qquad \sigma_1 = \frac{V_1}{K_m k_{out}}, \qquad \sigma_2 = \frac{V_1}{K_m k_{out}}, \tag{6.5}$$

$$q_1 = \frac{K_{m1}}{K_{P1}}, \qquad q_2 = \frac{K_{P1}}{K_{P2}}, \qquad \delta = \frac{K_{P1}}{K_{m1}}, \qquad \varepsilon = \frac{k_{out}}{k_{tb}}, \tag{6.6}$$

will be employed together with a dimensionless time-scale $\tau = tk_{out}$. With the definitions of variables in Eq. (6.4) and Eq. (6.1) and the dimensionless parameters in Eq. (6.6) the extended four dimensional model reads

$$\boxed{\begin{aligned}
\frac{d\alpha}{d\tau} &= \nu - \sigma_1 \frac{\alpha\gamma}{\alpha+1} \\
\frac{d\beta_1}{d\tau} &= q_1\sigma_1 \frac{\alpha\gamma}{\alpha+1} - \sigma_2 \frac{\beta_1(\delta\beta_1+1)(\beta+1)^2}{L_2+(\delta\beta_1+1)^2(\beta+1)^2} \\
\frac{d\beta_2}{d\tau} &= q_2\sigma_2 \frac{\beta_1(\delta\beta_1+1)(\beta_2+1)^2}{L_2+(\delta\beta_1+1)^2(\beta_2+1)^2} - \beta_2 \\
\frac{d\gamma}{d\tau} &= \frac{1}{\varepsilon L_1} - \gamma \left[\frac{(\alpha+1)^2(\beta_1+1)^2+L_1}{\varepsilon L_1(\alpha+1)^2(\beta_1+1)^2} \right]
\end{aligned}} \tag{6.7}$$

It can readily be shown, using Tihonov's First Theorem, that the extended model in Eq. (6.7) can by approximated by the three dimensional model in Eq. (6.2) if $\varepsilon \to 0$, that is if the allosteric transition is fast. The validity of the four-dimensional model can be shown formally by a detailed reduction using the method outlined in Appendix B for a single enzyme reaction.

6.3 Fast Allosteric Transition

It was previously noted that the three dimensional model in Eq. (6.2) exerts chaotic oscillations for $k_{out} = 2.0$ and $\nu_{in} = 0.45$ sec^{-1}, $L_1 = 5.0 \cdot 10^8$, $L_2 = 100$, $\sigma_1' = \sigma_2' = 10$ sec^{-1}, $q_1 = 50$, $q_2 = 0.02$ and $\delta = 0.0$. The dimensionless parameters used in Eq. (6.7) are related to the dimensional parameters in Eq. (6.2) through the relations

$$\nu = \frac{v_{in}}{K_{m1} k_{out}}, \qquad \sigma_1 = \frac{\sigma_1'}{k_{out}}, \qquad \sigma_2 = \frac{\sigma_2'}{k_{out}}, \tag{6.8}$$

and the extended model in Eq. (6.7) is therefore ensured to exert chaotic oscillations, in the limit of $\varepsilon \to 0$, by setting

$$\nu = 0.225, \qquad \sigma_1 = \sigma_2 = 5.0, \tag{6.9}$$

and keeping the other parameters as in Tab. (6.1). Using ν as bifurcation parameter and setting $\varepsilon = 10^{-12}$ the system undergoes a wide range of different bifurcations as depicted in the bifurcation diagram in Fig. (6.1). The extended model allows for a unique single steady state solution for a given value of ν which can be either stable or unstable. In the bifurcation diagram in Fig. (6.1) the steady state value of α, denoted α_0, is plotted with full lines when the steady state solution is stable and with broken lines when the steady state solution is unstable. The periodic or aperiodic solutions are outlined by maximum value of α, denoted α_M, observed during oscillations. The stability of the periodic and aperiodic solutions is indicated by full lines when stable and broken lines when unstable. The stability of the steady state is determined by the eigenvalues of the Jacobian matrix, whereas the stability of the periodic solutions is obtained by computation of Floquet multipliers. The different types of dynamic behaviors are summarized in Tab. (6.2) and discussed below.

Catalogue of dynamic behaviors

Steady state. When the value of ν is very low $\nu \lesssim 0.001$, intermediate, $0.264 < \nu \leq 0.594$, and high, $\nu > 3.380$ a steady state is the only stable solution and the system will settle in this steady state. When ν increases from zero, the steady state becomes unstable through a Hopf-bifurcation at $\nu = 9.97 \cdot 10^{-4}$ (not shown) and regains its stability through another super-critical Hopf bifurcation at $\nu = 0.264$.

The steady state looses stability once more at a sub-critical Hopf bifurcation at $\nu = 0.850$ causing the destruction of an unstable limit cycle. Between $\nu = 0.594$ and $\nu = 0.850$ a steady state coexists with a stable periodic solution. Finally, the steady state becomes stable at a super-critical Hopf bifurcation at $\nu = 3.380$ and it remains stable for all higher values. Due to the low amplitude oscillations observed close to a super-critical Hopf bifurcation, this bifurcation is often called a *soft excitation*.

Limit-cycle Oscillations. When the steady state solution reverses stability through Hopf bifurcations, a periodic solution is either generated or destroyed. When ν is increasing from zero, a stable limit cycle solution labeled LC_1 in Fig. (6.1) is generated at a super-critical Hopf bifurcation at $\nu = 9.97 \cdot 10^{-4}$. The limit cycle is associated with an instability that can be assigned to the first auto-catalytic feedback loop and shows bursting oscillations when it couples to the second instability generating mechanism (discussed below). The limit cycle looses stability at the entry into the chaotic region (see below) but regains stability through a saddle-node bifurcation at $\nu = 0.219$. Finally, LC_1 is destroyed at the super-critical Hopf bifurcation at $\nu = 0.264$. A limit cycle reappears at a saddle-node bifurcation of periodic solutions at $\nu = 0.594$ where a stable and an unstable branch are generated. The latter is destroyed at the sub-critical

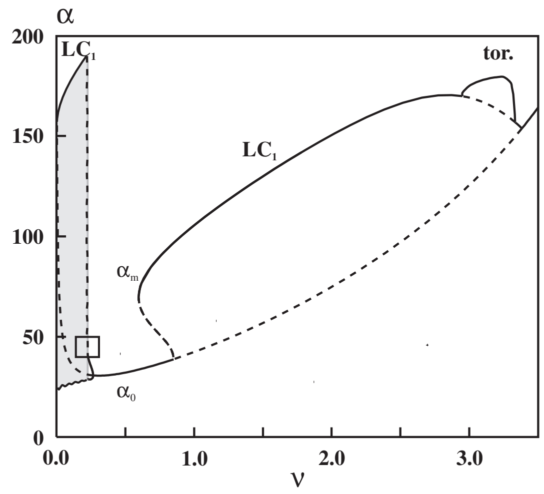

Fig. 6.1: Bifurcation diagram of the extended model Eq. (6.7) when the allosteric transition is fast ($\varepsilon = 10^{-12}$). Broken lines indicates that the steady state solution, labeled with α_0, is unstable. α_M indicate the maximum value of α during oscillations. When the steady state is unstable a stable periodic solution, labeled LC_1, exists. The parameter values are as in Eq. (6.9) and the system undergoes a series of period doublings at about $\nu = 0.226$ leading to chaos. The period doubling sequence is illustrated by the blowup in Fig. (6.2). In the shaded region below $\nu = 0.223$ the system shows complex periodic oscillations (bursting). The occurrence of chaos and bursting is expected from the prior investigations presented in Tab. (6.1). The co-existence of a stable periodic solution and a stable steady state between 0.594 and 0.850 is also expected. The instability of LC_1 is a new finding in this model. The bifurcations of the LC_1 limit cycle are torus bifurcations leading to the torus attractor shown in Fig. (6.3).

Hopf bifurcation for $\nu = 0.850$. This limit cycle, which is also labeled LC_1 in Fig. (6.1), following Decroly and Goldbeter (Decroly & Goldbeter, 1982), has a short period and can be assigned to an instability generated by the second autocatalytic feedback loop. The LC_1 limit cycle reverses stability twice through torus bifurcations at $\nu = 2.984$ and $\nu = 3.331$ before being destroyed at a super-critical Hopf bifurcation at $\nu = 3.380$.

Hard Excitation. At the saddle-node bifurcation at $\nu = 0.594$ a pair of periodic solutions, one stable and one unstable, are generated. At the same time, the steady state solution is stable and the unstable limit cycle separates the basins of attraction for the coexisting stable attractors. The coexistence of a stable steady state and a stable limit cycle is often referred to as hard excitation. When the system rests in the steady state, a perturbation that brings the system into the basin of attraction of the limit cycle will cause the onset of high amplitude oscillations. The unstable limit cycle is destroyed when it collides with the stable periodic solution at $\nu = 0.850$ where the steady state reverses its stability and the stable limit cycle becomes the only stable attractor of the system.

Birhythmicity. The fate of the stable limit cycle LC_1 generated at the super-critical Hopf-bifurcation at $\nu = 0.264$ is illustrated in the blowup in Fig. (6.2).

Parameter range	Observed behavior
$\nu \lesssim 0.001$	Steady state
$0.001 \lesssim \nu \leq 0.219$	Complex periodic oscillation (bursting)
$0.219 < \nu \leq 0.226$	Period doubling bifurcations and chaos
$0.226 < \nu \leq 0.227$	Two stable limit cycles of which one undergoes period doubling bifurcations
$0.227 < \nu \leq 0.264$	One limit cycle
$0.264 < \nu \leq 0.594$	Steady state
$0.594 < \nu \leq 0.850$	Steady state and one stable limit cycle (hard excitation)
$0.850 < \nu \leq 2.948$	One limit cycle
$2.948 < \nu \leq 3.331$	Quasi-periodicity
$3.331 < \nu \leq 3.380$	One limit cycle
$3.380 < \nu$	Steady state

Tab. 6.2: Summary of different types of dynamic behavior of the extended model at varied ν. Only stable attractors are considered. The allosteric transition is fast ($\varepsilon = 10^{-12}$) and the four dimensional model may successfully be reduced to a three dimensional model showing the same types of dynamic behavior. The quasi-periodic oscillations have not previously been reported.

Lowering the value of ν from 0.264 one observes, at $\nu \approx 0.227$, a saddle-node bifurcation which generates a new stable limit cycle, labeled LC_2, and an unstable limit cycle. The unstable limit cycle separates the basin of attraction of the LC_1 and LC_2 and the two stable limit cycles coexist analogously to the coexistence between a stable steady state and a stable limit cycle in the region of hard excitation. The limit cycle LC_1 is destroyed (or created, depending on preference) in a saddle-node bifurcation at $\nu = 0.2251$.

Period Doubling and Chaos. The stable periodic solution generated at the saddle-node bifurcation for $\nu = 0.227$ undergo a period doubling bifurcation when decreasing ν. At the period doubling point the LC_2 limit cycle becomes unstable and a new limit cycle emerges. The new limit cycle is illustrated in Fig. (6.2) by its alternating higher and lower maxima. The first period doubling bifurcation is followed by a sequence of period doublings when ν is decreased and limit cycles of period $2^2, 2^3, 2^4, \ldots$ emerge. The sequence of bifurcations comprises the well-known period doubling route to chaos and leads to a cycle of period 2^∞. The period doubling route to chaos is illustrated in the bifurcation diagram Fig. (6.2) where the limit cycles of period 1, 2 and 4 are illustrated together with the chaotic behavior at $\nu = 0.225$. When ν is decreased below 0.225 the system leaves the chaotic region and settles on a high amplitude oscillation with a complex bursting pattern. This transition may involve some type of intermittency (Decroly & Goldbeter, 1982).

Complex Periodic Oscillations (bursting). The trademark of complex peri-

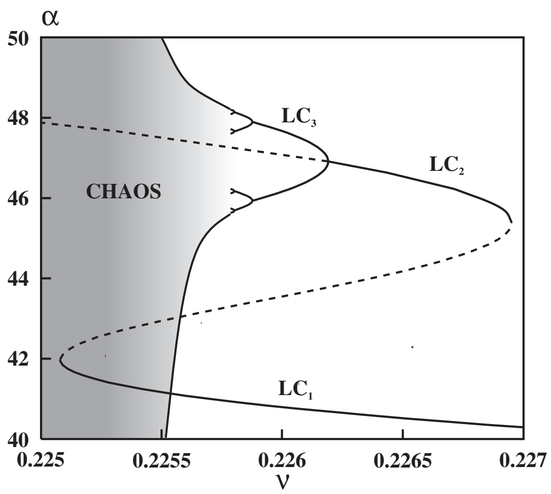

Fig. 6.2: Period doubling route to chaos through variation of ν. The bifurcation diagram is an enlargement of the square in Fig. (6.1). The stable limit cycle LC_2 is generated at a saddle-node bifurcation at ≈ 0.227 and undergoes a period doubling bifurcation which generates the limit cycle labeled LC_3. The period doubling continues and finally a limit cycle with infinite period is stabilized and the oscillations becomes chaotic. Between 0.225 and 0.227 the stable LC_1 coexists with LC_2 or another attractor, generated through the period doubling sequence. The basins of attractions of these attractors are separated by the unstable periodic solution indicated with broken the line.

odic oscillations or bursting oscillations is a series of sharp bursts after a period of relative quiescence in one of the variables in the system. Bursting oscillations may be understood in terms of a slow passage though a Hopf-bifurcation (Decroly & Goldbeter, 1987; Holden & Erneux, 1993). Bursting oscillation occurs on the limit cycle denoted LC_1 which is the only stable attractor between the Hopf-bifurcation at about $\nu = 0.001$ (not shown) and the period doubling bifurcations starting at about $\nu = 0.219$.

Quasi-periodicity. In the region between the Hopf-bifurcations at $\nu = 0.850$ and $\nu = 3.340$ the steady state is unstable and the system will show sustained oscillatory behavior. The limit cycle labeled LC_1 in Fig. (6.1) is the only stable attractor until it changes stability at a torus bifurcation for $\nu = 2.948$. The torus bifurcation is super-critical and a torus of vanishing width emerges. As ν is further increased, the width of the torus increases and the characteristic donut-shaped attractor emerges. When the first enzyme of the reaction can be considered in a quasi-steady state, which is the case here where $\varepsilon = 10^{-12}$, the level of γ will be determined solely by the value of α and β and the α, β_1, β_2 phase space will represent the whole phase space of the system. The location of the torus in the α, β_1, β_2 phase space is outlined in Fig. (6.3) for $\nu = 3.1$ where the "hole" in the torus is indicated by an arrow. The motion along the torus may be periodic or aperiodic depending on whether or not the phases of the two oscillations coincide. The torus is destroyed at $\nu = 3.331$ where the limit cycle regains its stability.

Fig. 6.3: The shape of the torus attractor showing the quasi-periodic motion in α, β_1, β_2 phase space for $\nu = 3.2$ and a fast allosteric transition ($\varepsilon = 10^{-12}$). The torus is tilted as compared with the typical representation of a torus and the arrow indicates the "hole" in its donut-shaped structure. The motion on the torus may be either periodic or aperiodic. The latter seems to be the case here as the phase trajectories do not coincide. It has not previously been reported that this reaction scheme can show quasi-periodic behavior.

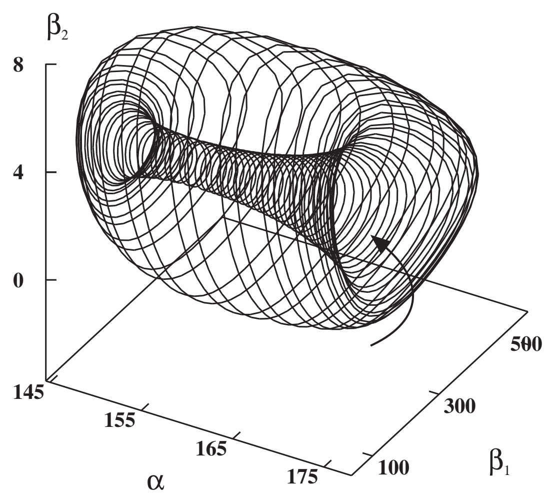

6.4 Effects of a Slow Allosteric Transition

The coupled auto-catalytic enzyme reaction scheme composed of oligomeric allosteric enzymes is thus able to show a wide range of different dynamic behaviors when the allosteric transition is fast, i.e. $\varepsilon \to 0$. However, if the allosteric transition is slowed down, e.g. increasing ε, the complex dynamic modes are readily inhibited as investigated next.

6.4.1 Bursting Oscillations

When $\nu = 0.2$ and $\varepsilon = 10^{-9}$, the integral solution of Eq. (6.7) shows bursting oscillations as depicted in Fig. (6.4a) where the time-dependent behavior of β_1 is recorded. During the first 500 time-units of integration the level of β is very low. Shortly after $\tau = 500$ the level of β_1 increases dramatically and a series of 10 high amplitude bursts is observed. After the bursts, the value of β_1 returns to a low level and stays quiescent until another series of bursts is initiated at about $\tau = 1600$. The subsequent series of bursts are identical indicating that the system evolves on a periodic solution of non-trivial geometry. An illustration of the phase

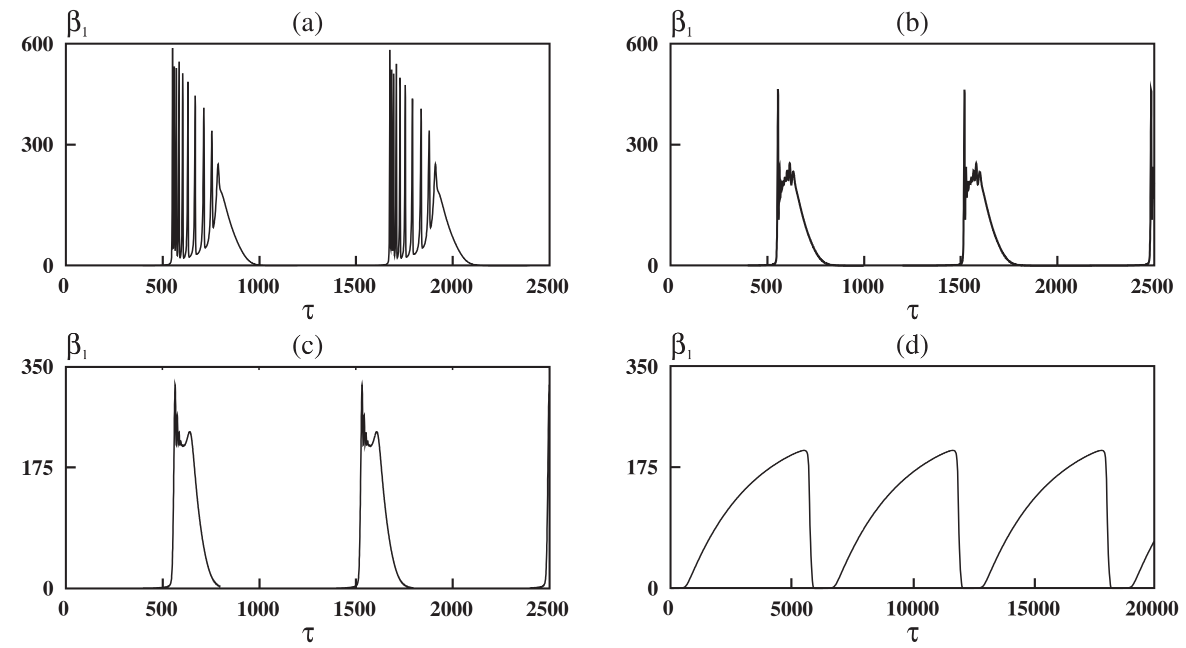

Fig. 6.4: Effect of a slow allosteric transition of the bursting pattern for $\nu = 0.2$. The other parameters are as in Fig. (6.1). The integral solution of β_1 is shown for different values of ε: (a) 10^{-9}, (a) 10^{-8}, (b) 10^{-7}, (c) 10^{-4}.

plane trajectory of the bursting oscillations can be found elsewhere (Decroly & Goldbeter, 1987) and it is associated with a linear part for the quiescent state, and a spiraling part resulting in a series of bursts. The bursting pattern arises through the coupling of two instability generating mechanisms. Initially, the catalytic activity of the first enzyme is low causing α to accumulate. The production of β_1 is low and the low inflow of β_1 to the second enzyme causes the latter to operate in the steady state region. When a critical level in α is reached, the auto-catalytic loop involving the first enzyme is triggered, and the rate of converting α to β_1 is increased. The increased catalytic activity of the first enzyme causes the inflow of β_1 to the second enzyme to increase, and the second enzyme becomes activated as a critical level of β_1 is reached. As the auto-catalytic loop of the second enzyme is triggered, β_1 is converted rapidly into β_2 causing the removal of β_1 and a corresponding lowered activity of the first enzyme. Transiently, the level of α is increasing until sufficient β_1 has accumulated to trigger another round of fast β_2 production. After the final burst, the stock of α has been depleted rendering the first enzyme unable to produce the flow of β_1 required for the second enzyme switch into a state of high catalytic activity. Instead, the second enzyme is operating with a steady activity which keeps the level of both β_1 and β_2 low. Actually, the level of α can be taken as a slowly varying bifurcation parameter of the second enzyme (Decroly & Goldbeter, 1987), and the bursting pattern can be understood as a slow passage through a Hopf bifurcation (Holden & Erneux, 1993).

The bursting pattern changes from a series of 10 bursts observed at $\varepsilon \lesssim 10^{-9}$ to a series of eight peaks when $\varepsilon = 10^{-8}$ as illustrated in Fig. (6.4b). The time span between the first and the last burst is decreased, indicating that the second enzyme leaves the oscillatory mode earlier when the allosteric transition of the first enzyme is slowed down. When ε is increased to 10^{-7} the behavior is very similar to that observed for $\varepsilon = 10^{-8}$ as shown in Fig. (6.4c). When $\varepsilon = 10^{-7}$, the height of the first burst is significantly lowered and is followed by only four bursts instead of the eight peaks observed for $\varepsilon = 10^{-8}$. The decreased ability to produce bursting oscillations when the allosteric transition is slowed down arises from a decreased ability of the first enzyme to respond fast when α and β_1 change. At a slow allosteric transition, the auto-catalytic feedback is weakened and the transition from a mode where α accumulates to a mode where α is quickly converted into product is less sharp. As a result, the changes in the level of β_1 produced by the second auto-catalytic loop (i.e. the bursts) do not alter the catalytic activity of the first enzyme, as the slow allosteric transition hinders a fast change in the rate of converting α into β_1 and the depletion of α is hardly influenced by the fluctuations in β_1 produced by the second enzyme. When the allosteric transition is slowed further, the bursting oscillation is replaced by a smooth oscillation as shown for $\varepsilon = 10^{-4}$ in Fig. (6.4d). At this point, the coupling between the two instability generating mechanisms is inhibited to the degree where the action of the second enzyme does not influence the behavior of the system.

6.4.2 Quasi-periodic Oscillations

The effect of a slow allosteric transition on the quasi-periodic oscillations observed when $\varepsilon = 10^{-12}$ is investigated in Fig. (6.5) where the integral solution of α is shown for various values of ε. The value of ν is 3.0 and the other parameters are as in Tab. (6.2). In Fig. (6.5a) the value of ε is 10^{-11} and the quasi-periodic behavior is clearly reflected in the integral solution of α. Before the system passes the torus bifurcation in Fig. (6.1) through an increase in ν, the system evolves along a stable limit cycle (not shown) with a short period and a low amplitude in α. The limit cycle returns to the same point in a Poincaré section once during each period. When the torus bifurcation is passed, and the limit cycle becomes unstable, the rapid low amplitude oscillation is still present but is now entangled with a higher amplitude oscillation located in the Poincaré section. This behavior seems to arise as the two instability generating mechanisms are operating simultaneously in an

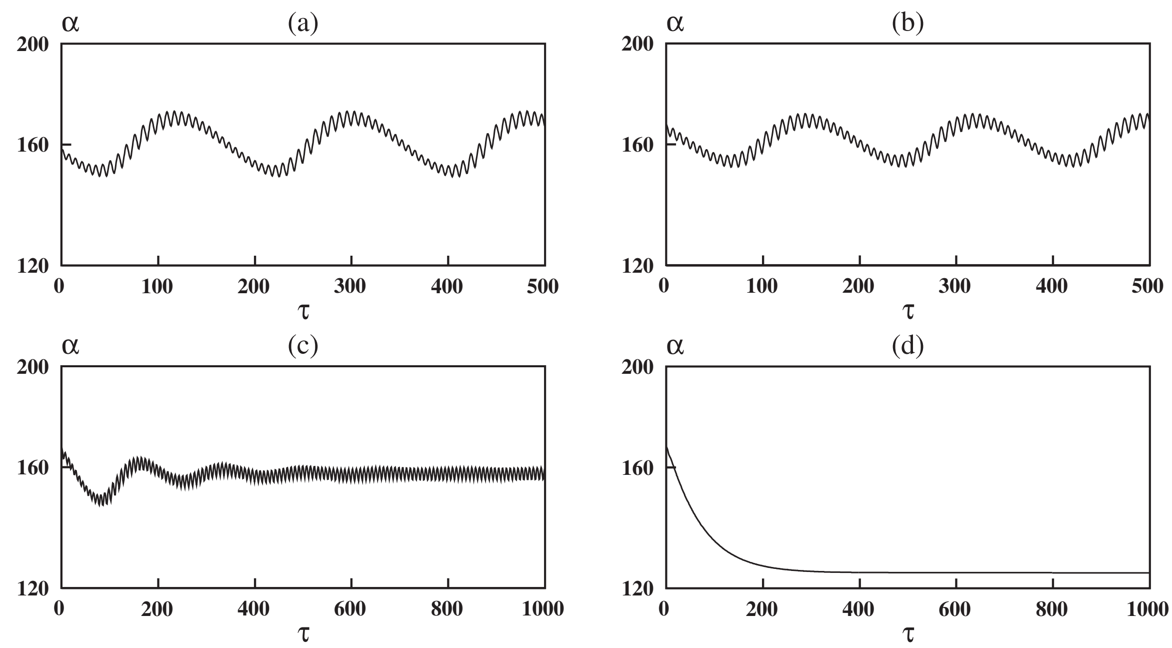

Fig. 6.5: The effect of a slow allosteric transition on the quasi-periodic oscillations. The plots show the behavior of the integral solution of α for (a): $\varepsilon = 10^{-11}$, (b): $\varepsilon = 10^{-10}$, (c): $\varepsilon = 10^{-9}$ and (d): 10^{-8}.

oscillatory mode, with the low amplitude oscillation arising from the second auto-catalytic feedback loop. In the region of bursting oscillations discussed above, the two auto-catalytic loops coupled through changes in the flow of β_1 and the second enzyme operated in an oscillatory fashion when the catalytic activity of the first enzyme was sufficiently large. In the quasi-periodic region, the conversion of α to β_1 is high at all times, and the flow of β_1 to the second enzyme is such that the second enzyme operates in an oscillatory mode. The mean value in β_1 is for the oscillations in Fig. (6.5a) about 250 (not shown). The high amplitude oscillations introduced as the first enzyme starts to oscillate independently do not affect the catalytic activity of the second enzyme as the catalytic activity of the first enzyme remains sufficiently high during the slow oscillations in the Poincaré section.

In Fig. (6.5b) the value of ε is increased to 10^{-10}. The amplitude of the slow oscillation regulated by the first auto-catalytic feedback is slightly lower than the amplitude for $\varepsilon = 10^{-12}$ and its period is increased slightly. The fast, low amplitude oscillations regulated by the second auto-catalytic loop seem unchanged and the two instability generating mechanisms do not appear to be strongly correlated in this region of parameter space. When $\varepsilon = 10^{-9}$ the torus is replaced by a fast oscillating periodic orbit solution as shown in Fig. (6.5c) as the slow oscillation in the Poincaré section of the fast oscillation becomes unstable. Choosing an initial condition close to the unstable torus, the phase trajectory converges to the stable periodic solution which initially follows the shape of the torus. At this value of ε the first enzyme does not operate in an oscillatory mode as the slow allosteric transition can not support oscillatory behavior. When $\varepsilon = 10^{-8}$, the system converges toward a stable steady state with a steady state value of α at about 125, as shown in Fig. (6.5d). Numerical investigations, which have not been included here, show that the transition from the rapid oscillations observed at $\varepsilon = 10^{-9}$ to the steady state observed at $\varepsilon = 10^{-8}$ takes place through a super-critical Hopf bifurcation at $\varepsilon = 5.25 \cdot 10^{-9}$.

6.4.3 Chaotic Oscillations

When $\varepsilon = 10^{-9}$ and $\nu = 0.224$ the system shows chaotic oscillations as outlined in Fig. (6.6a) and which is also reported in the non-normalized original version of the truncated model (Decroly & Goldbeter, 1982). The level of α ranges from a minimum at about 10 to a maximum just below 60. When $\varepsilon = 10^{-8}$, the system has escaped the chaotic region of parameter space and the chaotic attractor is replaced by a limit cycle. As shown in Fig. (6.6b), the limit cycle that replaces the chaotic attractor produces bursting oscillations similar to those observed in Fig. (6.4). When $\varepsilon = 10^{-7}$ the limit cycle depicted in Fig. (6.6)c still produces bursts but the bursts can only be seen in the integral solutions of β_1 and β_2.

The bursts are not reflected in the level of α because the slow allosteric transition does not allow the enzyme to change activity sufficiently fast when β_1 has bursting behavior. At $\varepsilon = 10^{-4}$, no bursting is observed in neither α nor β_1 similar to the behavior for $\nu = 0.2$ and $\varepsilon = 10^{-4}$ depicted in Fig. (6.4d).

6.5 From Complex to Simple Behavior

In the previous sections, the effect of a slow allosteric transition was discussed in some detail for three different complexes of oscillations types; bursting, quasi-periodicity and chaos. Of these three phenomena, quasi-periodicity showed the highest sensibility towards a slowed allosteric transition as the attractor changes from a torus to a simple limit cycle when ε is changed from 10^{-10} to 10^{-9}. The chaotic oscillations also shows sensibility toward increased ε, and for $\nu = 0.224$ chaos is not observed when $\varepsilon \lesssim 10^{-9}$. Instead, a bursting oscillation is observed. The bursting type oscillations seems to be more robust toward a slow allosteric transition than the chaotic and quasi-periodic oscillations. The transition from bursting oscillations to simple periodic behavior is smooth and cannot be detected

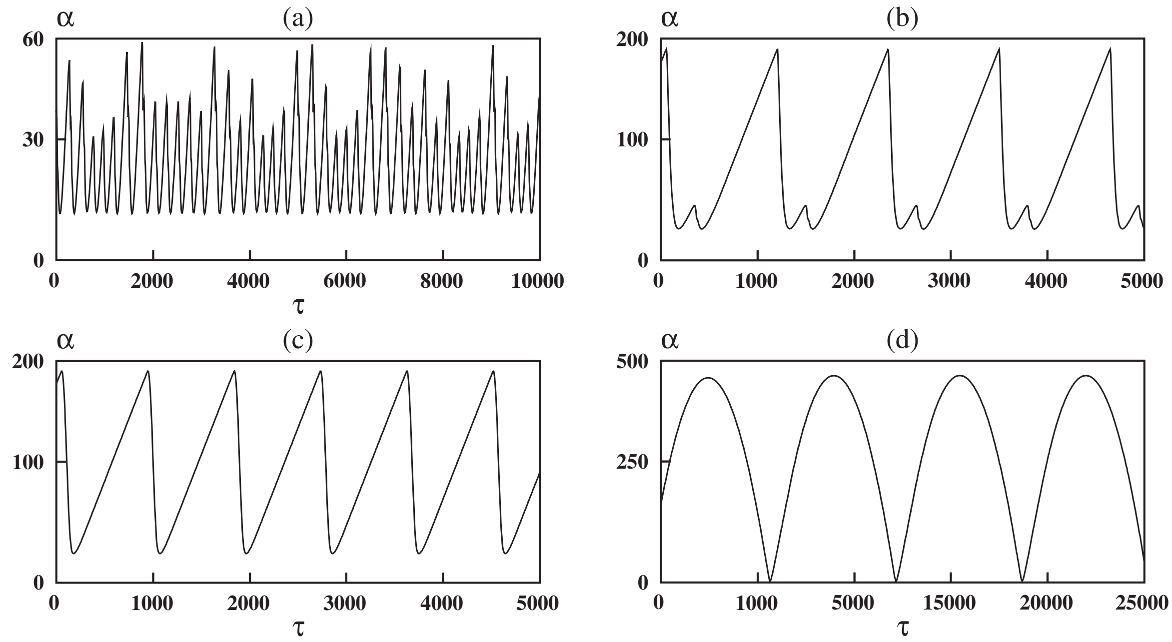

Fig. 6.6: The effect of a slow allosteric transition on the chaotic behavior observed for $\varepsilon = 10^{-12}$ and $\nu = 0.224$. The behavior of α is recorded at different values of ε such that $\varepsilon = 10^{-9}$ in (a), $\varepsilon = 10^{-8}$ in (b), $\varepsilon = 10^{-7}$ in (c) and $\varepsilon = 10^{-4}$ in (d).

by evaluation of the Floquet multipliers. However it is apparent from Fig. (6.4) and Fig. (6.6) that bursting oscillations are also inhibited by a slow allosteric transition.

In Fig. (6.7) the result of a two-dimensional bifurcation analysis in ν and ε is presented to discuss the effect of a slow allosteric on all the different dynamic behaviors observed in the one-dimensional bifurcation diagram in Fig. (6.1). The different behaviors will be discussed in order of appearance for increased ν. At very low values of ν, the steady state solution is stable for all values of ε. The transition through a super-critical Hopf bifurcation to the region where bursting oscillations are observed is located at such a low value of ν that it coincides with the ε-axis. As discussed above, the transition from bursting oscillations to simple oscillations is smooth and is not detectable through the investigation performed here. However, by examination of the integral solutions presented in Fig. (6.4) and Fig. (6.6) one may be convinced that the emergence of bursting oscillations is inhibited by a slow allosteric transition, and it is therefore likely that the oscillations are of a simple type, or at least appear smooth, when ε is above about 10^{-7}. The dark shaded region labeled "Period-Doubling" in Fig. (6.7)

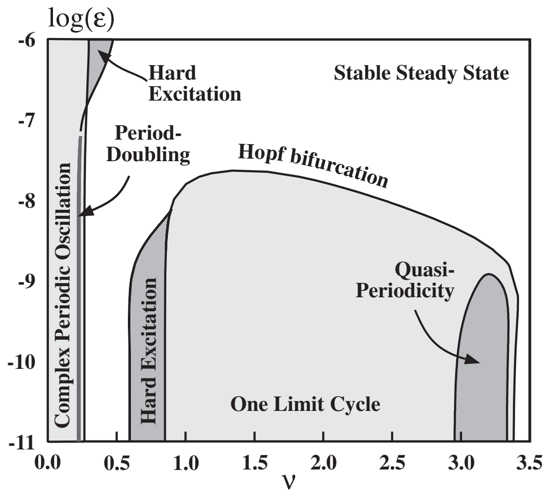

Fig. 6.7: Two-dimensional bifurcation diagram in ν, ε showing the interdependence of the emergence of simple and complex non-steady behavior and the rate of the allosteric transition. When the parameter ε associated with the rate of the allosteric transition is below 10^{-8}, non-steady behavior is dominant with only a narrow range where the stady state solution is stable. When $\varepsilon < 10^{-8}$ a wide range of nonlinear behaviors can be observed including chaos, bursting, quasi-periodicity, birhythmicity and hard excitation. The transition from bursting to simple oscillation is smooth and not detectable by examination of the Floquet multipliers. The chaotic oscillations are confined to the region outlined by the location of the first period-doubling bifurcation. The region of birhythmicity lies close to the period-doubling and has been omitted for clarity. When $\varepsilon > 10^{-8}$ most of these phenomena cannot be observed and the bifurcation diagram is dominated by a stable steady state solution. When $\varepsilon > 10^{-8}$ non-steady behavior occurs only for $\nu < 0.5$ but only simple periodic behavior and hard excitation is observed. A slow allosteric transition is thus a potent inhibitor of the emergence of complex behavior in enzyme reaction systems composed of auto-catalytic oligomeric enzymes.

outlines the location of the first period-doubling bifurcation of the limit cycle LC_3 in Fig. (6.2). The existence of chaotic oscillations is not guaranteed in this region but will, if present, be confined to this region. From the observations made in Fig. (6.6) it seems unlikely that chaos exists at values of ε below at least 10^{-8}. Just above the dark shaded region that outlines the location of the period-doubling bifurcation, a full line is drawn. This line represents the location of a saddle-node bifurcation of the periodic solution and is associated with birhythmicity and hard excitation. When the ε is below about 10^{-7}, where the saddle-node bifurcation overlaps the shaped region, there is a narrow region where the system has birhythmic behavior. This region has been omitted for clarity. When i. $\varepsilon > 10^{-7}$, the saddle-node bifurcation overlaps with the region of a stable steady state solution and the system has, in the labeled region, a phenomena of hard excitation. Hard excitation is also observed when $\varepsilon = 10^{-12}$ and ν is between 0.594 and 0.850 as written in Tab. (6.2). When ε exceeds 10^{-9} this region starts to contract and is vanishing at about $\varepsilon = 10^{-8}$. The boundary labeled "Hopf bifurcation" in Fig. (6.7) outlines a super-critical Hopf bifurcation where the low amplitude rapid periodic solution observed in the light shaded region is destroyed and the steady state becomes stable. Inside the light shaded region, there exists a region where a torus is stable. In Fig. (6.5) it was observed that the torus becomes unstable somewhere between $\varepsilon = 10^{-10}$ and $\varepsilon = 10^{-9}$ when $\nu = 3.0$. In Fig. (6.7) it is observed that the torus bifurcation does not occur before ε is above 10^{-9} when ν is approximately 3.2. The emergence of aperiodic oscillations (i.e. chaotic and/or quasi-periodic oscillations) thus seem impossible when ε is higher than 10^{-9}. When ε is above approximately 10^{-8} the bifurcation diagram in Fig. (6.7) is dominated by a stable steady state solution and dynamic behavior more complex than a simple limit cycle and hard excitation is not possible.

The dimensionless parameter ε represents the ratio of first order constant k_{tb} associated with the transition from the active R-form of E_1 to the inactive T-form and the first order rate constant k_{out} associated with removal of the second product P_2. When the inverse of k_{out} is of the order of seconds, as in the original investigations (Decroly & Goldbeter, 1982, 1985, 1987), the above results predict that the rate constant for the $R \to T$ transition must be higher than 10^8 $sec.^{-1}$ for complex dynamic behavior to emerge. According to Klonowski (Klonowski, 1983), a quasi-steady state can be assumed a system of the type in Eq. (6.7) when the system is given enough time to reach the singular point of the adjoined system (see Chapter 3). This time is longer than $\tau_c = |\varepsilon \ln(\varepsilon)|$ (Klonowski, 1983) and the enzyme can be assumed in a quasi-steady state when $\tau \gg \tau_c$. By inserting the definitions $\tau = k_{out}t$ and $\varepsilon = k_{out}/k_{tb}$ the critical time reads, in dimensional form,

$$t_c = \frac{\tau_c}{k_{out}} = \frac{|\varepsilon \ln(\varepsilon)|}{k_{out}} = \frac{|\ln(\varepsilon)|}{k_{tb}}, \tag{6.10}$$

which, with the above estimates, yields roughly $t_c = 1.0 \cdot 10^{-7}$ *sec.* This value of t_c is an estimate of the maximum time required for establishment of a quasi-steady state between the states of the allosteric enzyme in order to allow for the emergence of complex dynamic behavior. It has been reported that yeast phosphofructokinase under various *in vitro* conditions establishes a quasi-steady state following an exponential rate law with an apparent first order constant ranging from about 1 $sec.^{-1}$ to about 8 $sec.^{-1}$ (Kurganov, 1981). This corresponds to a half-time of roughly 0.1 *sec.* for establishing a quasi-steady state *in vitro.* There may be objections to the relevance of comparing the two time estimates but the difference it to an extent where it seems reasonable to doubt that the proposed mechanism involving allosteric enzymes can lead to complex dynamic behavior such as chaos and quasi-periodicity *in vivo* as well as *in vitro.*

CHAPTER 7

Kinetic Cooperativity

Mechanisms other than cooperativity between subunits exists that can introduce sigmoidal dependencies in biochemical reaction networks. One of these is the apparent cooperativity observed in monomeric enzymes (Cornish-Bowden & Cárdenes, 1987; Neet, 1995). For obvious reasons cooperativity between subunits cannot be the source of the apparent cooperativity of monomeric enzymes. The apparent cooperativity is to be considered in an operational meaning, and apparent cooperativity arising from a reaction mechanism will here be referred to as *kinetic cooperativity* (Cornish-Bowden & Cárdenes, 1987).

In this chapter, a simple mechanism proposed by Goldbeter and Koshland (Goldbeter & Koshland, 1981, 1982, 1984) that introduces a high degree of kinetic cooperativity is revisited. It will be argued that the mechanism can be associated with an arbitrary high Hill coefficient and, as a limiting case, mimic Heaviside's unit function (see e.g. Speigel, 1994). The Heaviside function is an ideal on-off switch where only the states 0 and 1 are available and is very important in the theoretical studies of networks containing a large number of interacting species (see e.g. Kauffman, 1993). It will also be shown that kinetic cooperativity may give raise to sustained oscillations in a system composed of two Michaelis-Menten enzymes. Moreover, a simple method for threshold modulation is proposed.

7.1 Covalent Modification Mechanism

The covalent modification reaction scheme considered here comprises two monomeric Michaelis-Menten enzymes, denoted E_1 and E_2, which catalyze opposing reactions

$$
\begin{aligned}
W + E_1 &\underset{k_{b1}}{\overset{k_{f1}}{\rightleftarrows}} WE_1 \overset{k_{c1}}{\rightarrow} W^* + E_1 \\
W^* + E_2 &\underset{k_{b2}}{\overset{k_{f2}}{\rightleftarrows}} W^*E_2 \overset{k_{c2}}{\rightarrow} W + E_2
\end{aligned}
\tag{7.1}
$$

where W denotes some target molecule and W^* denotes the covalently modified W (Goldbeter & Koshland, 1981). This reaction scheme is relevant to, for example, opposing kinases and phosphatases which, respectively, add and remove a phosphate from another biological molecule. It is assumed that both modifications are irreversible and the reactions effectively can be considered only to involve one substrate.

7.1.1 Mathematical Description

The reactions in Eq. (7.1) are described using mass action kinetics and the rate equations for the change in the concentrations of W, WE_1, W^* and W^*E_2 are

$$
\begin{aligned}
\frac{d}{dt}[W] &= -k_{f1}[W][E_1] + (k_{b1} + k_{c1})[WE_1] - k_{c1}[WE_1] + k_{c2}[W^*E_2], \\
\frac{d}{dt}[WE_1] &= k_{f1}[W][E_1] - (k_{b1} + k_{c1})[WE_1], \\
\frac{d}{dt}[W^*] &= -k_{f2}[W^*][E_2] + (k_{b2} + k_{c2})[W^*E_2] - k_{c2}[W^*E_2] + k_{c1}[WE_1], \\
\frac{d}{dt}[W^*E_2] &= k_{f2}[W^*][E_2] - (k_{b2} + k_{c2})[W^*E_2]
\end{aligned}
\tag{7.2}
$$

The rate equations are complemented by conservation of total target concentration W^0 and total concentration E_1^0, E_2^0 of, respectively, E_1 and E_2 following

$$
\begin{aligned}
w_T &= [W] + [WE_1] + [W^*] + [W^*E_2], \\
e_1^0 &= [E_1] + [WE_1], \quad e_2^0 = [E_2] + [W^*E_2].
\end{aligned}
\tag{7.3}
$$

The mathematical description used here for the kinetic equations reaction is different from that used by Goldbeter and Koshland. The resulting normalized equations are identical to the previously obtained dimensional equations (Goldbeter & Koshland, 1981). Taking the conservation relations into consideration and defining new dimensionless variables

$$\beta = \frac{[W^*] + [W^*E_2]}{w_T}, \quad \gamma_1 = \frac{[WE_1]}{e_1^0}, \quad \gamma_2 = \frac{[W^*E_2]}{e_2^0}, \quad \tau = t\frac{k_{c2}e_2^0}{w_T}, \tag{7.4}$$

it is by now a standard exercise to obtain the normalized AODE's

$$\begin{aligned} \frac{d\beta}{d\tau} &= \delta\gamma_1 - \gamma_2 \\ \varepsilon_1 \frac{d\gamma_1}{d\tau} &= q_1(1 - \beta - \eta_1\gamma_1)(1 - \gamma_1) - \gamma_1 \\ \varepsilon_2 \frac{d\gamma_2}{d\tau} &= q_2(\beta - \eta_2\gamma_2)(1 - \gamma_2) - \gamma_2. \end{aligned} \tag{7.5}$$

The dimensionless constants are defined by

$$\begin{aligned} &\delta = \frac{V_1}{V_2}, \qquad \varepsilon_1 = \frac{e_1^0 k_{c1}}{w_T K_{m1} k_{f1}}, \qquad \varepsilon_2 = \frac{e_2^0 k_{c2}}{w_T K_{m2} k_{f2}}, \\ &q_1 = \frac{w_T}{K_{m1}}, \qquad q_2 = \frac{w_T}{K_{m2}}, \qquad \eta_1 = \frac{e_1^0}{K_{m1}}, \qquad \eta_2 = \frac{e_2^0}{K_{m2}}, \end{aligned} \tag{7.6}$$

where V_1, V_2 and K_{m1}, K_{m2} denote the maximum velocity and the Michaelis-Menten constant of, respectively, E_1 and E_2.

The structure of the AODE's in Eq. (7.5) allows for simplification through Tihonov's Second Theorem when ε_1 and ε_2 are small. The rate equations of γ_1 and γ_2 are uncoupled and the order at which ε_1 and ε_2 goes toward zero is not of importance as long both goes to zero (see Chapter 2). The reduced model obtained when the enzyme concentrations are low compared to the Michaelis-Menten constants and the terms involving η_1 and η_2 are negligible, is rather simple and the investigation of the simplified model will here be limited to this case. When $\varepsilon_1 \to 0$ and $\varepsilon_2 \to 0$ one obtains the quasi-steady state relations

$$\gamma_1 = \frac{q_1(1-\beta)}{1 + q_1(1-\beta)}, \qquad \gamma_2 = \frac{q_2\beta}{1 + q_2\beta}, \tag{7.7}$$

which can easily be shown to be stable by evaluation of the adjoined system describing the dynamics on the fast time-scales τ/ε_1 and τ/ε_2. Inserting the quasi-steady state values in Eq. (7.7) into Eq. (7.5), the covalent modification mechanism can be described by the single equation

$$\boxed{\frac{d\beta}{d\tau} = \frac{\delta q_1(1-\beta)}{1 + q_1(1-\beta)} - \frac{q_2\beta}{1 + q_2\beta}.} \tag{7.8}$$

7.1.2 Zeroth Order Ultra-sensibility

One can, when assuming that β is in a quasi-steady state, express the amount of covalently modified target, symbolized through β, as a function of the δ. The dimensionless parameter δ expresses the ratio of maximum velocity of the modifying enzymes E_1 and E_2. Setting the left hand side of Eq. (7.8) to zero one obtains the algebraic equation

$$(\delta - 1)\beta^2 - \left[\delta - 1 - \left(\frac{1}{q_1} + \frac{\delta}{q_2}\right)\right]\beta - \frac{\delta}{q_2} = 0 \tag{7.9}$$

which solves to

$$\beta = \frac{\phi + \sqrt{\phi^2 + 4(\delta - 1)\delta/q_2}}{2(\delta - 1)}, \tag{7.10}$$

where

$$\phi = \delta - 1 - \left(\frac{1}{q_1} + \frac{\delta}{q_2}\right). \tag{7.11}$$

The steady state concentration of covalently modified target enzyme is determined by the three parameters q_1, q_2 and δ in Eq. (7.10). These parameters can be subjects of biological regulation. The values of q_1 and q_2 can be altered through regulation of the total target concentration or by modulation of the Michaelis-Menten constants, for example through non-competitive inhibition. The ratio of maximal catalytic activity δ may be regulated by modulation of the activities of the enzymes. This can be mediated through activators/inhibitors or through synthesis/degradation. The values of q_1, q_2 and δ where the system switches from a state where non-modified target is dominating to a state where the level of modified enzyme W^* exceeds the level of W can be found by setting $\beta = 0.5$ in Eq. (7.10) and solving with respect to the parameter of interest. This way one obtains the threshold value in δ

$$\delta_{tr} = \frac{q_2(q_1 + 2)}{q_1(q_2 + 2)}. \tag{7.12}$$

In Fig. (7.1) the relative steady state level of modified target molecule β as predicted by Eq. (7.10) for varied δ is drawn with full lines. The values of q_1 and q_2 are for simplicity assumed to be equal and the threshold occurs from Eq. (7.12) at $\delta = 1.0$. When q_1 and q_2 are low, the steady state value of β follows δ as a hyperbolic curve similar to a Michaelis-Menten rate law. As q_1 and q_2 increases, the curve in Fig. (7.1) becomes increasingly sigmoidal.

The kinetic cooperativity observed in the covalent modification reaction mechanism has been coined *zeroth-order ultra-sensibility* (Goldbeter & Koshland, 1981). This seemingly peculiar name has been introduced because the sharp transition occuring for high values of q_1 and q_2 corresponds to an increased sensitivity in a biological signaling pathway as compared to the hyperbolic Michaelis-Menten rate law. High values of q_1 and q_2 indicate that the total concentration of target molecule is high compared to the Michaelis-Menten constants. In Michaelis-Menten terminology a high substrate level relative as to the Michaelis-Menten constant corresponds to a situation where an enzyme is saturated by its substrate and converts substrate into product at a constant rate (i.e. following zeroth order kinetics). Zeroth-order ultra-sensibility was introduced by Goldbeter and Koshland in the early 1980s (Goldbeter & Koshland, 1981, 1982) in response to investigations of Michaelis-Menten enzymes operating in the region of first-order kinetics. Since then, the covalent modification mechanism has been applied to abstract models of biochemical oscillators (Goryanin *et al.*, 1992; Dupont & Goldbeter, 1992; Goldbeter, 1996), to the behavior in biological signaling pathways (Goldbeter & Koshland, 1984; Erneux *et al.*, 1993; Huang & Ferrell, 1996; Ferrell, 1996), to the arising of thresholds in biological systems (Goldbeter & Wolpert, 1990; Goldbeter & Guilmot, 1996), to computational functions in biological systems (Arkin & Ross, 1994; Bray, 1995) and in models of the cell cycle (Goldbeter, 1991; Novak & Tyson, 1993a,b; Romond *et al.*, 1994; Novak & Tyson, 1995; Tyson *et al.*, 1996).

Fig. 7.1: Kinetic cooperativity in the covalent modification mechanism. The relative amount of covalently modified target molecule, denoted β, as a function of the ratios of maximum velocities, denoted δ, of the opposing Michaelis-Menten enzymes E_1 and E_2. The dimensionless parameters q_1 and q_2 representing the ratios of total concentration of target w_T to the Michaelis-Menten constants of E_1 and E_2 are taken to be equal with the value indicated at each curve. β is a hyperbolic function of δ for low values of q but becomes more and more sigmoidal as q increases.

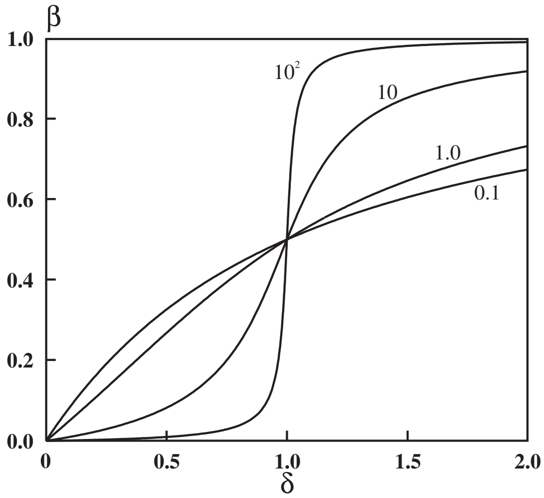

7.2 Oscillations in Monomeric Enzymes?

The high nonlinearity observed in the covalent modification reaction mechanism led to the suspicion that sustained oscillatory behavior may emerge in an open system with product feedback. Consider the reaction scheme

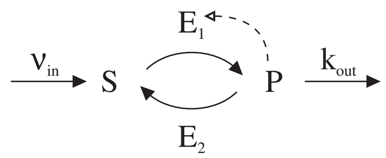

where the enzymes E_1 and E_2 are opposing Michaelis-Menten enzymes catalyzing a covalent modification of, respectively, S and P. The covalently modified target P is considered a ligand that through binding to E_1 can alter the activity of the enzyme. The molecular mechanism, which is discussed in detail in Appendix A, involves the binding of product to either the enzyme -substrate complex between E_1 and S or binding directly to E_1. The binding reactions are associated with two distinct dissociation constants denoted K_l and K_l' for dissociation of product from, respectively, the enzyme-effector complex and the enzyme-substrate-effector complex. As the modulation of the activity of E_1 may operate through binding of P in a binding site that is not located in the active site the reaction mechanism can be considered as a case of allosteric regulation. The regulation mechanism is, however, different from the allosteric mechanism discussed in Chapter 5 as cooperativity between subunits is not involved. The reaction system depicted above is open to the surroundings and substrate is supplied constantly with a rate given by v_{in} whereas the product is removed proportionally to the first order rate constant k_{out}.

7.2.1 Truncated Kinetic Equations

The covalent modification mechanism discussed in the previous sections of this chapter was assumed to take place in a closed system in which the total level of target molecule can be considered to be constant. When the system is open to the surroundings, the total target concentration is not appropriate to normalization as the total target concentration is no longer constant. Instead, the dimensionless variables

$$\alpha = \frac{[W]}{K_{m1}}, \qquad \beta = \frac{[W^*]}{K_l'}, \qquad \tau = tk_{out}, \tag{7.13}$$

will be employed. In Appendix A, it is shown through a detailed analysis of the mass action kinetic rate equations, that the dimensionless catalytic rate, with respect to removal of substrate, for a Michaelis-Menten enzyme subject to binding of a effector ligand is described by (see Eq. (A.30))

$$\frac{\sigma_1 \alpha(1+\delta\beta)}{(1+\rho\beta)+\alpha(1+\beta)}, \tag{7.14}$$

when the enzyme concentration is sufficiently low and the product dissociation is a fast equilibrating reaction. With the choice of normalized variables in Eq. (7.13) the dimensionless parameters in Eq. (7.14) are

$$\sigma_1 = \frac{k_{c1} e_1^0}{K_{m1} k_{out}}, \qquad \delta = \frac{k_{c2}}{k_{c1}}, \qquad \rho = \frac{K_l'}{K_l}. \tag{7.15}$$

The catalytic activity of the second enzyme E_2 that converts product into substrate is described by standard Michaelis-Menten type kinetics. The rate of substrate formation due to the action of E_2 can, when the dimensionless variables are as defined in Eq. (7.13), be written

$$\frac{\sigma_2 \beta}{K+\beta}, \tag{7.16}$$

where

$$\sigma_2 = \frac{k_{c2} e_2^0}{K_{m1} k_{out}}, \qquad K = \frac{K_{m2}}{K_l'}. \tag{7.17}$$

Taking into account the different normalizations of substrate and product in Eq. (7.13) by defining $q = \frac{K_{m1}}{K_l'}$ and defining the dimensionless flow parameter $\nu = v_{in}/K_{m1}/k_{out}$, the reaction system can be described by the rate equations

$$\begin{aligned} \frac{d\alpha}{d\tau} &= \nu - \frac{\sigma_1 \alpha(1+\delta\beta)}{(1+\rho\beta)+\alpha(1+\beta)} + \frac{\sigma_2 \beta}{K+\beta}, \\ \frac{d\beta}{d\tau} &= \frac{q\sigma_1 \alpha(1+\delta\beta)}{(1+\rho\beta)+\alpha(1+\beta)} - \frac{q\sigma_2 \beta}{K+\beta} - \beta. \end{aligned} \tag{7.18}$$

7.2.2 Phase Plane Analysis

The two-dimensional model in Eq. (7.18) is too complex for an analytic investigation of conditions needed for the emergence of sustained oscillatory behavior, as the total target concentration, which ensures a high sigmoidal function in a closed system without feedback, does no longer appear in the rate equations. A good place to start when searching for parameters where oscillations may occur is, in a two-dimensional system, to evaluate the nullclines, as sustained oscillations typically occur if the steady state (i.e. the intersection between the nullclines) are in a region where one of the nullclines is repelling. The β-nullcline of Eq. (7.18) is the curve $\beta^*(\alpha)$ obtained by solving

$$\frac{q\sigma_1\alpha(1+\delta\beta)}{(1+\rho\beta)+\alpha(1+\beta)} - \frac{q\sigma_2\beta}{K+\beta} - \beta = 0 \tag{7.19}$$

with respect to β. Here, the shape and stability of the β-nullcline is determined by numerical continuation of the steady state solution of the one-dimensional rate equation

$$\frac{d\beta}{d\tau} = \frac{q\sigma_1\alpha(1+\delta\beta)}{(1+\rho\beta)+\alpha(1+\beta)} - \frac{q\sigma_2\beta}{K+\beta} - \beta \tag{7.20}$$

where α is taken as a bifurcation parameter. The β-nullcline, which is independent of ν, is drawn with heavy lines in Fig. (7.2b) for $\sigma_1 = 10$, $\sigma_2 = 10$, $\delta = 10$, $\rho = 0.1$, $q = 0.1$ and $K = 10^{-4}$. The β nullcline is N-shaped and the one-dimensional equation in Eq. (7.20) undergoes a bifurcation where the single eigenvalue passes zero (a saddle-node bifurcation) when α passes the critical points indicated in Fig. (7.2b). Between the two bifurcation values in α the β-nullcline is repelling. The unstable β-nullcline is indicated by the broken heavy line. If the α-nullcline intersects the β-nullcline in the unstable region, the steady state solution of Eq. (7.18) will be unstable and sustained oscillations will typically emerge. The α-nullcline $\alpha^*(\beta)$ is obtained by steady state continuation of the one-dimensional rate equation

$$\frac{d\alpha}{d\tau} = \nu - \frac{\sigma_1\alpha(1+\delta\beta)}{(1+\rho\beta)+\alpha(1+\beta)} + \frac{\sigma_2\beta}{K+\beta}, \tag{7.21}$$

where β is taken as a parameter. The α nullcline is dependent on ν and the location of the α-nullcline in phase space can thus be altered when varying ν. The α-nullcline is drawn with thin lines in Fig. (7.2b) for three different values of ν.

When ν and β are both small the α-nullcline and β-nullclines are very close in phase space. This is expected as the rate equations for α and β in Eq. (7.18) will be almost proportional with q being the proportionality factor. For $\nu = 0.1$ the α-nullcline intersects the β-nullcline in the steady state point labeled 1 in Fig. (7.2b). This steady state solution is located before the saddle-node bifurcation in Eq. (7.20) and is a stable steady state. The convergence of a phase plane trajectory originating from the point $\alpha = 1.0$, $\beta = 0.001$ to the steady state solution labeled 1 in Fig. (7.2) is drawn with dotted lines. When $\nu = 1.0$ the shape of the α-nullcline is changed as compared to the shape predicted when $\nu = 0.1$ and the steady state, labeled 2 in Fig. (7.2b), has moved into the region where the β-nullcline is unstable. A stable limit cycle has been created with a location in the phase space outlined by dotted lines forming a closed trajectory around the unstable steady state. The integral solution of Eq. (7.18) for this point of parameter space is shown in Fig. (7.2) where the oscillatory solution of α is drawn with a heavy line and the level of β with thin lines. The oscillation is shown on a logarithmic scale as α oscillates at a level significantly higher than the level of β. When $\nu = 25$, the steady state labeled 3 in Fig. (7.2b) is located outside the unstable region of the β-nullcline and the steady state is stable. The convergence to this steady state is illustrated by the phase plane trajectory originating from the point $\alpha = 100$, $\beta = 1.0$ in the phase plane.

It is quite interesting that sustained oscillations may occur in a system involving only two Michaelis-Menten enzymes. A reconstructed open biochemical reaction system containing phosphofructokinase, which is indeed oligomeric and

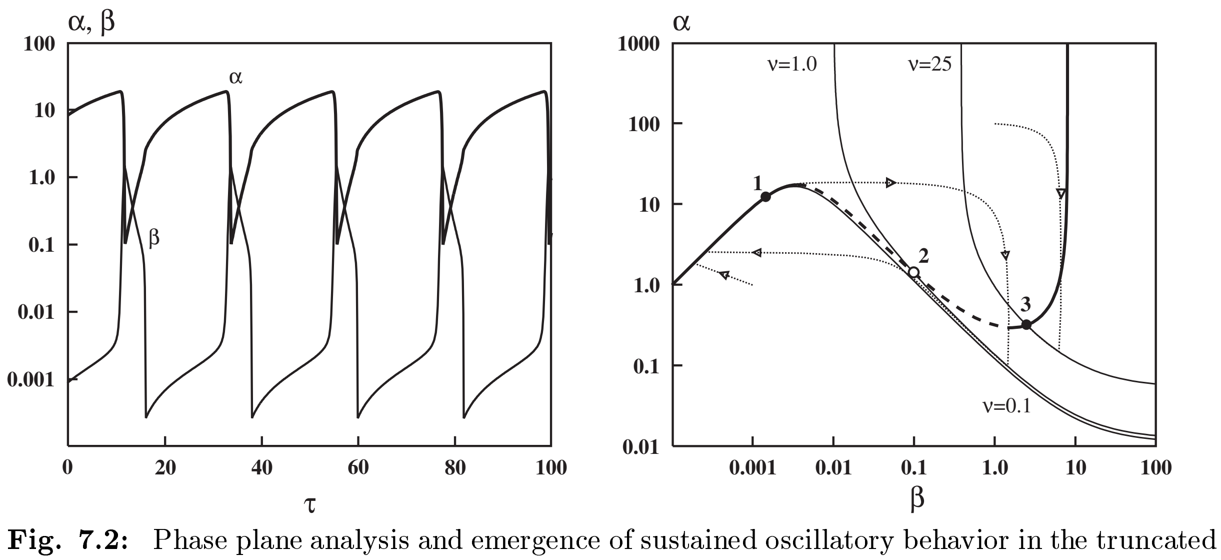

Fig. 7.2: Phase plane analysis and emergence of sustained oscillatory behavior in the truncated system in Eq. (7.18). Plot (a) illustrates the integral solution in α (heavy lines) and β (thin lines) when $\nu = 1.0$, $\sigma_1 = 10$, $\sigma_2 = 10$, $\delta = 10$, $\rho = 0.1$, $q = 0.1$ and $K = 10^{-4}$. Plot (b) shows location of the α- and β-nullclines for varied values of ν. The β-nullcline is drawn with a full heavy line when stable and with a broken line when unstable. Sustained oscillations are observed when the α-nullcline intersects the β-nullcline in the unstable region.

auto-catalytic, show hysteresis (i.e. bistability) but not sustained oscillations (Eschrich *et al.*, 1980). Sustained oscillations are reported when the reaction system contains the enzyme fructose 1,6-bisphosphatase (Eschrich *et al.*, 1983). Whereas phosphofructokinase adds a phosphate to fructose-1-phosphate the enzyme fructose 1,6-bisphosphatase removes this phosphorylation and operates in opposition to phosphofructokinase. Taken together, the two enzymes comprise a case of opposing covalent modification and the fact that sustained oscillations are not observed when phosphofructokinase is not opposed by the action of fructose 1,6-bisphosphatase suggests that the oscillations observed in glycolysis may arise from kinetic cooperativity and not the relatively weak cooperativity between the subunits of phosphofructokinase. Moreover, preliminary studies, which are not included here, show that even a spontaneous decomposition of the modified target into unmodified target is sufficient to destabilize the steady state when the rate of decomposition is high. Thus, only one Michaelis-Menten enzyme regulated through allostery is, in principle, required for the emergence of sustained oscillations.

7.3 Modulation of Thresholds

The variation in the level of a messenger is an effective way to trigger a response in a covalent modification reaction. In the covalent modification mechanism the steady state function in Eq. (7.10) was used to find the threshold value of the possible messenger dependent parameter δ. The threshold value δ_{tr} of δ is given by Eq. (7.12) and is a function of q_1 and q_2. This way the threshold δ_{tr} may be modulated by changing the total target concentration through synthesis or degradation or by affecting the Michaelis-Menten constants, for example through, non-competitive inhibition. Modulating the threshold one of these ways is not very effective when q_1 and q_2 are high, as seen from

$$\delta_{tr} = \frac{q_2(q_1+2)}{q_1(q_2+2)} \approx 1, \qquad q_1, q_2 \gg 2. \tag{7.22}$$

The threshold is therefore difficult to modulate if the reaction should have switch-like behavior at the same time (i.e. large values of q_1 and q_2).

Modulation of the threshold value δ_{tr} without affecting the switch-like properties of the covalent modification reaction may be accomplished by introducing a third enzyme E_3 catalyzing the same reaction as E_1. With the introduction of E_3

the mechanism is composed of the reactions

$$\begin{aligned}
W + E_1 &\underset{k_{b1}}{\overset{k_{f1}}{\rightleftarrows}} WE_1 \overset{k_{c1}}{\rightarrow} W^* + E_1, \\
W + E_3 &\underset{k_{b3}}{\overset{k_{f3}}{\rightleftarrows}} WE_3 \overset{k_{c3}}{\rightarrow} W^* + E_3, \\
W^* + E_2 &\underset{k_{b2}}{\overset{k_{f2}}{\rightleftarrows}} W^*E_2 \overset{k_{c2}}{\rightarrow} W + E_2,
\end{aligned} \tag{7.23}$$

which will be referred to as the extended covalent modification reaction. Mass action kinetic equations describing the behavior of the species Eq. (7.23) are

$$\begin{aligned}
\frac{d}{dt}[W] &= -k_{f1}[W][E_1] + (k_{b1}+k_{c1})[WE_1] - k_{f3}[W][E_3] + (k_{b3}+k_{c3})[WE_3] \\
&\quad - k_{c1}[WE_1] - k_{c3}[WE_3] + k_{c2}[W^*E_3], \\
\frac{d}{dt}[WE_1] &= k_{f1}[W][E_1] - (k_{b1}+k_{c1})[WE_1], \\
\frac{d}{dt}[WE_3] &= k_{f3}[W][E_3] - (k_{b3}+k_{c3})[WE_3], \\
\frac{d}{dt}[W^*] &= -k_{f2}[W^*][E_2] + (k_{b2}+k_{c2})[W^*E_2] - k_{c2}[W^*E_2] + k_{c1}[WE_1] + k_{c3}[WE_3], \\
\frac{d}{dt}[W^*E_2] &= k_{f2}[W^*][E_2] - (k_{b2}+k_{c2})[W^*E_2].
\end{aligned} \tag{7.24}$$

It is assumed that the total concentration of target and enzymes are conserved

$$\begin{aligned}
w_T &= [W] + [WE_1] + [WE_3] + [W^*] + [W^*E_2], \\
e_1^0 &= [E_1] + [WE_1], \quad e_2^0 = [E_2] + [W^*E_2], \quad e_3^0 = [E_3] + [WE_3],
\end{aligned} \tag{7.25}$$

where e_3^0 represents the total concentration of E_3. Employing the same dimensionless variables and dimensionless parameters as in Eq. (7.4) and Eq. (7.6) one can obtain the dimensionless equations

$$\begin{aligned}
\frac{d\beta}{d\tau} &= \delta\gamma_1 + \delta' - \gamma_2 \\
\varepsilon_1 \frac{d\gamma_1}{d\tau} &= q_1(1 - \beta - \eta_1\gamma_1 - \eta_3\gamma_3)(1 - \gamma_1) - \gamma_1 \\
\varepsilon_2 \frac{d\gamma_2}{d\tau} &= q_2(\beta - \eta_2\gamma_2)(1 - \gamma_2) - \gamma_2. \\
\varepsilon_3 \frac{d\gamma_1}{d\tau} &= q_3(1 - \beta - \eta_1\gamma_1 - \eta_3\gamma_3)(1 - \gamma_3) - \gamma_3
\end{aligned} \tag{7.26}$$

where

$$\gamma_3 = \frac{[WE_3]}{e_3^0}, \quad q_3 = \frac{e_3^0}{K_{m3}}, \quad \eta_3 = \frac{e_3^0}{w_T}, \quad \varepsilon_3 = \frac{e_3^0 k_{c3}}{w_T K_{m3} k_{f3}}, \quad \delta' = \frac{V_3}{V_2}, \tag{7.27}$$

and K_{m3} and V_3 are, respectively, the Michaelis-Menten constant and the maximal velocity of E_3. Tihonov's second theorem can be applied directly and the reduced system is especially simple when it is assumed that η_1, η_2 and η_3 are negligible. When ε_1, ε_2 and ε_3 all approach zero the quasi-steady state values of γ_1 and γ_2 are given in Eq. (7.7) whereas the quasi-steady state value of γ_3 is

$$\gamma_3 = \frac{q_3(1-\beta)}{1+q_3(1-\beta)}. \tag{7.28}$$

The singular points of the first, second and third adjoined systems can easily be shown to be stable and the reduced, third degenerate, system reads

$$\boxed{\frac{d\beta}{d\tau} = \frac{\delta q_1(1-\beta)}{1+q_1(1-\beta)} + \frac{\delta' q_1(1-\beta)}{1+q_1(1-\beta)} - \frac{q_2\beta}{1+q_2\beta}.} \tag{7.29}$$

The rate equation for β can be rearranged

$$\frac{d\beta}{d\tau} = \frac{\delta q_1(1-\beta)}{1+q_1(1-\beta)}\left[1+\frac{\delta' q_3(1+q_1(1-\beta))}{\delta q_1(1+q_3(1-\beta))}\right] - \frac{q_2\beta}{1+q_2\beta}. \tag{7.30}$$

The term in square brackets equals $1+\delta'/\delta$ when $q_3 = q_1$ and the threshold value δ_{tr} in δ is thus

$$\delta_{tr} = 1 - \delta', \tag{7.31}$$

if also $q_1 = q_2$. The modulation of the threshold is illustrated in Fig. (7.3) for an extended covalent modification reaction with a high degree of kinetic cooperativity. The values of q_1, q_2 and q_3 in the steady state curves depicted in Fig. (7.3) are equal and chosen to be 100. The kinetic cooperativity is therefore associated with a Hill coefficient of 51.0 predicted in Fig. (7.4). The threshold value δ_{tr} in δ where the system switches from a state where a mono-modified target dominates to a state where most of the target is covalently modified, follows the predictions made by Eq. (7.31), and δ_{tr} decreases when δ' increases. The modulation of the threshold occurs without any change in switch-like behavior of the reaction system. When δ' exceeds 1.0 the threshold in δ is vanishing as the catalytic activity of E_3 is sufficient to give a steady state value of β that exceeds 0.5.

7.4 Measure of Kinetic Cooperativity

A plausible measure of the ability of a biological system to produce a response ϕ to a stimuli S was provided in the mid-sixties by the *response coefficient* R_S (Koshland *et al.*, 1966) which is defined as the ratio of stimuli that produces a 90% response $S_{0.9}$ to the stimuli that produces 10% reasons $S_{0.1}$. This measure is not appropriate, however, if the response ϕ is not a symmetric function around the stimuli that produces a response of 0.5 (Goldbeter & Koshland, 1982). Another measure is given by the *control strength* C

$$C = \frac{d \ln \phi}{d \ln S} \tag{7.32}$$

(Higgens, 1965; Goldbeter & Koshland, 1982). In the covalent modification mechanism, this measure will correspond to

$$C = \frac{d \ln \beta}{d \ln \delta}. \tag{7.33}$$

There are many different methods for measuring responses in biological systems (Goldbeter & Koshland, 1982) and they are all related to the steepness of the sigmoidal response function. It is proposed here, that a measure of sigmoidal dependency between stimuli δ and response β in Eq. (7.10) is provided by

$$n_h = \frac{d[\ln \beta/(1-\beta)]}{d \ln \delta}. \tag{7.34}$$

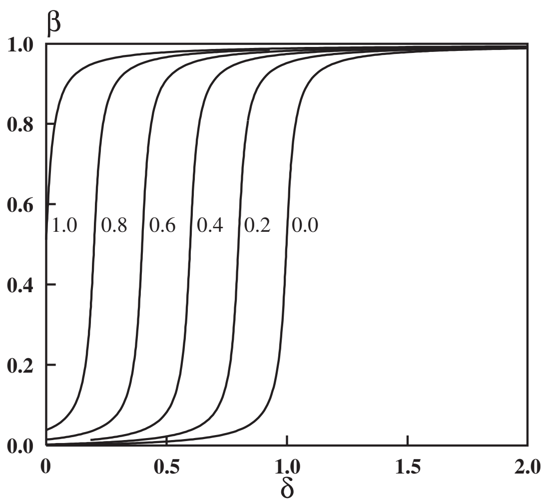

Fig. 7.3: Steady state levels of the covalently modified target molecule W^* predicted by Eq. (7.29) as a function of δ for different values of δ'. The value of δ' is indicated for each curve. The values of q_1, q_2 and q_3 equal 100. When the activity of E_3 is zero, the threshold where W^* switches from the low to the high state occurs at $\delta = 1.0$ as in Fig. (7.1). At increased activities of E_3 (i.e. increasing δ') the threshold in δ is lowered in accordance with Eq. (7.31) and the threshold in δ will be non-existent when δ' is higher than unity. The modulation of the threshold through δ' does not affect the highly switch-like operation of the simple mechanism and offers itself as a way to introduce additional control in biological systems where tight regulation is required.

This measure is obviously inspired by the Hill coefficient of a cooperative oligomeric enzyme and is a reasonable measure when cooperativity is to be considered in the context: "if it looks like cooperativity then it is cooperativity" (quote from Cornish-Bowden & Cárdenes, 1987). An operational Hill coefficient given by Eq. (7.34) offers itself as a link between the traditional definition by enzymologist and the sigmoidal response functions in the theory of biological regulation. Accepting that cooperativity between subunits and kinetic cooperativity are, on the level of overall organization, in fact two sides of the same coin allows for a more comprehensive perspective on biological regulation.

In Fig. (7.4) the Hill plots, $\ln(\beta/(1-\beta))$ versus $\ln(\delta)$, of the steady state function in Eq. (7.10) are drawn with the same values of q_1 and q_2 as in Fig. (7.1). It is noted that the Hill coefficient here is associated with a biochemical signal regulating the maximum activity of at least one of the enzymes and not with the binding of subsequent substrate molecules which is the usual application of the Hill rate law. In the Hill plots in Fig. (7.4) the largest slope determines the Hill constant. The largest slope occurs, as expected, at the threshold value of $\delta = 1$ at $ln(\delta) = 0$. The Hill constant reflecting the kinetic cooperativity is

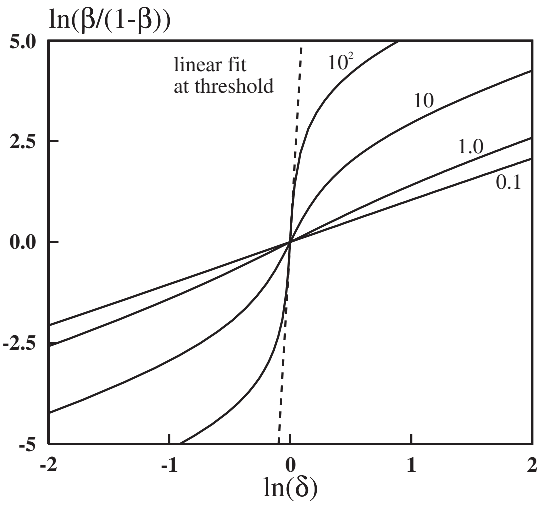

Kinetic Cooperativity

q_1, q_2	n_h	q_1, q_2	n_h
0.01	1.00	10	6.00
0.1	1.05	25	13.5
0.5	1.25	50	25.6
1.0	1.50	100	51.0
2.5	2.25	500	248
5.0	3.50	1000	482
7.5	4.75	10000	2312

Estimates of Hill constants at δ=1

Fig. 7.4: Hill plots and measurement of Hill constants associated with the kinetic cooperativity observed in the covalent modification mechanism. q_1 and q_2 are equal and with the same values as in Fig. (7.1). The broken line illustrates the measurement of the Hill constant when q_1 and q_2 equal 100. The curve is a linear fit to the slope at the threshold $\delta = 1.0$. The table summarizes the Hill constants obtained at a wide range of q_1 and q_2.

estimated by the linear fit

$$n_h \approx \frac{|\ln(M(\delta_2)) - \ln(M(\delta_1))|}{|\ln(\delta_2) - \ln(\delta_1)|}, \qquad M(\delta) = \frac{\beta(\delta)}{1-\beta(\delta)}. \tag{7.35}$$

where δ_1 and δ_2 are chosen in the close neighborhood of the threshold in δ. In Fig. (7.4) the linear estimate of n_h when q_1 and q_2 equal 100 is illustrated with a broken line. The slope of this line corresponds to a Hill constant as high as 51.0. The Hill constants for other values of q_1 and q_2 are summarized in the table presented in Fig. (7.4) where the slope is estimated from the values of β obtained at $\delta_1 = 0.99$ and $\delta_2 = 1.01$. When q_1 and q_2 are below 0.01 the Hill constant is one corresponding to the hyperbolic curve of the Michaelis-Menten rate law. n_h increases slowly though 1.50 at q_1 and q_2 equal to 1.0 and a value of 6.0 at q_1 and q_2 equal to 10. This shows that a significant kinetic cooperativity is present in the system at relatively moderate ratios of total target concentration to the Michaelis-Menten constants. When q_1 and q_2 exceed 10 the Hill constant increases rapidly and becomes as large as 2312 at q_1 and q_2 equal to 10^4. At high values of q_1 and q_2 the transition is practically all or none and for $q_1, q_2 \to \infty$ the covalent modification mechanism mimics Heaviside's unit function.

An important question to address is whether a biological system can actually employ kinetic cooperativity through the covalent modification mechanism. There is no immediate biological reason to reject the covalent modification mechanism based on the requirement of high values of q_1 and q_2. Michaelis-Menten constants are typically of the order of about 10^{-5} M and total target concentrations in the range of 10^{-2} M to 10^{-4} M *in vivo* do not seem unreasonable. The low values of η_1 and η_2 are not unreasonable either, as the total enzyme concentrations may be in the range 10^{-9} M to 10^{-7} M. The value of δ may be under biological control as the ratio of maximal velocities can be altered through allosteric binding following Eq. (7.14) or through synthesis/degradation of the catalyzing enzymes. Criticism can also be directed at the assumptions of steady state and irreversible operation of the enzymes. This questions was addressed in the same publication in which zero-order ultra-sensibility was introduced (Goldbeter & Koshland, 1981) and may have an effect but do not represent a sufficient argument to discard the covalent modification scheme as a plausible mechanism for biological regulation. The Hill coefficients in Fig. (7.4) are undoubtedly overestimates of what occurs *in vivo* due to the assumptions of steady state and irreversible reactions but the mechanism cannot be disregarded based on biochemical or kinetic considerations. Moreover, it is possible that the catalyzing enzymes can be subject to traditional cooperativity between subunits if the enzymes are oligomeric. In that case, δ may be a nonlinear function of a signal and not be linear as in Fig. (7.4). Moreover, in phosphorylation cascades, where several covalent modification mechanisms are placed in series (Huang & Ferrell, 1996; Ferrell, 1996), preliminary studies, which are not included here, shows that the kinetic cooperativity is more than additive. The effective kinetic Hill coefficient is, for example, found to be 58.8 in cascade composed of six covalent modification mechanisms in series, each having a kinetic cooperativity of only 3.5 (Kærn, unpublished).

CHAPTER 8

Cell Cycle Regulation

In this chapter a biochemical reaction network that controls the early development of the South African frog *Xenopus leavis* is considered. The investigations are based on a previously proposed comprehensive mathematical model derived from the known biochemical reactions using Michaelis-Menten and mass-action kinetics (Novak & Tyson, 1993a,b). The early development of *Xenopus* is simple compared to higher mammals but dynamic mechanisms of the early development reflect the control mechanism of cell division of all higher organisms. The intensive experimental research of early development in *Xenopus* has made it possible to capture the control mechanism that regulates the activity of MPF (mitosis promoting factor). It has been suggested that the simple reaction network found in *Xenopus* reflects a *universal cell cycle engine* which is the fundamental control mechanism that allowed for periodic activation of MPF and subsequent cell division in the primitive cells from which all higher organisms originate.

8.1 Summary of the Cell Cycle

The general aspects of the cell cycle has been reviewed in detail elsewhere (e.g. Murray & Hunt, 1993) and only the key points needed for reference will be summarized here. The cell cycle of mammalian cells is made up of four subsequent phases denoted as G1, S, G2 and M. The normal state of a mammalian cell cycle is a quiescent resting state called G0, which is normally considered not to be a part of the cell cycle. A mammalian cell leaves its resting state in G0 and enters the S cell cycle in G1 when it receives the proper external signals for growth. During the G1 phase, the cell prepares for DNA replication and the cell mass increases through nutrient uptake followed by protein synthesis. In late G1, at the so-called restriction point, the cell decides whether to commit itself to a full cycle. If the cell does not receive the proper external signals, it is unable to pass the restriction point and the cell cycle arrests in G1. If the cell passes the G1 checkpoint, the cell has then committed itself to enter S phase and replicate its DNA. When the G1 checkpoint is passed, the "master brake" pRB protein complex activates transcription factors which initiate replication of the DNA.

When the DNA has been correctly copied and arranged, the cell enters G2 and prepares to divide. When the DNA is damaged or the DNA replication is not yet completed, the cell arrests in the G2 to M phase transition. If the cell is unable to repair the damage and therefore is unable to pass the G2 checkpoint, the cell activates its self-termination (apoptosis) through the protein encoded by the gene p53. When the G2 checkpoint is passed, the cell continues through G2. At this stage of the cell cycle, all the components required for division are present. Mitosis (M phase) starts when the chromosomes segregate and ends when the cell divides. The activity that regulates the entry into mitosis is called MPF (mitosis promoting factor) which has been found to oscillate during the cell cycle with a maximum activity during mitosis. MPF initiates all the events required for mitosis and it is one of the key regulatory activities of the cell cycle. After successful division, the daughter cell can select to rest in G0, choose alternative cell cycles or proceed through G1 and the restriction point to enter another cell cycle. The G1, S, and G2 phases are collectively called interphase and the cycle for a normal somatic cell may vary from 24 to 96 hours, depending on cell type. In a typical animal cell cycle, G1 lasts 12 hours, S phase lasts 6 hours, G2 6 lasts hours, and mitosis lasts about 30 minutes.

One of the prefered specimens in studies of the cell cycle is the South African frog *Xenopus leavis* because of the rapid synchronous divisions that occur immediately after its egg has been fertilized. In the early development of *Xenopus*, the checkpoints in G1 and G2 are largely suppressed and the regulation of MPF takes place without the feedback that complicates the division of more advanced cells. The *Xenopus* egg does not require any external signals, additional uptake of nutrients or successful DNA replication in order to divide. The oocyte has produced all the components required for division during maturation and fertilization sets off a series of repeated divisions called the early embryonic cell cycles. The first division takes about 75 minutes and is followed by 11 synchronous divisions lasting approximately 30 minutes each. The early stage of development ends with two divisions of increased duration. At this stage in development, called the mid blastula transition (MBT), the S-phase of the cell cycle elongates (Howe & Newport, 1996) and successful DNA replication is necessary for further divisions (Rempel *et al.*, 1995). The proteolytic system that becomes active at the MBT appears to be regulated by a cell autonomous timing mechanism, not by the size of the cell, (Howe & Newport, 1996) but the exact mechanism awaits further study.

8.2 The Cell Cycle Engine

MPF has been found to be a kinase composed of the subunits Cdc2 and cyclin B. The active site is located on the Cdc2 subunit and the kinase activity of Cdc2 depends strongly on association with cyclin B. The cyclin B subunit has a purely regulating function and possesses no catalytic activity. The Cdc2 is often referred to as Cdk1 (cyclin dependent kinase one) and it is the first member of a whole family of cyclin dependent kinases. The cyclin B subunit (or more correctly cyclin B1) is the second member of a large family of cyclins and it is sometimes simply called cyclin. The level of Cdc2 remains constant throughout the early embryonic cell cycles, whereas cyclin B is constantly synthesized but periodically degraded.

The model used in the present investigation is a variant of the comprehensive model by Bela Novak and John Tyson (Novak & Tyson, 1993a,b) which will be referred to as the NT-model. The original publications should be consulted for a detailed background of the model and references. The biochemical reactions constituting the proposed model of cell cycle engine are presented in Fig. (8.1). When cyclin B is synthesized and released to the cytosol, it readily associates with Cdc2 to form a Cdc2-cyclin B heterodimer as illustrated in Fig. (8.1a). The kinase activity of the heterodimer is controlled by phosphorylation of the Cdc2 subunit. The Cdc2 subunit contains the active site and three important regulatory phosphorylation sites: phosphorylation on residues Thr14 and Tyr15 inhibits the activity of the Cdc2-cyclin B complex whereas phosphorylation on residue Thr161 is required for activity. The inhibition is stronger than the activation and only the phosphorylation state, in which Thr161 is phosphorylated and both Thr14 and Tyr15 are unphosphorylated, has significant activity. In *Xenopus leavis*, the two inhibitory sites are phosphorylated simultaneously and only the phosphorylation state of Tyr15 is considered.

The phosphorylation state of the Cdc2-cyclin B complex is controlled by two pairs of opposing kinases and phosphatases. The residue Thr161 is phosphorylated and dephosphorylated by the enzymes CAK and INH. Those activities are constant during the early embryonic cleavages. The phosphorylation state of the residues Thr14 and Tyr15 is regulated by the kinase Wee1 and the phosphatase

Cdc25 as sketched in Fig. (8.1b). Wee1 and Cdc25 themselves are highly regulated phosphoproteins. Phosphorylated Wee1 is inactive and it has been suggested that MPF, directly or indirectly, is responsible for the inactivation of Wee1. MPF is known to directly phosphorylate Cdc25 and the mutual activation of Cdc25 and MPF constitute a well characterized auto-catalytic feedback loop. The extension to the NT-model proposed here is the inclusion of the kinase Cdk2-cyclin E which also acts on Cdc25. The experimental basis for including this kinase is discussed in detail below. Deactivation of MPF at the end of mitosis occurs through decomposition of the MPF heterodimer as the cyclin B subunit is degraded. The inactivation is illustrated in Fig. (8.1c) where the cyclin B subunit is labeled for destruction by the Ubiquitin-conjugating enzyme (UbE) activated indirectly by MPF through the intermediary enzyme IE. In the present scheme, MPF activates IE by phosphorylation and phosphorylated IE (IE-P) activates the Ubiquitin-conjugating enzyme (UbE*) that labels the cyclin B subunit for proteolytic destruction. For simplicity, it is assumed that Ubiquitin labeled cyclin B is degraded independently of its association with Cdc2 and that the Cdc2 subunit immediately loses all phosphates when the Cdc2-cyclin B complex dissociates.

The inclusion of Cdk2-cyclin E activity in the model of the early cell cycles of *Xenopus* is motivated by the recently published experimental results by Guadagno

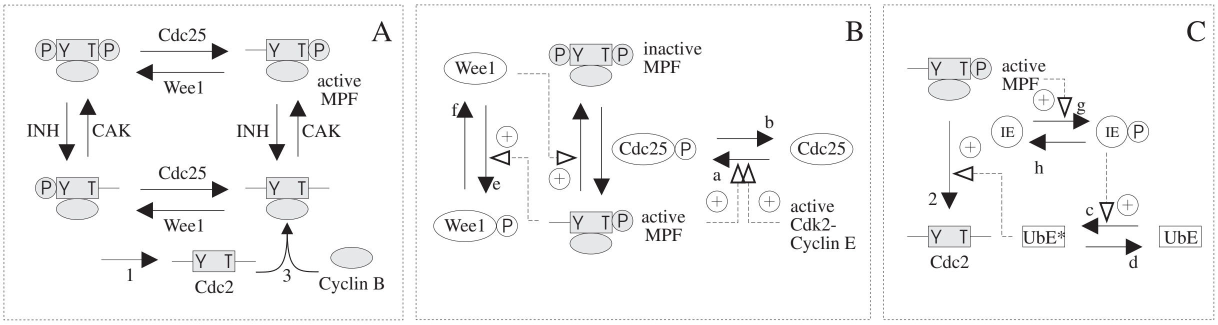

Fig. 8.1: Biochemical reactions of the cell cycle engine. A: Regulation of the Cdc2-cyclin B heterodimer by phosphorylation on the inhibitory Thr14/Tyr15 site and the activating Thr161 residue by the CAK/INH and Wee1/Cdc25 respectively. The heterodimer is formed by association between newly synthesized cyclin B and free Cdc2. B: Regulation of Wee1 and Cdc25. MPF phosphorylates Wee1 directly or indirectly which reduces its catalytic activity. Cdc25 becomes activated upon phosphorylation by either MPF or active Cdk2-cyclin E complex. C: Degradation of the cyclin B subunit through the Ubiquitin pathway. MPF activates the Ubiquitin conjugating enzyme (UbE) indirectly through phosphorylation of the intermediary enzyme IE. The active form of UbE target cyclin B for destruction independent of cyclin B association to Cdc2 and the phosphorylation state of the Cdc2-cyclin B heterodimer.

and Newport (Guadagno & Newport, 1996). In the presented experiments, it was observed that *Xenopus* egg extracts treated with the potent Cdk2 inhibitor Cip1 ($p21^{cip1}$) (Harper *et al.*, 1993) do not enter mitosis. Instead, Cdc2-cyclin B accumulates in the inactive phosphorylated form and the cell cycle is arrested in the G2 to M phase transition. The block to mitosis is reported not to be due to a direct inhibition of MPF by Cip1 or the presence of unreplicated DNA. Restoring Cdk2-cyclin E activity to Cip1-treated extracts reverses the block to mitosis and the immunodepletion of Cdk2 blocks the initiation of mitosis even in the absence of Cip1. The accumulation of Thr14/Tyr15 phosphorylated Cdc2-cyclin B complexes in the absence of Cdk2 activity indicates that the activity of the inhibitory phosphorylation on Thr14/Tyr15 exceeds the activity of the opposing dephosphorylation by Cdc25. On this basis, Guadagno and Newport conclude (Guadagno & Newport, 1996) that the Cdk2-cyclin E complex is a positive regulator of MPF. How then, does Cdk2-cyclin E regulate the phosphorylation state of MPF? In absence of Cip1, Cdc25 becomes phosphorylated well before mitosis while this phosphorylation is completely absent in Cip1 treated extracts (Guadagno & Newport, 1996). Cdc25 has been found to be phosphorylated *in vitro* by Cdk2-cyclin E (Izumi & Maller, 1995) and direct or indirect phosphorylation of Cdc25 by Cdk2-cyclin E could therefore be a plausible mechanism by which Cdk2-cyclin E up-regulates the activating phosphorylation of the Cdc2-cyclin B complex (Guadagno & Newport, 1996).

The activity of Cdk2-cyclin E shows low amplitude oscillations during the cell cycle of *Xenopus* (Gabrielli *et al.*, 1992b). Recently, it has been found that Cdk2-cyclin E *in vivo* peaks twice in each cycle, consistent with a role for Cdk2-cyclin E in both S-phase and mitosis (Hartley *et al.*, 1996). Even though the kinase activity changes during the early cell cycles the total level of Cdk2-cyclin E complex remains constant until the mid-blastula transition where cyclin E is degraded (Hartley *et al.*, 1996; Howe & Newport, 1996).

Cdc25 has been shown to phosphorylate Cdk2 complexes (Gabrielli *et al.*, 1992a) and the Cdk2-cyclin E complex is probably regulated in a manner similar to that controlling the activity of MPF (Hoffman *et al.*, 1994; Pines, 1996). However, the constant cyclin B synthesis and the periodic degradation of cyclin B is responsible for the periodic activity of MPF during early development of *Xenopus* (Murray *et al.*, 1989; King *et al.*, 1996). This is not the case for cyclin E which is not synthesized nor degraded during the embryonic divisions and the Cdk2-cyclin E activity is not controled by dissociation/association of the Cdk2-cyclin E complex (Rempel *et al.*, 1995). Details of the molecular regulation and function of regulation of Cdk2 kinase activity at the S/G2 transition awaits further investigations (Guadagno & Newport, 1996). Meanwhile, it seems reasonable to assume that active Cdk2-cyclin E directly phosphorylates Cdc25 as shown in Fig. (8.1b), and to approximate the low amplitude oscillations by a mean activity. Although the reaction scheme in Fig. (8.1) is undoubtedly very simplistic as compared to the *in vivo* regulation of Cdk2-cyclin E as well as Cdc2-cyclin B and Cdc25 (see e.g. Izumi & Maller, 1995; Lee & Kirschner, 1996, for experiments not included here) the simple model reflects some important features of cell cycle regulation and the simple mechanism for threshold modulation discussed in the previous chapter.

8.3 Mathematical Description

The mathematical description of the reactions in Fig. (8.1) is identical to the method employed in the analysis of the NT-model (Novak & Tyson, 1993a). The reactions in Fig. (8.1a) follow second order mass action kinetics and the velocity of cyclin B synthesis, denoted v_1, is assumed to be constant. The enzymes Cdc25, Wee1, IE and UbE are assumed to be present in two activity states with some basal activity in the least active form. The pseudo first-order rate constants k_{Cdc25}, k_{Wee1} and k_{UbE} associated with the overall activity of these enzymes are then defined as a weighted sum of the activity of the two activity states. The total concentration of Cdc25, Wee1, IE and UbE is assumed to be constant and one activity state is sufficient to keep track of the total activity of these enzymes. The pseudo first-order constants k_{INH} and k_{CAK} are defined the same way as k_{Cdc25}, k_{Wee1} and k_{UbE} but the activity of these enzymes does not change during the early embryonic cell cycles and k_{INH} and k_{CAK} can be taken as constants. Whereas the reactions in Fig. (8.1a) follow mass action kinetics, the reactions in Fig. (8.1b) and Fig. (8.1c) are assumed to follow the Michaelis-Menten rate law. For simplicity, the effect of enzyme sharing is not taken into account.

The set of AODE's describing the rate of change of the species in Fig. (8.1) is written in Tab. (8.1). The subscript on velocity, rate constants and Michaelis-Menten constant refers to the correspondingly labeled reaction in Fig. (8.1). The names of the enzymes are the same except the Cdc2-cyclin B heterodimer, cyclin B and the active Cdk2-cyclin E complex are named HD, cycB and Cdk2. The phosphorylation state or the heterodimer is indicated with superscript P to the left or right for phosphorylation on residue Thr14/Tyr15 and Thr161 respectively. Active Cdc2-cyclin B complex (or HD^P) is simply denoted MPF. The Cdc2 subunit is neither synthesized nor degraded and the total amount of Cdc2 is constant. Mass conservation implies

$$1 = \frac{[HD] + [{}^{P}HD] + [{}^{P}HD^{P}] + [MPF] + [Cdc2]}{[Cdc2]^{T}}, \tag{8.1}$$

where $[Cdc2]^T$ denotes the total concentration of Cdc2, and one of the species composed by a Cdc2 subunit can be expressed in terms of the other four Cdc2-containing species. Therefore, the reaction system can be fully described by nine linear independent rate equations. The concentrations of each enzyme is eliminated by recasting the system with variables that express fractions of the total enzymes instead of variables with units of concentrations. The parameters in the concentration-less description and their basal values are as defined in Tab. (8.2).

The regulation of Cdc25 activity through the combined action of active MPF and active Cdk2-cyclin E corresponds to a covalent modification reaction mechanism where two enzymes operate in parallel. To see this, consider the rate equation for the relative amount of Cdc25 in the covalently modified form (i.e. phosphorylated Cdc25) obtained from Tab. (8.1)

$$\begin{aligned}\frac{d}{dt}\beta =& \frac{k_{a1}[MPF]/[C25]^T(1-\beta)}{K_{a1}/[C25]^T+(1-\beta)} - \frac{v_b\beta}{K_b/[C25]^T+\beta} \\ &+ \frac{k_{a2}[Cdk2]/[C25]^T(1-\beta)}{K_{a2}/[C25]^T+(1-\beta)}\end{aligned} \tag{8.2}$$

where $[C25]^T$ denotes the total concentration of Cdc25 and β denotes the relative level of phosphorylated Cdc25, i.e. $\beta = [C25^P]/[C25]^T$. When $K_{a2} = K_{a1}$, the relative level of more active Cdc25 can be rearranged into

$$\frac{d}{dt}\beta = (\delta+\delta')\frac{q_1(1-\beta)}{1+q_1(1-\beta)} - \frac{v_b q_2\beta}{1+q_2\beta}. \tag{8.3}$$

where

$$q_1 = \frac{[C25]^T}{K_{a1}}, \quad q_2 = \frac{[C25]^T}{K_b}, \quad \delta = \frac{k_{a1}[MPF]}{[C25]^T}, \quad \delta' = \frac{k_{a2}[Cdk2]}{[C25]^T}. \tag{8.4}$$

Eq. (8.3) is similar to Eq. (7.29) obtained for the covalent modification mechanism with two enzymes operating in parallel. In Eq. (7.29) the additional enzyme, represented through δ', acts to modulate the value in δ needed to switch the system into a state dominated by the covalently modified target. Thus, by assuming that Cdk2-cyclin E directly phosphorylates Cdc25, Cdk2 kinase activity acts as a modulater of the threshold in MPF activity needed to shift the relative level of Cdc25 from unphosphorylated to phosphorylated form.

$$\begin{aligned}
\frac{d}{dt}[cycB] =& v_1 - k_{UbE}[cycB] - k_3[cycB][Cdc2] \\
\frac{d}{dt}[HD] =& k_{INH}[MPF] - (k_{Wee1} + k_{CAK} + k_{UbE})[HD] + k_{C25}[^P HD] - k_3 \\
\frac{d}{dt}[^P HD] =& k_{Wee1}[HD] - (k_{C25} + k_{CAK} + k_{UbE})[^P HD] + k_{INH}[^P HD^P] \\
\frac{d}{dt}[^P HD^P] =& k_{Wee1}[MPF] - (k_{INH} + k_{C25} + k_{UbE})[^P HD^P] + k_{CAK}[^P HD] \\
\frac{d}{dt}[MPF] =& k_{CAK}[HD] - (k_{INH} + k_{Wee1} + k_{UbE})[MPF] + k_{C25}[^P HD^P] \\
\frac{d}{dt}[Cdc2] =& k_{UbE}([HD] + [^P HD] + [^P HD^P] + [MPF]) - k_3[cycB][Cdc2] \\
\frac{d}{dt}[C25^P] =& \frac{k_{a1}[MPF]([C25^T] - [C25^P])}{K_{a1} + ([C25^T] - [C25^P])} - \frac{v_b[C25^P]}{K_b + [C25^P]} + \frac{k_{a2}[Cdk2]([C25^T] - [C25^P])}{K_{a2} + ([C25^T] - [C25^P])} \\
\frac{d}{dt}[Wee1] =& \frac{k_e[MPF]([Wee1^T] - [Wee1])}{K_e + ([Wee1^T] - [Wee1])} - v_f[Wee1]K_f + [Wee1] \\
\frac{d}{dt}[IE^P] =& \frac{k_g[MPF]([IE^T] - [IE]^P)}{K_g + ([IE^T] - [E^P])} - \frac{v_h[IE^P]}{K_h + [IE^P]} \\
\frac{d}{dt}[UbE^*] =& \frac{ck_c[MPF]([UbE^T] - [UbE^*])}{K_c + ([UbE^T] - [UbE^*])} - \frac{v_d[UbE^*]}{K_d + [UbE^*]}
\end{aligned}$$

$$\begin{aligned}
k_{C25} &= k'_{C25}([C25^T] - [C25^P]) + k''_{C25}[C25^P] \\
k_{Wee1} &= k'_{Wee1}([Wee^T] - [Wee1]) + k''_{Wee1}[Wee1] \\
k_{UbE} &= k'_{UbE}([UbE^T] - [UbE^*]) + k''_2[UbE^*]
\end{aligned}$$

Tab. 8.1: Mathematical description of the cell cycle engine. HD denotes the Cdc2-cyclin E heterodimer with superscript P on the left for Thr14/Tyr15 phosphorylation and on the right for Thr161 phosphorylation. Cyclin B is denoted by cycB and Cdk2 denotes active Cdk2-cyclin E kinase. In the first six rate equations it is assumed that the reactions obey mass action kinetics with apparent first order rate constants k_{C25}, k_{Wee1}, k_{UbE} and k_3 being the second order rate constant for the irreversible association between free cyclin B and Cdc2. In remaining rate equations it is assumed that the reactions obey the Michaelis-Menten rate law. The total concentrations (denoted by T) of Cdc25, Wee1, IE and UbE are constant and only the most active state of the enzymes needs to be included. As discussed in the text, the Cdk2-cyclin E complex can be assumed to have constant activity during the early embryonic cell cycles of *Xenopus*. The overall catalytic activities of Cdc25, Wee1 and UbE is given through the apparent first order rate constants k_{C25}, k_{Wee1} and k_{UbE} where $'$ and $''$ denotes, respectively, the second order rate constants associated with the most and the least active state of the enzymes.

8.4 Autonomous Oscillations

The arising of autonomous oscillations in the original model is treated in detail elsewhere (Novak & Tyson, 1993a) through the phase plane analysis of a two-dimensional approximation. With the parameters written in Tab. (8.2) the variant model that includes Cdk2-cyclin E is in a region of parameter space where the steady state solution is unstable and a periodic solution is stable. The inclusion of Cdk2-cyclin E as a constant activity is not expected to alter the general dynamic features of the system and it not surprising that autonomous oscillations are indeed observed. The integral solutions of MPF and the inactive double phosphorylated Cdc2-cyclin B complex are shown in Fig. (8.2) where the activity of MPF is drawn with heavy line, whereas the relative concentration of doubly phosphorylated Cdc2-cyclin B complex (inactive MPF) is drawn in a thin line. The broken vertical lines separate the time into regions where the level of inactive MPF increases or decreases and here the lines are used to define two phases of the cell cycle with different general features. In the phase labeled S-phase in Fig. (8.1), the level of inactive MPF is increasing as the activity of the inhibitory Wee1 ki-

Dimensionless parameters

$[Cdk2]/[C25]^T = 0.04$	$K_{a1}/[C25]^T = 0.1$	$K_{a2}/[C25]^T = 0.1$
$K_b/[C25]^T = 0.1$	$K_c/[UbE]^T = 0.01$	$K_d/UbE^T = 0.01$
$K_e/[Wee1]^T = 0.3$	$K_f/[Wee1]^T = 0.3$	$K_g/[IE]^T = 0.01$
$K_h/[IE]^T = 0.01$		

Dimensional conststants (units min^{-1})

$k_1/[Cdc2]^T = 0.0145$	$k_3/[Cdc2]^T = 1.0$	$k'_{C25}[C25]^T = 0.1$
$k''_{C25}[C25]^T = 0.8$	$k'_{Wee1}[Wee1]^T = 0.2$	$k''_{Wee1}[Wee1]^T = 3.0$
$v'_{UbE}[UbE]^T = 0.015$	$v''_{UbE}[UbE]^T = 1.0$	$k_{CAK} = 0.25$
$k_{INH} = 0.025$	$k_{a1}[Cdc2]^T/[C25]^T = 1.0$	$k_{a2}[Cdc2]^T/[C25]^T = 1.0$
$v_b/[C25]^T = 0.1$	$k_c[Cdc2]^T/[UbE]^T = 0.1$	$v_d/[UbE]^T = 0.095$
$k_e[Cdc2]^T/[Wee1]^T = 1.33$	$v_f/[Wee1]^T = 0.1$	$k_g[Cdc2^T]/[IE]^T = 0.65$
$v_h/[IE]^T = 0.087$		

Tab. 8.2: Basal parameters used in the analysis of the early embryonic cell cycles. Most of the parameters are identical to those employed by Novak and Tyson (Novak & Tyson, 1993b) expect minor changes to v_1 and k_b/UbE^T and a change of k'_{C25}, k''_{C25}, k'_{Wee1}, k''_{Wee1} such that the inhibitory phosphorylation of Cdc2-cyclin B dominates in the absence of Cdk2-cyclin E.

nase exceeds that of the activating Cdc25 phosphatase. The cyclin B degradation is low and the level of active MPF is slowly increasing. When the activity of MPF reaches a critical level, the balance between phosphorylation/dephosphorylation of the inhibitory Thr14/Tyr15 residues is switched as the activity of Cdc25 exceeds that of Wee1. The activity of MPF self-amplifying though auto-catalysis with Cdc25 as the stockpiled doubly phosphorylated Cdc2-cyclin B is converted into MPF by Cdc25. This marks the entry into M-phase in Fig. (8.1) where the level of Thr14/Tyr15 phosphorylated Cdc2-cyclin B complexes is decreasing rapidly. The increase in MPF activity in M-phase marks the entry into mitosis where the proteolytic degradation of cyclin B, after a time-lag, is initiated. The Cdc2-cyclin B complexes starts to decompose as the rate of proteolysis increases and the activity of MPF decreases rapidly. When MPF is low, the balance between the activities of Cdc25 and Wee1 favors inhibitory phosphorylation of the Cdc2-cyclin B complex and cyclin B degradation ceases. Inactive MPF starts to accumulate as the system reenters the phase denoted S-phase in Fig. (8.1). This also marks the point where the cell enters a new S phase.

8.5 Absence of Cdk2-cyclin E

Xenopus egg extracts, where Cdk2-cyclin E activity has been depleted or is inhibited, fails to activate MPF (Guadagno & Newport, 1996). The present model may indeed reproduce this observation when the depletion of Cdk2-cyclin E is

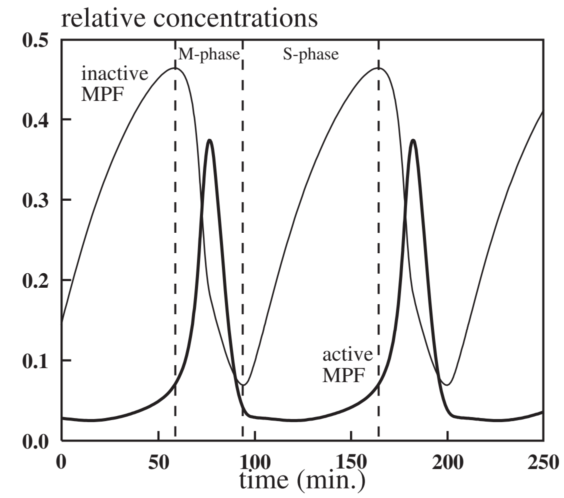

Fig. 8.2: Oscillations in the activity of MPF (heavy line) and the level of double phosphorylated Cdc2-cyclin B (inactive MPF) when the parameters are as defined in table 2. During S phase, the Cdc2-cyclin B complex accumulates in the inactive double phosphorylated form. When active MPF reaches a critical level, the auto-catalytic feedback loop is triggered as the overall catalytic activity of Cdc25 exceeds that of Wee1. Cdc25 removes the inhibitory phosphorylation on residues Thr14/Tyr15 of the Cdc2 subunit and increases the level of active MPF. Active MPF initiates the degradation of cyclin B and, as the Cdc2-cyclin B complexes decomposes, the cell exits mitosis and enters a new S phase.

mimicked by setting $[Cdk2]/Cdc2^T = 0$ in Tab. (8.2). In Fig. (8.3), the integral solutions of MPF, doubly phosphorylated Cdc2-cyclin B and free cyclin B are drawn with, respectively, solid heavy, solid thin and dotted lines.

In the absence of Cdk2-cyclin E activity the system settles in a steady state corresponding to a G2 arrest of the cell cycle. Cdc2-cyclin B complexes accumulates in the inactive Thr-14/Tyr-15 phosphorylated form and the activity of MPF remains to low to trigger self-amplification through activation of Cdc25. The accumulation of Thr-14/Tyr-15 phosphorylated Cdc2-cyclin B complexes in the absence of Cdk2-cyclin E is also observed experimentally (Guadagno & Newport, 1996). In addition to showing that the cell cycle arrests in the absence of Cdk2-cyclin E activity, Fig. (8.3) reproduces an experiment by Guagdano and Newport where in which addition of cyclin B to Cdk2-depleted or Cip1 treated extracts readily activates mitosis (Guadagno & Newport, 1996). When, in Fig. (8.3), the level of free cyclin B is increased after 500 min. to a level of 0.4, corresponding to injection of free cyclin B, the cyclin B immediately binds to free Cdc2. As the inhibitory phosphorylation is favored, the newly formed Cdc2-cyclin B complexes accumulate to a large extent in the Thr14/Tyr15 form as seen by the increased level of doubly phosphorylated Cdc2-cyclin B (thin line). However, the increase in the total amount of Cdc2-cyclin B complexes affects the overall distribution of phosphorylation states and a slight increase in the activity of MPF is also present. The increased activity of MPF is sufficient to slightly favor dephosphorylation of Thr14/Tyr15. The auto-catalytic loop is triggered and inactive doubly phosphorylated Cdc2-cyclin B is rapidly dephosphorylated resulting in a sharp increase in

Fig. 8.3: Depletion of Cdk2-cyclin E halts the cell cycle but is rescued by injection of free cyclin B. The parameters are as in Tab. (8.2) except that the absence of Cdk2-cyclin E activity is mimicked by setting $[Cdk2]/Cdc2^T = 0$. In the absence of Cdk2-cyclin E the MPF activity (heavy line) remains low whereas Thr-14/Tyr-15 phosphorylated Cdc2-cyclin B complexes (thin line) accumulates. The system settles in a steady state and the cell cycle is halted corresponding to a G2 arrest. Injection of cyclin B (dotted line) after 500 min. overcomes the G2 arrest and results in a single peak in the activity of MPF corresponding to an activation of mitosis.

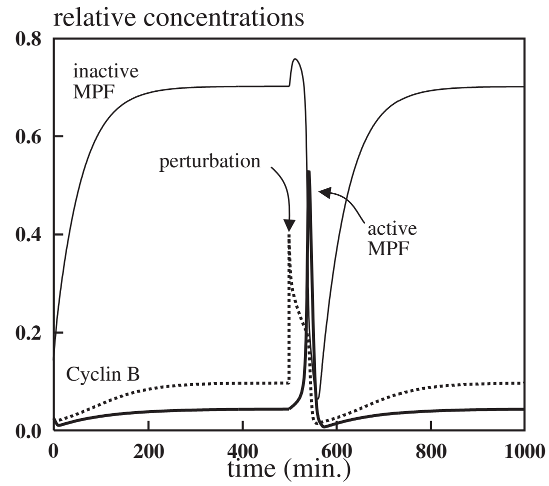

MPF activity. The increased activity of MPF then initiates cyclin B degradation and the Cdc2-cyclin B complexes start to decompose causing a decrease in the total level of Cdc2-cyclin B complexes. As the MPF activity returns to a low state, proteolysis ceases and the system resettles in the steady state.

8.6 Onset of Repeated Divisions

The transition from autonomous oscillations observed in the presence of Cdk2-cyclin E to the G2-arrest observed in the absence of Cdk2 kinase activity is investigated further by establishing a bifurcation diagram taking $[Cdk2]/[Cdc2]^T$ as a bifurcation parameter and keeping all other parameters as in Tab. (8.2). This diagram is presented in Fig. (8.4). The bifurcation diagram in Fig. (8.4) is divided into two regions by the vertical broken line at relative Cdk2-cyclin E activity of about 0.0014. This line represents a critical value in Cdk2-cyclin E activity where the system changes dynamic behavior. When the activity of Cdk2-cyclin E is below 0.0014, three distinct steady state solutions, labeled SS_1, SS_2 and SS_3, with different activities of MPF coexist. The steady state solutions labeled SS_2 and SS_3 are drawn with broken lines to indicate that they are unstable, whereas SS_1 is drawn with a solid line to indicate that this steady state is stable. The SS_1 steady state is the only stable solution when the Cdk2-cyclin E activity is

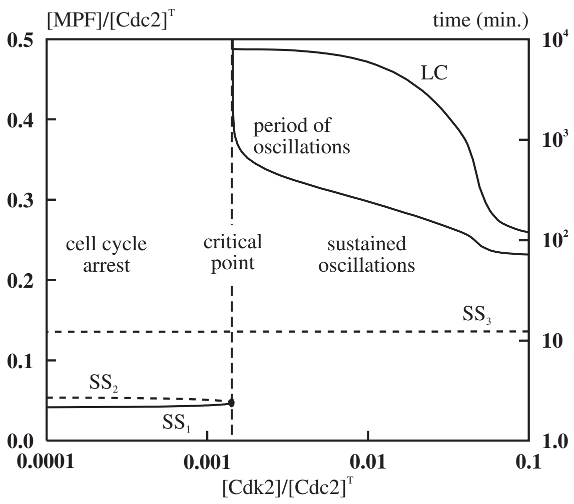

Fig. 8.4: Bifurcation diagram with $[Cdk2]/[Cdc2]^T$ as a bifurcation parameter. All other parameters are as in Tab. (8.2). In the diagram, solid lines indicates either the MPF activity when the steady state is stable or the maximum activity of MPF when the periodic solution is stable. Broken lines indicate unstable steady states. At activities of Cdk2-cyclin E below 0.0014 a steady state with a low activity of MPF is the only stable solution. The system will converge toward the stable steady state corresponding to the G2-arrest observed in Fig. (8.3). At Cdk2-cyclin E activities above 0.0014 the only stable solution is a periodic solution and the system will show sustained oscillatory behavior corresponding to the behavior observed in Fig. (8.2). The transition from steady state to autonomous oscillations occurs through a so-called omega explosion as discussed in the text.

below the critical value. The cell cycle will arrest in a state with low MPF activity as observed in Fig. (8.3). When the Cdk2-cyclin E activity is above 0.0014 only the steady state SS_3 will exist as the other steady state solutions are destroyed at the critical point as discussed below. The SS_3 solution is unstable and the system will converge to a stable periodic solution and sustained oscillations as in Fig. (8.2) are observed. The stable periodic solution is depicted by the curve labeled LC corresponding to the maximum activity of MPF during oscillations as well as the period between subsequent peaks of MPF. The amplitude in MPF and the period of oscillation decrease when the activity of Cdk2 increases but the periodic solution seems to be stable for all values of $[Cdk2]/[Cdc2]^T$ above 0.0014.

The transition from the steady state to sustained oscillations at increased Cdk2-cyclin E activity occurs through a so-called omega explosion (Thompson & Stewart, 1986). The four planes presented in Fig. (8.5) are schematic illustrations of the dynamic changes as $[Cdk2]/[Cdc2]^T$ passes the critical point in Fig. (8.4). The planes labeled D and C illustrate the dynamic behavior of the system when the activity of Cdk2-cyclin E is, respectively, above and at the critical value. The planes labeled B and A illustrate the dynamic behavior when $[Cdk2]/[Cdc2]^T$ is below 0.0014 corresponding to an arrest of the cell cycle. Each of the planes should be seen as a phase plane where steady states appear as points, periodic solutions appear as closed curves and the arrows outline parts of phase plane trajectories. The solid and broken lines traversing all four phase planes outline stable and unstable steady states. A projection of these lines on the plane of the paper correspond to a one-parameter continuation as in Fig. (8.4). The plane labeled A

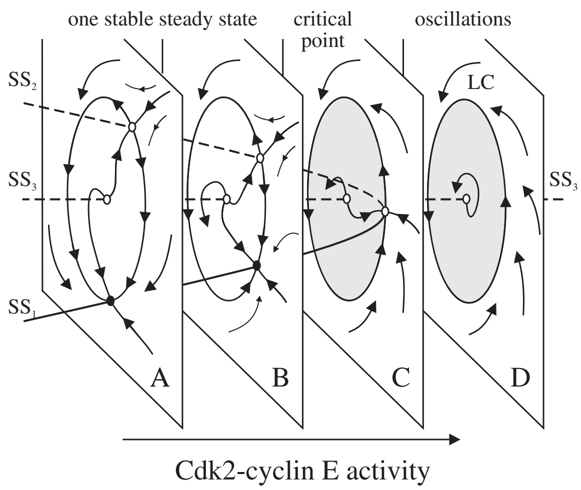

Fig. 8.5: Schematic illustration of the transition from a stable periodic solution to a stable steady state through an omega explosion. The activity of Cdk2-cyclin E is the bifurcation parameter. For high values of Cdk2-cyclin E activity (left hand side) a stable closed orbit exists around an unstable steady state and the system oscillates. At the critical point of the bifurcation parameter a steady state solution appears on the periodic orbit through a saddle-node bifurcation generating a homoclinic orbit. When the Cdk2-cyclin E activity increases, the homoclinic orbit is destroyed and the saddle-node splits into a saddle and a stable node (modified from Thompson & Stewart, 1986).

in Fig. (8.5) correspond to a low activity of Cdk2-cyclin E, e.g $[Cdk2]/[Cdc2]^T = 10^{-4}$, where three steady state solutions SS_1, SS_2 and SS_3 coexist. The steady state solutions indicated by white circles are unstable whereas the steady state indicated by a filled circle is stable. The unstable steady states solutions labeled SS_2 and SS_3 are, respectively, an unstable saddle point and an unstable spiral, whereas the stable steady state labeled SS_1 is a stable node. When initiating the system in a point close to the unstable saddle point SS_2 the system will converge to stable node SS_1 following a phase trajectory going either in or out of the plane of the paper. The phase trajectory will itself converge toward a trajectory called the heteroclinic connection which is an unstable manifold of SS_2 and a stable manifold of SS_1. In the two-dimensional representation in Fig. (8.5) the saddle and the node is linked through two heteroclinic connections which constitute a heteroclinic cycle. The heteroclinic cycle is important as it will be replaced by a stable periodic orbit when the Cdk2-cyclin activity increases. When the activity of Cdk2-cyclin E is increased slightly, for example to $[Cdk2]/[Cdc2]^T = 10^{-3}$, the unstable spiral is unchanged but the unstable saddle SS_2 and the stable node SS_1 approach each other as illustrated in the phase plane labeled B in Fig. (8.5) and seen in Fig. (8.4). As the two steady states solutions come closer to each other,the length of one of the heteroclinic connections is decreased and will vanish when the critical point is reached. In the phase plane labeled C, the unstable saddle and the stable node collide in a saddle-node bifurcation corresponding to the critical point $[Cdk2]/[Cdc2]^T = 0.0014$ in Fig. (8.4). At this point the non-vanishing heteroclinic connection is replaced by a closed trajectory called a homoclinic orbit of infinite period. The homoclinic orbit is structurally unstable (i.e. it only exist in the critical point) and it is replaced by a stable limit cycle when the activity of Cdk2-cyclin E is increased. This transition is illustrated in Fig. (8.5) in the phase plane labeled D, and is found numerically in Fig. (8.4). Initially, the stable periodic solution labeled LC will have a very high period, as observed in Fig. (8.4), but it will decrease with the Cdk2-cyclin E activity as the system moves away from the critical point.

The omega explosion may be an advantageous dynamic mechanism of the G2 checkpoint as only a state of low MPF is available in the absence of Cdk2-cyclin E activity. This is advantageous as compared to, for example, a bistable mechanism (Thron, 1996) or a system where a stable steady state and a stable periodic solution coexists, because the cell cycle may, respectively, arrest in a state of high MPF activity or initiate repeated division when the system experience a perturbation. The omega explosion is robust in the sense that after a transient the system will return to a uniquely defined state which can be either a steady state with low MPF activity or repeated divisions, depending on the activity of Cdk2-cyclin E. Moreover, the presence of a homoclinic orbit strongly influences the period of oscillations in the neighborhood of the critical point. This may be advantageous in cell cycle regulation as the Cdk2-cyclin E activity, or a similar effector, can be used to control the timing between divisions by elongation of the S phase. The correlation between the period and the activity of Cdk2-cyclin E also offers itself as a dynamic explanation for the increased period of the cell cycle observed at the mid-blastula transition where cyclin E is degraded (Rempel *et al.*, 1995) and Cdk2 kinase activity is inhibited (Shou & Dunhphy, 1996).

8.7 Threshold Modulation through Cdk2

The early embryonic cell cycle is driven by the constant synthesis of cyclin B which results in a steady accumulation of Cdc2-cyclin B complexes (Murray & Kirschner, 1989). When one of these complexes, for example MPF, reaches a critical level, mitosis is initiated and the cell starts to divide. However, in the absence of Cdk2 kinase activity mitosis is never initiated. To investigate the correlation between the activity of Cdk2-cyclin and the cyclin B synthesis rate further, a two-dimensional bifurcation analysis with v_1 and $[Cdk2]/[Cdc2]^T$ as bifurcation parameters was performed. The result is presented in Fig. (8.6) where the bifurcations are traced out in $v_1, [Cdk2]/[Cdc2]^T$ parameter space. All other parameters are as in Tab. (8.2). The two-dimensional bifurcation diagram

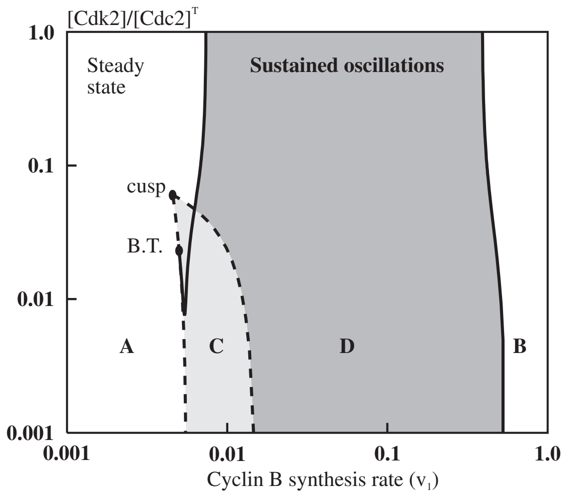

Fig. 8.6: Two-dimensional bifurcation diagram that outlines the regions of different dynamic behaviors of the cell cycle engine at varied activity of Cdk2-cyclin E and varied rate of cyclin B synthesis. In region A and B, a single steady state is stable. In region C, the system has a total of three steady state solutions of which either one or two are stable (see text). In region D, a stable periodic orbit evolves around an unstable steady state. The transition from the multi-stable region C to region D, where the cell cycle engine shows autonomous oscillations, occurs through an omega explosion as discussed in Fig. (8.5). When the value of $[Cdk2]/[Cdc2]^T$ increases, the region with three steady states is destroyed through a cusp bifurcation and the system passes directly from region A to region C through a super-critical Hopf-bifurcation generated at the Takens-Bogdanov (B.T.) bifurcation.

in Fig. (8.6) is divided into four regions labeled A, B, C and D, which correspond to regions of different dynamic behavior. In both regions A and B, the system has a single stable steady state, whereas three steady states coexist in region C. In region D, the only steady state solution is unstable and the cell cycle evolves along a stable periodic solution. At a low value of v_1 (i.e. low cyclin B synthesis rates) the integral solution of the system predicts (not shown) that the cell cycle arrests in a stable steady state where the level of MPF as well as the level of all other Cdc2-cyclin B complexes are low. Very high cyclin B synthesis rates also result in a steady state as shown in region B of Fig. (8.6). Numerical investigations (not shown) predict relatively low levels of all Cdc2-cyclin B complexes in this arrest and it would be interesting to investigate whether the predicted steady state is observed experimentally. The transition from autonomous oscillations in region D to the arrest in region B occurs through a super-critical Hopf bifurcation and high rates of cyclin B synthesis tend to lower the amplitude in the MPF activity during oscillations. Interestingly, there in no bifurcation in Cdk2-cyclin E when v_1 is above 0.02. High cyclin B synthesis rates (i.e. overexpression of cyclin B) may thus result in sustained oscillations even in the absence of Cdk2-cyclin E activity. At moderate values of v_1, a low activity of Cdk2-cyclin E arrests the cell cycle in region C of Fig. (8.6). In this region three steady states coexist and the transition from cell cycle arrest to sustained oscillations occurs through the omega explosion as depicted in Fig. (8.5). The multi-stable region is destroyed (or generated) in a cusp bifurcation where two saddle-node bifurcations, drawn with broken lines, collide (see e.g. Perko, 1996). For values of $[Cdk2]/[Cdc2]^T$ above the cusp bifurcation, the transition from cell cycle arrest in region A to sustained oscillations in region B occurs through a Hopf bifurcation which is drawn with solid line in Fig. (8.6). Numerical studies (not shown) has shown that the Hopf bifurcation is super-critical. The Hopf bifurcation is generated (or destroyed) at a Bogdanov-Takens bifurcation indicated by the point B.T. in Fig. (8.6). In the B.T. bifurcation, two eigenvalues have zero real parts as in a Hopf bifurcation, but the imaginary parts of the two eigenvalues are also zero as in the saddle-node bifurcation (see e.g. Scott, 1993; Perko, 1996). When the value of $[Cdk2]/[Cdc2]^T$ is below and close to the Bogdanov-Takens bifurcation the leftmost saddle-node bifurcation drawn in a broken line and the leftmost Hopf-bifurcation drawn in a solid line are close and a homoclinic orbit will exist (Scott, 1993). Below the B.T., the leftmost Hopf bifurcation indicates that one of the steady states SS_2 or SS_3, which are unstable for low values of $[Cdk2]/[Cdc2]^T$, may become stable as a pair of eigenvalues traverses the imaginary axis. Numerical evaluation shows that the steady state SS_3 is stable in the narrow range of v_1 where two Hopf-bifurcations coexist in region C. The level of MPF in this steady state is high and the system is thus bistable.

8.8 Cdk2 and Cell Cycle Checkpoints

It is well established that Cdk2-cyclin E is an important factor in the G1 checkpoint and it has recently been suggested that the the ever-present Cdk2 activity may account for the absence of a G1 checkpoint in the early divisions of *Xenopus* (Rempel *et al.*, 1995). The present model is directed toward the mechanism that triggers mitosis and does not take into account the complex mechanisms that allow the cell to enter S-phase. An extended model including a mathematical description of G1 regulation mechanism (e.g. Obeyesekere *et al.*, 1995) may be able to take the G1 checkpoint into account.

The analysis made here investigates how inclusion of Cdk2-cyclin E activity, which have been shown to be essential for the entry into mitosis (Guadagno & Newport, 1996), may alter the behavior of the existing comprehensive NT-model of the cell cycle engine (Novak & Tyson, 1993a,b). When the Cdk2-cyclin E kinase complex is incorporated into the NT-model, the model can reproduce several recent experimental observations, and can be added to the long list of experimental observations already reproduced by the comprehensive model. Through a detailed bifurcation analysis a plausible dynamic mechanism for the G2/M transition emerges. The mechanism, which is called an omega explosion, can halt the cell cycle in a uniquely defined state if the proper conditions (for example high Cdk2-cyclin E activity) are not given. Moreover, the omega explosion provides a highly sensitive mechanism for adjustment of the period between subsequent divisions which may be crucial if other tasks (for example DNA replication or repair) needs to be performed before the onset of mitosis.

In the paper by Novak and Tyson (Novak & Tyson, 1993a) it is suggested that the presence of unreplicated DNA halts the cell cycle through activation of the enzymes opposing the phosphorylation of Cdc25 and Wee1. However, it has been suggested, based on experimental data, that Cdk2 is part of the mechanism that ensures that mitosis is not initiated before DNA replication is completed (Gabrielli *et al.*, 1992a). If unreplicated DNA cause an inhibitory phosphorylation of Cdk2, which is indeed what is observed experimentally (Gabrielli *et al.*, 1992a), the extended NT-model may present a plausible mechanism by which the progress of DNA replication is mediated. Inhibition of Cdk2 by unreplicated DNA may provide an explanation for the observed oscillations in Cdk2 kinase activity and a more sophisticated model should incorporate this connection. Other elaborated models should also include stoichiometric inhibitors of the Cdc2-cyclin B complexes (Thron, 1996; Lee & Kirschner, 1996) and the apparent lack of Thr14/Tyr15 phosphorylation of Cdc2 during the early embryonic cycles (Hartley *et al.*, 1996).

The important role of Cdk2 for maintenance of the G2 checkpoint has recently been established experimentally in human cells (Walker *et al.*, 1995). In these experiments, human cells that overexpress Cdk2 fail to down-regulate Cdk2 kinase activity following DNA damage by gamma-irradiation and show G2 checkpoint defects. The conclusion made by the authors is that misregulation of Cdk2 contributes to the failure of G2 checkpoint control by allowing premature entry into mitosis. The signal of damaged DNA is mediated through p53 activation of the Cdk2 inhibitor p21 (Petrocelli *et al.*, 1996; Weinberg, 1996) and appears to affect the activity of Cdc25 (Lees, 1995). The detailed mechanism has not been established but it seems plausible that Cdk2 kinase activity, through a mechanism similar to that proposed herein for Cdk2-cyclin E in *Xenopus*, may also account for G2 checkpoint failure following DNA damage in mammalian cells. Considering that high levels of Cdk2-cyclin E activity in the present model allows for rapid, repeated divisions of the embryonic cell it is conceivable that many tumors cells, whose trademark is indeed rapid, repeated cell divisions, lack a functional p53 gene (Weinberg, 1996; Elledge, 1996) and fail to activate the Cdk2 inhibitor p21.

CHAPTER 9

Summary of Results

The aim of this thesis has been to shed light on selected topics from the theory of biological regulation with emphasis on the theoretical models of instability generating molecular mechanisms and sigmoidal biological response functions. Starting from established theories of chemical kinetics and enzymology, the dynamic and static behavior of a number of biologically relevant reaction schemes has been investigated.

To make these investigations possible, the basis of the most fundamental simplification methods in biochemical and chemical kinetics, the quasi-steady state approximation (QSSA) (Klonowski, 1983), had to be reconsidered. This has led to the formulation of an extended method for applying the QSSA, which can be used here where the existing methods failed to provide an appropriate level of detail. The proposed method is somewhat complex when compared to the standard implementation of the QSSA. Where the standard QSSA is typically based on a postulated quasi-steady state, the extended simplification method is based on a number of kinetic requirements. Through the extended simplification method, a number of conditions that validate the simplified mathematical description emerge in a direct and natural way. These conditions are typically a requirement of low enzyme concentrations, fast equilibration between the enzyme and molecules that bind to the enzyme and fast equilibrating internal transitions (i.e. allosteric transitions of allosteric enzymes). The validity conditions for applying the QSSA to biochemical reaction systems have been, until now, limited to the Michaelis-Menten reaction (Murray, 1993; de la Selva *et al.*, 1996; Borghans *et al.*, 1996). The extended simplification method presented herein can be applied to chemical reaction systems containing any number of species and reactions in order to provide a detailed investigation of theoretical models of biological systems.

The first instability generating mechanism subject to the following investigation is a model of an auto-catalytic dimeric allosteric enzyme, previously studied intensively through an approximation composed of two rate equations obtained through the standard QSSA approach (see Goldbeter, 1996, for survey). There is experimental evidence suggesting that the postulated quasi-steady state assumed in the derivation of the two-dimensional model is violated. *In vitro* measurements confirm that the allosteric transition may be slow and that a quasi-steady state between conformations in an allosteric enzyme may require minutes to be established (Kurganov, 1981). The change in dynamic behavior of a three-dimensional model that takes into account a possible slow allosteric transition is quite surprising. A slow allosteric transition may have a dual effect on the ability of the mechanism to produce sustained oscillatory behavior measured through the range of a key regulatory parameter ν. When the rate of the allosteric transition is below a critical value, a slow allosteric transition increases the range in ν where oscillations are observed. This indicates that a slow allosteric may enhance the potency of the mechanism and that the two-dimensional model may underestimate the possibility of allowing sustained oscillatory behavior. When including a slow allosteric, the resulting three-dimensional model predicts oscillatory behavior in a region of parameter space where the two-dimensional model does not. When the rate of the allosteric transition is above the critical value, the oscillatory mode is inhibited and eventually vanishes. The effects of a slow product dissociation reaction, high enzyme concentrations and a slow Michaelis-Menten reaction are also investigated. The effect of a high enzyme concentration is a decreased ability to show sustained oscillatory behavior but the effect does not seem to be critical. The dynamic effect of a slow product dissociation reaction and a slow Michaelis-Menten reaction is also vanishing. However, when a slow product dissociation rate and a slow rate of the Michaelis-Menten reaction are analyzed together, the dynamic effect is similar to that observed for a slow allosteric transition. Another quite interesting result is that a slow allosteric transition may cause a number of saddle-node bifurcations of periodic solutions. This introduces coexistence of two stable periodics at the same point in parameter space. It has previously been reported that such birhythmic behavior does not occur in this reaction scheme and additional enzymes are to be included before more complex dynamic phenomena can be observed.

A reaction mechanism which allows for the emergence of complex dynamic behaviors in biological systems is provided by a mechanism where two auto-catalytic oligomeric enzymes are coupled in series. This model has previously been reported to show a wide range of dynamic behaviors including simple oscillations, hard excitation, birhythmicity, chaos and bursting oscillations (Decroly & Goldbeter, 1982, 1985, 1987). Through a detailed numerical analysis of a normalized version of the mechanism, it has been found that the list of complex behaviors observed in the model is to be extended with the phenomenon of quasi-periodicity. The model analyzed herein allows for an investigation of the dynamic effect of a slow allosteric transition in one of the enzymes. Through an evaluation of the integral solutions obtained at varied rates of the allosteric transition, it is observed that the bursting, chaotic and quasi-periodic oscillations are sensitive to a slow allosteric transition. The complex behaviors, which are observed when the allosteric transition is fast, degenerate to simple periodic behavior when the rate of the allosteric transition is decreased. A two-dimensional bifurcation analysis reveals that only simple oscillations and hard excitation are possible when the allosteric transition is fast. Although a high rate constant cannot be discarded as physically unreasonable for an intra-molecular rearrangement of atoms, the experimental support of a slow allosteric transitions sheds doubt that this mechanism alone can account for the emergence of complex dynamics in biology.

Many theoretical models of biological regulatory systems involve a sigmoidal dependency that is typically taken into account through a Hill type equation. The sigmoidal dependency is usually interpreted as arising though cooperativity between subunits in an oligomeric enzyme. The steepness of the sigmoidal function is measured through the Hill coefficient obtained from *in vitro* experiments on isolated enzymes. The experimentally observed Hill coefficient is typically not higher than three, although values up to eight have been reported (see e.g. Hunding & Sørensen, 1997, and references therein). Some monomeric enzymes may have an apparent Hill coefficient that is slightly higher than one. Cooperativity between subunits is obviously not present in a monomeric enzyme and the meaning of the Hill coefficient has to be reconsidered. The most direct redefinition of cooperativity is the statement "if it looks like cooperativity, it is cooperativity" (Cornish-Bowden & Cárdenes, 1987). Here, it is argued that interpretation of cooperativity should not only be considered in the perspective of isolated enzymes but should also include sigmoidal response functions that arise from the kinetics of the system. A covalent modification reaction mechanism composed of Michaelis-Menten type enzymes has been reported to give very steep sigmoidal functions (Goldbeter & Koshland, 1981). As reported herein, the nonlinearity introduced by the covalent modification mechanism allows for the emergence of sustained oscillatory behavior in the absence of cooperativity in the traditional context. It is intriguing that a reconstituted biochemical reaction containing phosphofructokinase, which is used as the basis for the oscillatory model containing a single auto-catalytic dimeric allosteric enzyme, does not show sustained oscillatory behavior (Eschrich *et al.*, 1980). When the enzyme fructose 1,6-bisphosphatase is included in the system, sustained oscillatory behavior is observed (Eschrich *et al.*, 1983). The enzymes phosphofructokinase and fructose 1,6-bisphosphatase comprise a covalent modification reaction scheme indicating that it may not be the conventional cooperativity between subunits that solely causes the oscillations observed in the glycolysis.

By allowing an extended perspective of the concept of cooperativity which includes the sigmoidal dependencies arising from kinetic considerations, it is possible to measure and compare kinetic cooperativity through kinetic Hill coefficients. The result of estimating the ranges of kinetic Hill coefficients is quite stunning. Where the conventional cooperativity is not associated with Hill coefficients exceeding eight, the Hill coefficient of the covalent modification mechanism can in fact be arbitrarily large and can easily exceed a value of several hundred under reasonable biochemical conditions and act as a biochemical switch. A simple extension to the covalent modification mechanism that allows for effective control of the threshold value which is needed to switch the trigger is presented. Many enzymes, that is, literally thousands and maybe the majority of all enzymes, are *in vivo* regulated through covalent modification. The high kinetic cooperativity observed in the covalent modification mechanism may therefore be crucial for the understanding of *in vivo* biological regulation. The potential of kinetic cooperativity as a means of precise regulation in biological systems ranging from the control of metabolism, the regulation of DNA transcription, the regulation of the cell cycle, to cellular automata, far exceeds the traditional concept of cooperativity between subunits. It is therefore suggested that the present emphasis on the structures and functions of isolated enzymes are replaced by a kinetic perspective where the properties of single enzymes are integrated in networks of interacting species. If a higher level of understanding of biological self-regulation is to be achieved, one must consider whole reaction networks composed of a large number of interacting biochemical species and the coherent behavior of such a system. The structure and function of isolated enzymes (or genes) is indeed an important and central science but may not be sufficient to account for the high self-regulation of biological systems.

In the final chapter of this thesis, a comprehensive model of the cell cycle (Novak & Tyson, 1993a,b) is investigated. The model comprises a relatively large number of Michaelis-Menten enzymes operating through phosphorylation and dephosphorylation. The model is a case example of biological self-regulation through coherent operation of multiple enzymes. The overall dynamic behavior of the system cannot be explained by considering each enzyme reaction independently. An understanding of cell cycle regulation can only be achieved by considering the system as a whole. Through a detailed review of recent experimental results, the cell cycle model (the NT-model) is extended to include the kinase Cdk2-cyclin E as a modulator of a critical threshold. By doing so, a number of experimental results are reproduced. A detailed bifurcation analysis of the extended model suggests that the G2 to M-phase checkpoint may be related to a so-called omega explosion. The omega explosion can halt the cell cycle in a uniquely defined state if proper requirements, for example high Cdk2-cyclin E activity, are not met. Moreover, the omega explosion provides a highly sensitive mechanism for adjustment of the period between division by variation which may be crucial if other tasks, such as DNA replication or repair need to be performed before the onset of mitosis. It is also possible that Cdk2 kinase activity, through a similar mechanism, can account for G2 checkpoint failure following DNA damage in mammalian cells as these cells fail to down-regulate the activity of Cdk2 kinase complexes.

APPENDIX A

Ligand Binding to a Michaelis-Menten Enzyme

A Michaelis-Menten enzyme may be subject to regulation through binding of ligand in either an allosteric site or directly in the active site. The reaction scheme is composed of several different reactions, each associated with distinct characteristic time-scales. In this Appendix, the full mass kinetic description of the ligand binding reaction scheme is reduced to appropriate low dimensional models using the extended method in Chapter 2. The detailed kinetic considerations serve as an example of the truncation of a complex reaction system and may direct further studies of the minimal instability generating mechanism introduced in Chapter 7.

The binding of ligand L to a Michaelis-Menten enzyme can be described by the schematic reaction below:

$$
\begin{array}{ccccc}
S+E+L & \underset{k_{sb}}{\overset{k_{sf}}{\rightleftarrows}} & C_1+L & \xrightarrow{k_c} & E+P+L \\
k_{lf}\downarrow\uparrow k_{lb} & & k'_{lf}\downarrow\uparrow k'_{lb} & & \\
S+EL & \underset{k'_{sb}}{\overset{k'_{sf}}{\rightleftarrows}} & C_2 & \xrightarrow{k'_c} & EL+P
\end{array}
$$

The substrate S can combine to either free enzyme E or to the enzyme-ligand complex EL and produce an enzyme-substrate complex C_1 or an enzyme-substrate-ligand complex C_2. The catalytic constant k_c of the enzyme-substrate complex may be altered when ligand is bound such that $k_c \neq k'_c$. When k_c is higher than k'_c the ligand will have an inhibitory effect, whereas $k'_c > k_c$ indicates a case of activation.

The above reaction scheme comprises 10 elementary reactions and, applying the law of mass action, one obtains seven rate equations describing the change in concentrations measured in standard units of molar per second.

$$
\begin{aligned}
\frac{d}{dt}[S] &= -\, k_{sf}[S][E] + k_{sb}[C_1] - k'_{sf}[S][EL] + k'_{sb}[C_2], \\
\frac{d}{dt}[L] &= -\, k_{lf}[E][L] + k_{lb}[EL] - k'_{lf}[C_1][L] + k'_{lb}[C_2], \\
\frac{d}{dt}[C_1] &= +\, k_{sf}[E][S] - (k_{sb}+k_c)[ES] - k'_{lf}[C_1][L] + k'_{lb}[C_2], \\
\frac{d}{dt}[C_2] &= k'_{sf}[S][EL] - k'_{sb}[C_2] + k'_{lf}[C_1][L] - k'_{lb}[C_2], \\
\frac{d}{dt}[EL] &= -\, k'_{sf}[S][EL] + (k'_{sb}+k_c)[C_2] - k_{lf}[E][L] + k_{lb}[EL], \\
\frac{d}{dt}[E] &= -\, k_{sf}[E][S] + (k_{sb}+k_c)[ES] - k_{lf}[E][L] + k_{lb}[EL].
\end{aligned}
\tag{A.1}
$$

The total amount of enzyme, substrate and ligand is conserved and the conservation relations of the system reads.

$$[S]+[C_1]+[C_2]+[P] = s^0, \qquad [L]+[EL]+[C_2] = l^0, \tag{A.2}$$

$$[E]+[EL]+[C_1]+[C_2] = e^0. \tag{A.3}$$

The number of linearly independent AODE's required to fully describe the change in all concentrations is therefore only four.

The conversion of substrate through the enzyme-substrate complex C_1 and the enzyme-substrate-ligand complex C_2 are associated with the two Michaelis-

Menten constants

$$K_m = \frac{k_{sb} + k_c}{k_{sf}}, \qquad K'_m = \frac{k'_{sb} + k'_c}{k'_{sf}}, \tag{A.4}$$

for C_1 and C_2 respectively. The dissociation of ligand from the enzyme-ligand complex EL and the enzyme-substrate-ligand complex C_2 is associated with the dissociation constants

$$K_l = \frac{k_{lb}}{k_{lf}}, \qquad K'_l = \frac{k_{lb}}{k_{lf}}. \tag{A.5}$$

The four constants are not independent as

$$K'_m = \frac{[EL]_q[S]_q}{[C_2]_q} = \frac{[E]_q[S]_q}{[C_1]_q}\frac{[EL]_q}{[E]_q[L]_q}\frac{[C_1]_q[L]_q}{[C_2]_q} = \frac{K'_l}{K_l}K_m, \tag{A.6}$$

which will be useful when deriving dimensionless rate equations.

A.1 Full Dimensionless Model

The ligand binding reaction system described by the dimensional rate equations in Eq. (A.1) is normalized by defining the dimensionless variables

$$\alpha = \frac{[S]}{K_m}, \quad \gamma_1 = \frac{[C_1]}{e^0}, \quad \gamma_2 = \frac{[C_2]}{e^0}, \quad \gamma_3 = \frac{[EL]}{e^0}, \quad \tau = k_\tau t, \tag{A.7}$$

where k_τ is an arbitrary constant with units of inverse time. For clarity of the following derivations the dependent variables

$$\gamma_4 = \frac{[E]}{e^0}, \quad \beta = \frac{[L]}{K'_l}, \tag{A.8}$$

will be employed although they are to be replaced by appropriate combinations of the independent variables in Eq. (A.7). The constant k_τ is introduced for generality of the derivation and is to be replaced by an apparent first order rate constant.

In normalized form the conservation of total enzyme and total ligand reads

$$1 = \gamma_1 + \gamma_2 + \gamma_3 + \gamma_4, \qquad \beta + \eta(\gamma_3 + \gamma_2) = \beta^0, \tag{A.9}$$

where $\eta = e^0/K'_l$ and $\beta^0 = [L]^0/K'_l$. It will be assumed that the total enzyme concentration e^0 is much smaller than K'_l such that the term $\eta(\gamma_3+\gamma_2)$ is negligible and β can be taken as a parameter reflecting the total concentration of ligand.

The detailed normalization of the rate equation is shown in Tab. (A.1). The normalization yields the nine dimensionless parameters

$$\epsilon = \frac{e^0}{K_m}, \quad \sigma = \frac{k_c e^0}{K_m k_\tau}, \quad \delta = \frac{k_c'}{k_c}, \quad \varrho = \frac{K_l'}{K_l}, \tag{A.10}$$

$$\varepsilon_1 = \frac{k_\tau}{k_{sb}+k_c}, \quad \varepsilon_1' = \frac{k_\tau}{k_{sb}'+k_c'}, \quad \varepsilon_2 = \frac{k_\tau}{k_{lb}}, \quad \varepsilon_2' = \frac{k_\tau}{k_{lb}'}, \tag{A.11}$$

where ε_1 and ε_1' is associated with the Michaelis-Menten reactions of C_1 and C_2

$$\begin{aligned}
\frac{d}{dt}[S] =& -k_{sf}[S][E] + k_{sb}[C_1] - k_{sf}'[S][EL] + k_{sb}'[C_2] \\
=& -\frac{d}{dt}[C_1] - \frac{d}{dt}[C_2] - k_c[C_1] - k_c'[C_2] = -\frac{d}{dt}([C_1]+[C_2]) - k_c[C_1]\left(1+\frac{k_c'[C_2]}{k_c[C_1]}\right) \Rightarrow \\
\frac{d\alpha}{d\tau} =& -\frac{e^0}{K_m}\frac{d}{d\tau}(\gamma_1+\gamma_2) - \frac{k_c e^0 \gamma 1}{K_m k_\tau}\left(1+\frac{k_c'\gamma_2}{k_c\gamma_1}\right) = -\epsilon\frac{d}{d\tau}(\gamma_1+\gamma_2) - \sigma\gamma_1\left(1+\delta\frac{\gamma_2}{\gamma_1}\right) \\
\frac{d}{dt}[C_1] =& k_{sf}[S][E] - (k_{sb}+k_c)[C_1] - k_{lf}'[C_1][L] + k_{lb}'[C_2] \\
=& (k_{sb}+k_c)\left(\frac{[S]}{K_m}[E] - [C_1]\right) + k_{lb}'\left([C_2] - [C_1]\frac{[L]}{K_l'}\right) \Rightarrow \\
\frac{d\gamma_1}{d\tau} =& \frac{k_{sb}+k_c}{k_\tau}(\alpha\gamma_4 - \gamma_1) + \frac{k_{lb}'}{k_\tau}(\gamma_2 - \gamma_1\beta) = \frac{1}{\varepsilon_1}(\alpha\gamma_4-\gamma_1) + \frac{1}{\varepsilon_2'}(\gamma_2-\gamma_1\beta) \\
\frac{d}{dt}[C_2] =& k_{sf}'[S][EL] - (k_{sb}'+k_c')[C_2] + k_{lf}'[C_1][L] - k_{lb}'[C_2] \\
=& (k_{sb}'+k_c')\left(\frac{K_l[S]}{K_l'K_m}[EL] - [C_2]\right) + k_{lb}'\left([C_1]\frac{[L]}{K_l'} - [C_2]\right) \Rightarrow \\
\frac{d\gamma_2}{d\tau} =& \frac{k_{sb}'+k_c'}{k_\tau}\left(\frac{K_l}{K_l'}\alpha\gamma_3 - \gamma_2\right) + \frac{k_{lb}'}{k_\tau}(\gamma_1\beta - \gamma_2) = \frac{1}{\varepsilon_1'}\left(\frac{\alpha\gamma_3}{\varrho} - \gamma_2\right) + \frac{1}{\varepsilon_2'}(\gamma_1\beta - \gamma_2), \\
\frac{d}{dt}[C_3] =& -k_{sf}'[EL][S] + (k_{sb}'+k_c')[C_2] - k_{lb}[EL] + k_{lf}[E][L] \\
=& (k_{sb}'+k_c')\left([C_2] - [EL]\frac{K_m[S]}{K_m'K_m}\right) + k_{lb}\left([E]\frac{K_l'[L]}{K_lK_l'} - [EL]\right) \Rightarrow \\
\frac{d\gamma_3}{d\tau} =& \frac{k_{sb}'+k_c'}{k_\tau}\left(\gamma_2 - \frac{K_l}{K_l'}\gamma_3\alpha\right) + \frac{k_{lb}}{k_\tau}\left(\gamma_4\beta\frac{K_l'}{K_l} - \gamma_3\right) = \frac{1}{\varepsilon_1'}\left(\frac{\gamma_2-\gamma_3\alpha}{\varrho}\right) + \frac{1}{\varepsilon_2}(\gamma_4\beta\varrho - \gamma_3)
\end{aligned}$$

Tab. A.1: Detailed derivation of a linearly independent set of normalized rate equations that describes the binding of a general ligand to a Michaelis-Menten enzyme. The dimensionless constants and variables are discussed in the text and the dependent variable $\gamma_4 = 1-(\gamma_1+\gamma_2+\gamma_3)$ is used for clarity.

whereas ε_2 and ε_2' are parameters associated with the ligand binding reactions. It will, for simplicity and without a great loss of generality, be assumed that $\varepsilon_1 = \varepsilon_1'$ and that $\varepsilon_2 = \varepsilon_2'$. A set of linearly independent AODE's is obtained from Tab. (A.1) by replacing of the dependent variable γ_4 with $1 - \gamma_1 - \gamma_2 - \gamma_3$, and the dimensionless description of the ligand binding scheme reads

$$\begin{aligned}
\frac{d\alpha}{d\tau} =& -\frac{\epsilon}{\varepsilon_1}\left(\alpha(1-\gamma_1-\gamma_2-\gamma_3) - \gamma_1 + \frac{\alpha\gamma_3}{\varrho} - \gamma_2\right) - \sigma(\gamma_1 + \delta\gamma_2),\\
\frac{d\gamma_1}{d\tau} =& \frac{1}{\varepsilon_1}(\alpha(1-\gamma_1-\gamma_2-\gamma_3) - \gamma_1) + \frac{1}{\varepsilon_2}(\gamma_2 - \gamma_1\beta),\\
\frac{d\gamma_2}{d\tau} =& \frac{1}{\varepsilon_1}\left(\frac{\alpha\gamma_3}{\varrho} - \gamma_2\right) + \frac{1}{\varepsilon_2}(\gamma_1\beta - \gamma_2),\\
\frac{d\gamma_3}{d\tau} =& \frac{1}{\varepsilon_1}\left(\gamma_2 - \frac{\gamma_3\alpha}{\varrho}\right) + \frac{1}{\varepsilon_2}\left((1-\gamma_1-\gamma_2-\gamma_3)\beta\varrho - \gamma_3\right).
\end{aligned} \tag{A.12}$$

The left hand sides of the rate equations in Eq. (A.12) contain several distinct parameters and Tihonov's theorems do not apply. Instead the extended method presented in Chapter 2 is employed.

A.2 Fast Substrate Equilibration

In this section, an approximation to the full description in Eq. (A.12) is derived for the case where the Michaelis-Menten type reactions are fast equilibrating but the dissociation of ligand from the enzyme-ligand complex and the enzyme-substrate-ligand complex cannot be considered as a fast reaction.

Let $\varepsilon_1 \to 0$ such that $\varepsilon_1/\varepsilon_2 \to 0$. Changing the time-scale in Eq. (A.12) to $\tau_1 = \tau/\varepsilon_1$ one obtain

$$\begin{aligned}
\frac{d\alpha}{d\tau_1} &= -\epsilon\frac{d}{d\tau_1}(\gamma_1 + \gamma_2), & \frac{d\gamma_1}{d\tau_1} &= \alpha(1-\gamma_1-\gamma_2-\gamma_3) - \gamma_1,\\
\frac{d\gamma_2}{d\tau_1} &= \frac{\alpha\gamma_3}{\varrho} - \gamma_2, & \frac{d\gamma_3}{d\tau_1} &= \gamma_2 - \frac{\alpha\gamma_3}{\varrho}.
\end{aligned} \tag{A.13}$$

It is noted that the variable α change on the fast time-scale and α cannot be parameterized on the fast time-scale τ_1. As α is supposed to be a slow changing variable it is required that the rate of change of α is negligible on the fast time-scale. This requirement can be met if the value of ϵ is sufficiently low. It is therefore assumed that $\varepsilon_0 << K_m$ such that $\epsilon \to 0$. From the definition of the dimensionless constants, it is observed that

$$\varepsilon_1 = \frac{k_\tau}{k_{sb}+k_c} \leq \frac{k_\tau}{k_c} = \frac{e^0}{K_m\sigma} = \frac{\epsilon}{\sigma}, \tag{A.14}$$

and assuming $\epsilon \to 0$ therefore implies $\varepsilon_1 \to 0$. It is also seen that γ_2 and γ_3 are linearly dependent on the fast time-scale. The linear dependency implies that the total amount of γ_2 and γ_3 is conserved. This is taken into account by defining constant $y_1 = \gamma_2 + \gamma_3$. When replacing γ_3 by $y_1 - \gamma_2$ one obtains the adjoint system of first order

$$\begin{aligned} \frac{d\gamma_1}{d\tau_1} &= \alpha(1-\gamma_1-y_1)-\gamma_1, \\ \frac{d\gamma_2}{d\tau_1} &= \frac{\alpha(y_1-\gamma_2)}{\varrho} - \gamma_2. \end{aligned} \tag{A.15}$$

One notes that the adjoined system of first order degenerates to the adjoined system of the Michaelis-Menten reaction (see Chapter 2) when $y_1 = 0$ in the rate equation for γ_1 and when $y_1 = 1$ in the rate equation for γ_2. These cases correspond, respectively, to the situation where no ligand is present and in the situation where the enzyme only exists in enzyme-ligand complexes.

The eigenvalues of the Jacobian matrix of the adjoint system of first order reads

$$det(\mathbf{J}-\lambda\mathbf{I}) = det\begin{bmatrix} -\alpha-1-\lambda & 0 \\ 0 & -1-\alpha/\varrho-\lambda \end{bmatrix} \Rightarrow \begin{cases} \lambda_1 &= -\alpha-1, \\ \lambda_2 &= -1-\alpha/\varrho \end{cases}. \tag{A.16}$$

It is easily verified that the eigenvalues of the Jacobian matrix are always negative, as α and ϱ are positive. The singular point of the adjoint system of first order will therefore always be stable. In the singular point of the adjoint system of first order one can obtain the algebraic equations

$$\begin{aligned} \alpha(1-\gamma_1-y_1)-\gamma_1 = \alpha\gamma_4-\gamma_1 = 0 &\Rightarrow \gamma_1 = \alpha\gamma_4, \\ \alpha(y_1-\gamma_2)/\varrho-\gamma_2 = \alpha\gamma_3/\varrho-\gamma_2 = 0 &\Rightarrow \gamma_2 = \alpha\gamma_3/\varrho, \end{aligned} \tag{A.17}$$

which determine the quasi-steady state values of γ_1 and γ_2 when the Michaelis-Menten type reactions are fast equilibrating. Reevaluating the conservation relation for total enzyme in Eq. (A.9) by inserting $\gamma_1 = \alpha\gamma_4$ and $\gamma_2 = \alpha\gamma 3/\varrho$, one obtains the quasi-steady value of the dependent variable γ_4

$$\gamma_4 = \frac{1}{\alpha+1}\left(1-\gamma_3\left(1+\frac{\alpha}{\varrho}\right)\right). \tag{A.18}$$

The quasi-steady state value of γ_4 is then inserted into $\gamma_1 = \alpha\gamma_4$ and the quasi-steady state value of enzyme-substrate complex in Eq. (A.19) is obtained.

$$\gamma_1 = \frac{\alpha}{\alpha+1}\left(1 - \gamma_3\left(1 + \frac{\alpha}{\varrho}\right)\right). \tag{A.19}$$

As the quasi-steady state value of γ_2 is given by the expression $\gamma_2 = \alpha\gamma_3/\varrho$, the quasi-steady state is determined solely by the level of enzyme-ligand substrate γ_3 and the level of substrate α.

As the singular point of the adjoined system of first order is stable, the variables γ_1 and γ_2 will tend to their quasi-steady state values infinitely fast when $\varepsilon_1 \to 0$. When γ_1 and γ_2 have reached quasi-steady state the rate equations of γ_1 and γ_2 will be zero on the time-scale τ and the rate terms arising from the Michaelis-Menten type reactions are nullified. The degenerate system of first order is obtained from the full description in Eq. (A.12) by inserting of the quasi-steady state values of γ_1 and γ_2 and neglecting all terms involving ε_1.

$$\boxed{\begin{aligned}\frac{d\alpha}{d\tau} &= -\sigma(\gamma_1 + \delta\gamma_2) = -\sigma\left[\frac{\alpha}{\alpha+1}\left(1 - \gamma_3\left(1 + \frac{\alpha}{\varrho}\right)\right) + \delta\frac{\alpha\gamma_3}{\varrho}\right],\\ \frac{d\gamma_3}{d\tau} &= \frac{1}{\varepsilon_2}(\gamma_4\beta\varrho - \gamma_3) = \frac{1}{\varepsilon_2}\left[\frac{\beta\varrho}{\alpha+1}\left(1 - \gamma_3\left(1 + \frac{\alpha}{\varrho}\right)\right) - \gamma_3\right].\end{aligned} \quad \text{(A.20)}}$$

It is noted that if no ligand is present, $\beta = 0$, then $\gamma_3 = 0$ and the degenerate system in Eq. (A.20) reduces to the Michaelis-Menten rate law

$$\frac{d\alpha}{d\tau} = -\frac{\sigma\alpha}{\alpha+1} \tag{A.21}$$

.

A.3 Fast Ligand Equilibration

In this section an appropriate approximation of Eq. (A.12) is derived for the case where the dissociation of ligand from the enzyme-ligand complex and the enzyme-substrate-ligand complex are fast reactions, whereas the Michaelis-Menten type reactions are considered to be slow.

When $\varepsilon_2 \to 0$ such that $\varepsilon_2/\varepsilon_1 \to 0$ the rate equations in Eq. (A.12) will be given by

$$\frac{d\alpha}{d\tau_2} = -\epsilon \frac{d}{d\tau_2}(\gamma_1 + \gamma_2), \qquad \frac{d\gamma_1}{d\tau_2} = \gamma_2 - \gamma_1\beta,$$
$$\frac{d\gamma_2}{d\tau_2} = \gamma_1\beta - \gamma_2, \qquad \frac{d\gamma_3}{d\tau_2} = \gamma_4\beta\varrho - \gamma_3, \tag{A.22}$$

on the fast time-scale $\tau_2 = \tau/\varepsilon_2$. It is immediately observed that γ_1 and γ_2 are linearly dependent. The level of substrate, represented by α, therefore has a zero rate of change on the fast time-scale even if ϵ is not small and the requirement of separation of time-scales is met. Expressing the conservation of the sum of γ_1 and γ_2 on the fast time-scale by defining $y_2 = \gamma_1 + \gamma_2$, one obtains the adjoint system of first order

$$\begin{aligned} \frac{d\gamma_2}{d\tau_2} &= (y_2 - \gamma_2)\beta - \gamma_2, \\ \frac{d\gamma_3}{d\tau_2} &= -\gamma_3 + (1 - y_2 - \gamma_3)\beta\varrho. \end{aligned} \tag{A.23}$$

with a Jacobian matrix defined by

$$\mathbf{J} = \begin{bmatrix} -\beta - 1 & 0 \\ 0 & -1 - \beta\varrho \end{bmatrix}. \tag{A.24}$$

The eigenvalues of the Jacobian can easily be shown to be guaranteed negative and any singular solution of the adjoint system of first order will be stable.

The values of γ_2 and γ_3 that nullify the left hand side of Eq. (A.23) are

$$\gamma_2 = \gamma_1\beta, \qquad \gamma_3 = \gamma_4\beta\varrho, \tag{A.25}$$

which, inserted into the conservation of total enzyme, yields the expression in Eq. (A.26) that determines the quasi-steady state value of γ_3.

$$\gamma_3 = \frac{1 - \gamma_1(1+\beta)}{1 + \beta\varrho}. \tag{A.26}$$

The degenerate solution of first order is then obtained from the full description by ignoring the terms involving ε_2 and replacing γ_2 with $\gamma_1\beta$, and γ_3 with Eq. (A.26).

$$\begin{aligned} \frac{d\alpha}{d\tau} &= \frac{\epsilon}{\varepsilon_1}(\beta+1)\left[\gamma_1 - \frac{\alpha(1-\gamma_1(\beta+1))}{1+\beta\varrho}\right] - \sigma\gamma_1(1+\delta\beta), \\ \frac{d\gamma_1}{d\tau} &= \frac{1}{\varepsilon_1}\left[\frac{\alpha(1-\gamma_1(\beta+1))}{1+\beta\varrho} - \gamma_1\right] \end{aligned} \tag{A.27}$$

A.4 Reduced Model

In this section an approximation of the full description in Eq. (A.12) is derived for the case in which both the Michaelis-Menten and the ligand dissociation reaction are fast equilibrating reactions. The approximation can be derived from either Eq. (A.20) or Eq. (A.27) depending on whether $\varepsilon_1/\varepsilon_2 \to 0$ or $\varepsilon_2/\varepsilon_1 \to 0$, but will yield identical degenerate systems.

Consider the case $\varepsilon_1, \varepsilon_2 \to 0$ such that $\varepsilon_1/\varepsilon_2 \to 0$. The degenerate system of first order in Eq. (A.20) is then used to derive a degenerate system of second order. From Eq. (A.20) the adjoined system of second order is given by

$$\frac{d\gamma_3}{d\tau_2} = \frac{\beta\varrho}{\alpha+1}\left(1-\gamma_3\left(1+\frac{\alpha}{\varrho}\right)\right)-\gamma_3, \tag{A.28}$$

where $\tau_2 = \tau/\varepsilon_2$. The singular solution of the adjoint system of second order is easily shown to be stable and independent of the quasi-steady state value of γ_3. By nullifying the adjoint system of second order, the expression

$$\gamma_3 = \frac{\beta\varrho}{1+\beta\varrho+\alpha(1+\beta)}, \tag{A.29}$$

is obtained for the quasi-steady state value of γ_3. Inserting the quasi-steady state value of γ_3 into the rate equation for α in Eq. (A.20) one, obtains the degenerate system of second order given by

$$\boxed{\frac{d\alpha}{d\tau} = -\frac{\sigma\alpha(1+\delta\beta)}{(1+\beta\varrho)+\alpha(1+\beta)}} \tag{A.30}$$

.

When $\varepsilon_1, \varepsilon_2 \to 0$ such that $\varepsilon_2/\varepsilon_1 \to 0$ the degenerate system of second order is obtained from Eq. (A.27). The smallness of ε_1 is ensured when $\epsilon \to 0$. In this case, the adjoined system of second order is given by

$$\frac{d\gamma_1}{d\tau_1} = \frac{\alpha(1-\gamma_1(\beta+1))}{1+\beta\varrho}-\gamma_1, \tag{A.31}$$

where $\tau_1 = \tau/\varepsilon_1$. The singular solution of the adjoint system of second order will always be stable and the quasi-steady state value of γ_1 will be given by

$$\gamma_1 = \frac{\alpha}{1+\beta\varrho+\alpha(1+\beta)}. \tag{A.32}$$

Inserting the quasi-steady state value of γ_1 into the rate equation for α in Eq. (A.27), one readily obtains the degenerate system of second order given by Eq.

(A.30) The degenerate system obtained by the standard method, where it is assumed that $\varepsilon_1 = \varepsilon_2$ will also given by Eq. (A.30).

The dimensional form of the reaction rate $v = -d[S]/dt$ obtained from Eq. (A.30) is given by

$$v = \frac{k_c e_0 \left(1 + \frac{k_c'}{k_c}\frac{[L]}{K_l'}\right)[S]}{K_m\left(1 + \frac{[L]}{K_l}\right) + [S]\left(1 + \frac{[L]}{K_l'}\right)} \tag{A.33}$$

which coincides with the rate equation obtained without normalization of the rate equation and by considering the Michaelis-Menten type reactions and the reversible ligand dissociations reactions independently (see e.g. Christensen, 1993). The degenerate system of second order in Eq. (A.30) is a valid approximation of the full model in Eq. (A.12) when $\eta, \epsilon, \varepsilon_2 \to 0$. In dimensional form these requirements read

$$e^0 \ll K_l, \qquad e^0 \ll K_m, \qquad k_\tau \ll k_{lb}, \tag{A.34}$$

and a sufficiently low enzyme concentration and a sufficiently high rate constant for the dissociation of ligand from enzyme ensures that Eq. (A.33) is valid after a short time period needed to establish the quasi-steady state between the different enzyme species.

APPENDIX **B**

Product Activation of an Oligomeric Allosteric Enzyme

In this Appendix, appropriate low dimensional descriptions of the instability generating mechanism discussed in Chapter 5 will be derived. For convenience, the schematic illustration of the reactions involved in the mechanism reappear in Fig. (B.1). The system considered in Chapter 5 is open to the surroundings and substrate is supplied constantly at a rate determined by v_{in}. The product is removed from the system proportionally to the first order rate constant k_{out}. The elementary reactions outlined in Fig. (B.1) are transformed into a set of autonomous ordinary differential equations by applying the law of mass action. The derivation of the mass action kinetic equations for this system can be found elsewhere (Kærn, 1995). When described by MWC-theory the dimeric allosteric enzyme can exist in a inactive T-form and active R-form. Here, only R-exclusive binding is considered and the substrate and the effector is assumed to bind only to the active form. Each active binding states in Fig. (B.1) is uniquely defined by the number of substrate and product molecules bound to the active and the effector sites. The notation will be such that $[R_{ij}]$ represents the concentration of enzyme in the active R-conformation that binds i substrate in the active site and j product molecules in the effector site. The indices i, j will for a dimeric enzyme be limited to $i, j \in (0, 1, 2)$. The inactive binding state is denoted by T_{00}.

When the total enzyme concentration e^0 is conserved, the concentration of inactive enzyme can be taken as a dependent variable through the conservation relation

$$[T_{00}] = e^0 - \sum_{i,j=0}^{2} [R_{ij}]. \tag{B.1}$$

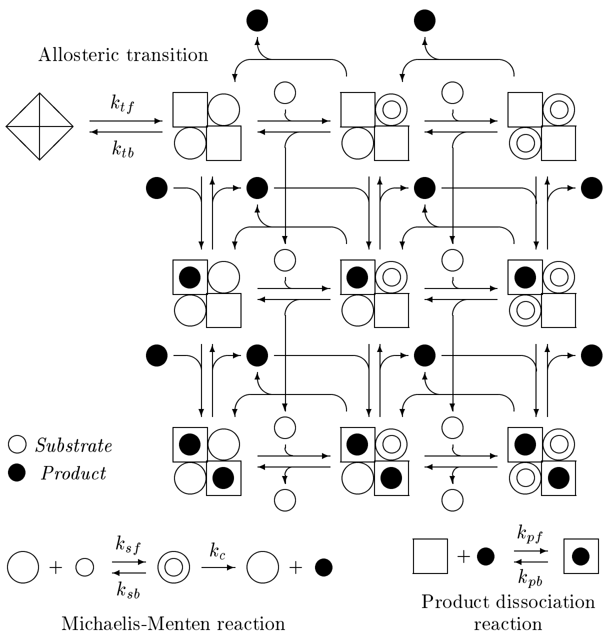

Fig. B.1: Elementary Reactions of a dimeric product activated allosteric enzyme described by the R-exclusive concerted MWC-model. The enzyme exists in an inactive T-conformation (diamond) and in an active R-conformation. The latter contains two active sites (circles) and two allosteric sites (squares). The elementary reactions comprises three sub-reactions and the rate constants in the system are defined in the labeled illustrations of the sub-reactions. The sub-reactions are identified as a Michaelis-Menten reaction, a product dissociation reaction and an allosteric transition. The exclusive binding of product to the R-conformation comprises an auto-catalytic feedback loop which, when the system is open to the surroundings, allows for the emergence of sustained oscillatory behavior. The figure is reproduced from Chapter 5 for convenience.

B.1 Full Dimensionless Model

The mass action kinetic rate equations obtained by applying the law of mass action to the elementary reactions outlined in Fig. (B.1) are normalized by defining the dimensionless variables

$$\alpha = \frac{[S]}{K_m}, \qquad \beta = \frac{[P]}{K_p}, \qquad r_{ij} = \frac{[R_{ij}]}{e^0}, \qquad \tau = tk_{out}, \tag{B.2}$$

and the dimensionless parameters

$$\begin{array}{cccc} \nu = \dfrac{v_{in}}{K_m k_{out}}, & \sigma = \dfrac{k_c e_0}{K_m k_{out}}, & q = \dfrac{K_p}{K_m}, & L, \\ \epsilon = \dfrac{e_0}{K_m}, & \varepsilon_1 = \dfrac{k_{out}}{k_{sb}+k_c}, & \varepsilon_2 = \dfrac{k_{out}}{k_{pb}}, & \varepsilon = \dfrac{k_{out}}{k_{tb}}. \end{array} \tag{B.3}$$

The normalization of the rate equations is presented in detail elsewhere (Hunding & Kærn, 1997) and the resulting linearly independent dimensionless AODE's can be written as in Tab. (B.1).

The full system appears rather complicated even though the allosteric enzyme is included using a minimal model. If the enzyme was not R-exclusive, which may indeed be the most frequent situation *in vivo* (Zhou *et al.*, 1989), the number of independent variables would be $2 \cdot 3 \cdot 3 - 1 + 2 = 19$ and if the enzyme were composed by four subunits and not R-exclusive the full model should include 51 independent AODE's (calculated by $2 \cdot 5 \cdot 5 - 1 + 2$). The MWC-model, as well as the sequential model (Koshland *et al.*, 1966), is a special case of a detailed mechanism proposed by Eigen (Eigen, 1968). The Eigen model is quite complex for a mathematical analysis as the full model would contain rate equations for $10^2 - 1 + 2 = 101$ species in the case of a dimeric enzyme and as many as $35^2 - 1 + 2 = 1226$ independent AODE's in the case of a tetrameric enzyme. The great number of variables makes numerical computation difficult as well as lowering the mathematical tractability.

B.2 Low Dimensional Models

The full dimensionless description in Tab. (B.1) is an example of a complex reaction system, as the right hand sides of the rate equations contain several parameters. The simplification methods which rely on the applicability of Tihonov's theorems fail except when the parameters ε, ε_1 and ε_3 are small and the Michaelis-Menten type reactions, the dissociation of product from the effector site and the allosteric transition, are fast equilibrating. In the following sections low dimensional approximations to the full description in Tab. (B.1) will be derived using the extended method presented in Chapter 2. The low dimensional models are appropriate for the investigations of the effect of having one or more slow enzyme reactions performed in Chapter 5 and 6. During the derivation, appropriate conditions for applying the QSSA are obtained and it is shown that fast equilibrating reactions may not be sufficient to ensure that the truncated descriptions are valid approximations of the full description in Tab. (B.1).

$$
\begin{aligned}
\frac{d\alpha}{d\tau} &= \nu + \frac{\epsilon}{\varepsilon_1}\left[\sum i r_{ij} - \alpha(2\sum r_{ij} - \sum i r_{ij})\right] - \sigma \sum i r_{ij} \\
\frac{d\beta}{d\tau} &= q\sigma \sum i r_{ij} + q\frac{\epsilon}{\varepsilon_2}\left[\sum j r_{ij} - \beta(2\sum r_{ij} - \sum j r_{ij})\right] - \beta \\
\frac{dr_{00}}{d\tau} &= \frac{1}{\varepsilon_1}(r_{10} - 2\alpha r_{00}) + \frac{1}{\varepsilon_2}(r_{01} - 2\beta r_{00}) + \frac{1}{\varepsilon}\left[\frac{1}{L}\left(1 - \sum r_{ij}\right) - r_{00}\right] \\
\frac{dr_{10}}{d\tau} &= \frac{1}{\varepsilon_1}\left[\alpha(2r_{00} - r_{10}) + 2r_{20} - r_{10}\right] + \frac{1}{\varepsilon_2}(r_{11} - 2\beta r_{10}) \\
\frac{dr_{20}}{d\tau} &= \frac{1}{\varepsilon_1}(\alpha r_{10} - 2r_{20}) + \frac{1}{\varepsilon_2}(r_{21} - 2\beta r_{20}) \\
\frac{dr_{01}}{d\tau} &= \frac{1}{\varepsilon_1}(r_{11} - 2\alpha r_{01}) + \frac{1}{\varepsilon_2}[\beta(2r_{00} - r_{01}) + 2r_{02} - r_{01}] \\
\frac{dr_{11}}{d\tau} &= \frac{1}{\varepsilon_1}[\alpha(2r_{01} - r_{11}) + 2r_{21} - r_{11}] + \frac{1}{\varepsilon_2}[\beta(2r_{10} - r_{11}) + 2r_{12} - r_{11}] \\
\frac{dr_{21}}{d\tau} &= \frac{1}{\varepsilon_1}(\alpha r_{11} - 2r_{21}) + \frac{1}{\varepsilon_2}[\beta(2r_{20} - r_{21}) + 2r_{22} - r_{21}] \\
\frac{dr_{02}}{d\tau} &= \frac{1}{\varepsilon_1}(r_{12} - 2\alpha r_{02}) + \frac{1}{\varepsilon_2}(\beta r_{01} - 2r_{02}) \\
\frac{dr_{12}}{d\tau} &= \frac{1}{\varepsilon_1}[\alpha(2r_{02} - r_{12}) + 2r_{22} - r_{12}] + \frac{1}{\varepsilon_2}(\beta r_{11} - 2r_{12}) \\
\frac{dr_{22}}{d\tau} &= \frac{1}{\varepsilon_1}(\alpha r_{12} - 2r_{22}) + \frac{1}{\varepsilon_2}(\beta r_{21} - 2r_{22})
\end{aligned}
$$

Tab. B.1: Full set of dimensionless AODE's describing the dynamics of an open autocatalytic allosteric enzyme reaction based on the elementary reactions in figure B.1. The variables α, β and r_{ij} represent substrate, product and active enzymes with i substrate and j molecules bound. All summations are taken over $i, j \in (0, 1, 2)$. The definitions of dimensionless variables and parameters are given in the text.

B.2.1 Fast Substrate Equilibration

The Michaelis-Menten type reactions in Fig. (B.1) can be considered fast equilibrating if $\varepsilon_1 \to 0$. Let $\varepsilon_1 \to 0$ such that $\varepsilon_1/\varepsilon_2 \to 0$ and $\varepsilon_1/\varepsilon \to 0$. Changing the time-scale to $\tau_1 = \tau/\varepsilon_1$, the full description in Tab. (B.1) yields

$$
\begin{aligned}
&\frac{d\alpha}{d\tau_1} = \epsilon\left[\gamma_1 - \alpha(2\gamma - \gamma_1)\right], \\
&\frac{dr_{00}}{d\tau_1} = r_{10} - 2\alpha r_{00}, \quad \frac{dr_{10}}{d\tau_1} = \alpha(2r_{00} - r_{10}) + 2r_{20} - r_{10}, \quad \frac{dr_{20}}{d\tau_1} = \alpha r_{10} - 2r_{20}, \\
&\frac{dr_{01}}{d\tau_1} = r_{11} - 2\alpha r_{01}, \quad \frac{dr_{11}}{d\tau_1} = \alpha(2r_{01} - r_{11}) + 2r_{21} - r_{11}, \quad \frac{dr_{21}}{d\tau_1} = \alpha r_{11} - 2r_{21}, \\
&\frac{dr_{02}}{d\tau_1} = r_{12} - 2\alpha r_{02}, \quad \frac{dr_{12}}{d\tau_1} = \alpha(2r_{02} - r_{12}) + 2r_{22} - r_{12}, \quad \frac{dr_{22}}{d\tau_1} = \alpha r_{12} - 2r_{22}.
\end{aligned}
\tag{B.4}
$$

The substrate level α cannot be parameterized on the fast time-scale τ_1 since the rate of change is not negligible as required by the simplification method. This condition can be ensured by choosing a sufficiently small value of ϵ. From the definitions of dimensionless parameters it is observed that

$$
\varepsilon_1 = \frac{k_{out}}{k_{sb} + k_c} \leq \frac{k_{out}}{k_c} = \frac{\epsilon}{\sigma} \tag{B.5}
$$

and $\epsilon \to 0$ therefore implies that $\varepsilon_1 \to 0$ when σ is of moderate value. When assuming that $\epsilon \to 0$, it is thus ensured that α can be treated as a parameter and the Michaelis-Menten reaction is a fast equilibrating reaction.

On the time-scale τ_1, the full description in Tab. (B.1) contains the linear dependencies

$$
\frac{dr_{00}}{d\tau_1} + \frac{dr_{10}}{d\tau_1} + \frac{dr_{20}}{d\tau_1} = 0, \quad \frac{dr_{01}}{d\tau_1} + \frac{dr_{11}}{d\tau_1} + \frac{dr_{21}}{d\tau_1} = 0, \quad \frac{dr_{02}}{d\tau_1} + \frac{dr_{12}}{d\tau_1} + \frac{dr_{22}}{d\tau_1} = 0, \tag{B.6}
$$

which can be taken into account by defining y_1, y_2 and y_3

$$
y_1 = r_{00} + r_{10} + r_{20}, \quad y_2 = r_{01} + r_{11} + r_{21}, \quad y_3 = r_{02} + r_{12} + r_{22}. \tag{B.7}
$$

The adjoint system of first order, which is linearly independent when the definitions in Eq. (B.7) are employed, can be obtained as in Eq. (B.8) where r_{00}, r_{01}

and r_{02} are replaced in accordance with Eq. (B.7).

$$\begin{aligned}
\frac{dr_{10}}{d\tau_1} &= \alpha(2(y_1 - r_{20}) - 3r_{10}) + 2r_{20} - r_{10}, & \frac{dr_{20}}{d\tau_1} &= \alpha r_{10} - 2r_{20}, \\
\frac{dr_{11}}{d\tau_1} &= \alpha(2(y_2 - r_{21}) - 3r_{11}) + 2r_{21} - r_{11}, & \frac{dr_{21}}{d\tau_1} &= \alpha r_{11} - 2r_{21}, \\
\frac{dr_{12}}{d\tau_1} &= \alpha(2(y_3 - r_{22}) - 3r_{12}) + 2r_{22} - r_{12}, & \frac{dr_{22}}{d\tau_1} &= \alpha r_{12} - 2r_{22}.
\end{aligned} \tag{B.8}$$

The Jacobian matrix of the adjoined system of first order is a diagonal block matrix

$$\mathbf{J} = \begin{pmatrix} \mathbf{M} & \mathbf{0} & \mathbf{0} \\ \mathbf{0} & \mathbf{M} & \mathbf{0} \\ \mathbf{0} & \mathbf{0} & \mathbf{M} \end{pmatrix}, \tag{B.9}$$

where $\mathbf{0}$ represents a two-dimensional square null-matrix and

$$\mathbf{M} = \begin{pmatrix} -3\alpha - 1 & -2\alpha + 2 \\ \alpha & -2 \end{pmatrix}. \tag{B.10}$$

The eigenvalues of the Jacobian matrix are triply degenerate eigenvalues of $\mathbf{M}$ and the stability of the singular point is therefore determined by

$$0 = det(\mathbf{M} - \lambda\mathbf{I}) = det \begin{pmatrix} -3\alpha - 1 - \lambda & -2\alpha + 2 \\ \alpha & -2 - \lambda \end{pmatrix} \Rightarrow \begin{cases} \lambda_1 & = -1 - \alpha, \\ \lambda_2 & = -2 - 2\alpha \end{cases}. \tag{B.11}$$

The substrate concentration α is always positive and the singular point is thus always stable.

The left hand sides of the rate equations in the adjoined system of first order in Eq. (B.8) are nullified when

$$\begin{aligned}
r_{10} &= 2\alpha r_{00}, & r_{20} &= \alpha/2 r_{10} = \alpha^2 r_{00}, \\
r_{11} &= 2\alpha r_{01}, & r_{21} &= \alpha/2 r_{11} = \alpha^2 r_{01}, \\
r_{12} &= 2\alpha r_{02}, & r_{22} &= \alpha/2 r_{12} = \alpha^2 r_{02},
\end{aligned} \tag{B.12}$$

which defines the quasi-steady state values of r_{10}, r_{20}, r_{11}, r_{21}, r_{12} and r_{22}. The quasi-steady state values are uniquely defined by the values of α, r_{00}, r_{01} and r_{02} and the singular point is always stable.

The degenerate system of second order is obtained by inserting the quasi-steady states in Eq. (B.12) into the full description in Tab. (B.1). The rate equations for r_{10}, r_{20}, r_{11}, r_{21}, r_{12}, r_{22} can then be omitted and all terms involving ε_1 are negligible. The degenerate system of first order then evaluates to

$$\frac{d\alpha}{d\tau} = \nu - 2\sigma\alpha(1+\alpha)(r_{00}+r_{01}+r_{02}), \tag{B.13a}$$

$$\frac{d\beta}{d\tau} = 2q\sigma\alpha(1+\alpha)(r_{00}+r_{01}+r_{02}) - \beta \tag{B.13b}$$

$$+q\frac{\epsilon}{\varepsilon_2}(1+\alpha)^2\left[(\beta+1)(r_{01}+2r_{02}) - 2\beta(r_{00}+r_{01}+r_{02})\right], \tag{B.13c}$$

$$\frac{dr_{00}}{d\tau} = \frac{1}{\varepsilon_2}(r_{01}-2\beta r_{00}) + \frac{1}{\varepsilon}\left[\frac{1}{L}(1-(\alpha+1)^2(r_{00}+r_{01}+r_{02})) - r_{00}\right], \tag{B.13d}$$

$$\frac{dr_{01}}{d\tau} = \frac{1}{\varepsilon_2}(\beta(2r_{00}-r_{01}) + 2r_{02} - r_{01}), \tag{B.13e}$$

$$\frac{dr_{02}}{d\tau} = \frac{1}{\varepsilon_2}(\beta r_{01} - 2r_{02}). \tag{B.13f}$$

which is an appropriate approximation of the full description in Tab. (B.1) when $\epsilon \to 0$.

At this stage in the reduction, it is convenient to introduce a new variable γ to represent the total amount of active enzyme

$$\gamma = \sum_{i,j=0}^{2} r_{ij} = (1+\alpha)^2(r_{00}+r_{01}+r_{02}). \tag{B.14}$$

The new variable is used to replace r_{00} by

$$r_{00} = \frac{\gamma}{(\alpha+1)^2} - (r_{01}+r_{02}), \tag{B.15}$$

and the degenerate system of first order in Eq. (B.13) reads

$$\begin{aligned}
\frac{d\alpha}{d\tau} &= \nu - 2\frac{\sigma\alpha\gamma}{1+\alpha}, \\
\frac{d\beta}{d\tau} &= 2q\frac{\sigma\alpha\gamma}{1+\alpha} + q\frac{\epsilon}{\varepsilon_2}\left[(\beta+1)(\alpha+1)^2(r_{01}+2r_{02}) - 2\beta\gamma\right] - \beta, \\
\frac{d\gamma}{d\tau} &= \frac{1}{\varepsilon}\left[\frac{1}{L}(1-\gamma) - \frac{\gamma}{(\alpha+1)^2} + (r_{01}+r_{02})\right], \\
\frac{dr_{01}}{d\tau} &= \frac{1}{\varepsilon_2}\left[2r_{02} - r_{01} + \beta\left(\frac{2\gamma}{(\alpha+1)^2} - 3r_{01} - 2r_{20}\right)\right], \\
\frac{dr_{02}}{d\tau} &= \frac{1}{\varepsilon_2}(\beta r_{01} - 2r_{02}).
\end{aligned} \tag{B.16}$$

The parameters ε_2 and ε in the degenerate system of first order occur, with the above variable transformation, in separate rate equations. Further simplification can be employed using Tihonov's second theorem as discussed in Chapter 2.

B.2.2 Slow Allosteric Transition

The degenerate system of first order written in Eqs. (B.16) can be used as basis for further simplification. Here, an approximation of the full model is derived for the case where only the allosteric transition cannot be considered to be fast equilibrating.

In the system written in Eq. (B.16), let $\varepsilon_2 \to 0$ such that $\varepsilon_2/\varepsilon \to 0$. The degenerate system of first order will, on the fast time-scale $\tau_2 = \tau/\varepsilon_2$, be described by the rate equations

$$\begin{aligned} \frac{d\beta}{d\tau_2} &= q\epsilon\left[(\beta+1)(\alpha+1)^2(r_{01}+2r_{02}) - 2\beta\gamma\right], \\ \frac{dr_{01}}{d\tau_2} &= 2r_{02} - r_{01} + \beta\left(\frac{2\gamma}{(\alpha+1)^2} - 3r_{01} - 2r_{20}\right), \\ \frac{dr_{02}}{d\tau_2} &= \beta r_{01} - 2r_{02}. \end{aligned} \tag{B.17}$$

As was observed for α during the derivation of the degenerate system of first order in Eq. (B.16), the variable β, which is to be considered a slow changing variable, has a non-zero rate of change on the fast time-scale τ_2. Tihonov's second theorem can therefore not be applied if the quantity $q\epsilon$ is not sufficiently small. In the case where q is of moderate level (i.e. where K_m and K_p are on comparable scales) the condition for applying Tihonov's second theorem is ensured when ϵ is sufficiently small. The requirement of a low value of ϵ is met as it is a necessary assumption for the validity of the degenerate system of first order in Eq. (B.16).

When $q\epsilon \to 0$ the adjoined system of second order, which is the adjoined system of the degenerate system of first order in Eq. (B.16), reads

$$\begin{aligned} \frac{dr_{01}}{d\tau_2} &= 2r_{02} - r_{01} + \beta\left(\frac{2\gamma}{(\alpha+1)^2} - 3r_{01} - 2r_{20}\right), \\ \frac{dr_{02}}{d\tau_2} &= \beta r_{01} - 2r_{02}. \end{aligned} \tag{B.18}$$

The rate equation for r_{01} in Eq. (B.18) reveals that the value of r_{02} in the singular point is given by $r_{02} = \beta r_{01}/2$. Replacing r_{02} by $\beta r_{01}/2$ in the rate equation for r_{02} in Eq. (B.18), one obtains the algebraic equations

$$\beta r_{01} - r_{01} + \beta\left(\frac{2\gamma}{(\alpha+1)^2} - 3r_{01} - \beta r_{01}\right) = 0 \Rightarrow \frac{2\beta\gamma}{(\alpha+1)^2} - r_{01}(1+\beta)^2 = 0.$$

The quasi-steady state values of $r_{01}$and r_{02} are thus determined by

$$r_{01} = \frac{2\beta\gamma}{(\alpha+1)^2(\beta+1)^2}, \qquad r_{02} = \frac{\beta^2\gamma}{(\alpha+1)^2(\beta+1)^2}. \tag{B.19}$$

The singular point of the adjoint system of second order can easily be shown to be stable by evaluating the eigenvalues of

$$\mathbf{J} = \begin{pmatrix} -3\beta - 1 & -2\beta + 2 \\ \beta & -2 \end{pmatrix}. \tag{B.20}$$

As the singular solution is always stable and the quasi-steady state values of r_{01} and r_{02} are uniquely defined by α, β and γ, one can obtain the degenerate system of second order. When the quasi-steady state values given in Eq. (B.19) for r_{01} and r_{02} are inserted into the degenerate system of first order in Eq. (B.16) the degenerate system of second order becomes

$$\begin{aligned} \frac{d\alpha}{d\tau} &= \nu - \frac{2\sigma\gamma\alpha}{\alpha+1}, \\ \frac{d\beta}{d\tau} &= \frac{2q\sigma\gamma\alpha}{\alpha+1} - \beta, \\ \varepsilon\frac{d\gamma}{d\tau} &= \frac{1}{L} - \gamma\left[\frac{(\alpha+1)^2(\beta+1)^2 + L}{L(\alpha+1)^2(\beta+1)^2}\right]. \end{aligned} \tag{B.21}$$

Eq. (B.21) is an appropriate approximation of the full mass kinetic description in Tab. (B.1) if $\epsilon \to 0$, $q\epsilon \to 0$ and $\varepsilon_2 \to 0$. From the definitions of ϵ, q and ε_2 in Eq. (B.3) these conditions are

$$e^0 \ll K_m, \qquad e^0 \ll K_p, \qquad k_{out} \ll k_{pb}. \tag{B.22}$$

B.2.3 Slow Product Dissociation

Tihonov's Second Theorem can also be used to simplify the degenerate system of first order in Eqs. (B.16) when the Michaelis-Menten reaction and the allosteric transition are fast equilibrating, but ε_2 cannot be considered small. The allosteric transition can be considered fast if ε is sufficiently close to zero.

Let $\varepsilon \to 0$, such that $\varepsilon/\varepsilon_2 \to 0$ in the system described by Eqs. (B.16). The adjoined system of second order is then given by

$$\frac{d\gamma}{d\tau_3} = \frac{1}{L}(1-\gamma) - \frac{\gamma}{(\alpha+1)^2} + (r_{01} + r_{02}), \tag{B.23}$$

where $\tau_3 = \tau/\varepsilon$. The adjoined system of second order is nullified when

$$\gamma = (\alpha+1)^2 \frac{L(r_{01} + r_{02}) + 1}{L + (\alpha+1)^2}, \tag{B.24}$$

and it is easily shown that the singular solution of the adjoined system of second order meets the conditions for applying Tihonov's second theorem. Inserting the quasi-steady state relation Eq. (B.24) into Eq. (B.16) one obtains the degenerate system of second order

$$\begin{aligned}
\frac{d\alpha}{d\tau} &= \nu - 2\sigma\alpha(\alpha+1)\frac{L(r_{01}+r_{02})+1}{L+(\alpha+1)^2}, \\
\frac{d\beta}{d\tau} &= 2q\sigma\alpha(\alpha+1)\frac{L(r_{01}+r_{02})+1}{L+(\alpha+1)^2} - \beta \\
&\quad + q\frac{\epsilon}{\varepsilon_2}\left[(\beta+1)(\alpha+1)^2(r_{01}+2r_{02}) - 2\beta(\alpha+1)^2\frac{L(r_{01}+r_{02})+1}{L+(\alpha+1)^2}\right], \\
\frac{dr_{01}}{d\tau} &= \frac{1}{\varepsilon_2}\left[2r_{02} - r_{01} + \beta\left(2\frac{L(r_{01}+r_{02})+1}{L+(\alpha+1)^2} - 3r_{01} - 2r_{20}\right)\right], \\
\frac{dr_{02}}{d\tau} &= \frac{1}{\varepsilon_2}(\beta r_{01} - 2r_{02}).
\end{aligned} \tag{B.25}$$

The model in Eq. (B.25) is a valid approximation of the full description in Tab. (B.1) if $\epsilon \to 0$ and $\varepsilon \to 0$. In dimensional form these conditions read

$$e^0 \ll K_m, \qquad k_{out} \ll k_{tb}. \tag{B.26}$$

B.2.4 Slow Michaelis-Menten Reaction

To derive an appropriate reduced description in the case where the Michaelis-Menten reaction is the only non-fast reaction, one has to start from the full description in Tab. (B.1). The derivation to follow below is similar to the derivations in the previous sections and details will be left out to avoid repetition.

Let $\varepsilon_2 \to 0$ such that $\varepsilon_2/\varepsilon_1 \to 0$ and $\varepsilon_2/\varepsilon \to 0$ in the full model described in Tab. (B.1). When $q\epsilon \to 0$ the roots of the adjoined system of first order yields the quasi-steady state relations

$$\begin{aligned}
r_{01} &= 2\beta r_{00}, & r_{02} &= \beta^2 r_{00}, \\
r_{11} &= 2\beta r_{10}, & r_{12} &= \beta^2 r_{10}, \\
r_{12} &= 2\beta r_{20}, & r_{22} &= \beta^2 r_{20}.
\end{aligned} \tag{B.27}$$

It is readily shown, that the singular point of the adjoined system of first order has ensured stability and the conditions for applying the extended method are met. Replacing r_{00} with

$$r_{00} = \frac{\gamma}{(\beta+1)^2} - (r_{01} + r_{02}), \tag{B.28}$$

the degenerate system of first order written in Eq. (B.29) can be written in a form where ε_1 and ε appear in separate rate equations.

$$\begin{aligned}
\frac{d\alpha}{d\tau} &= \nu + \frac{\epsilon}{\varepsilon_1}\left[(\alpha+1)(\beta+1)^2(r_{10}+2r_{20}) - 2\alpha\gamma\right] - \sigma(\beta+1)^2(r_{10}+2r_{20}),\\
\frac{d\beta}{d\tau} &= q\sigma(\beta+1)^2(r_{10}+2r_{20}) - \beta,\\
\frac{d\gamma}{d\tau} &= \frac{1}{\varepsilon}\left[\frac{1}{L}(1-\gamma) - \frac{\gamma}{(\beta+1)^2} + r_{10} + r_{20}\right],\\
\frac{dr_{10}}{d\tau} &= \frac{1}{\varepsilon_1}\left[2r_{20} - r_{10} + \alpha\left(\frac{2\gamma}{(\beta+1)^2} - 3r_{10} - 2r_{20}\right)\right],\\
\frac{dr_{20}}{d\tau} &= \frac{1}{\varepsilon_1}(\alpha r_{10} - 2r_{20}).
\end{aligned} \tag{B.29}$$

The degenerate system in Eq. (B.29) is an appropriate approximation of the full model in Tab. (B.1) when $\epsilon \to 0$ and $\varepsilon_2 \to 0$.

The degenerate system of first order in Eq. (B.29) can be further simplified using Tihonov's second theorem when ε is small. When $\varepsilon \to 0$ such that $\varepsilon/\varepsilon_1 \to 0$ one obtains the degenerate system of second order

$$\begin{aligned}
\frac{d\alpha}{d\tau} &= \nu - \sigma(\beta+1)^2(r_{10}+2r_{20})\\
&\quad + \frac{\epsilon}{\varepsilon_1}\left[(\alpha+1)(\beta+1)^2(r_{10}+2r_{20}) - 2\alpha(\beta+1)^2\frac{L(r_{10}+r_{20})+1}{L+(\beta+1)^2}\right],\\
\frac{d\beta}{d\tau} &= q\sigma(\beta+1)^2(r_{10}+2r_{20}) - \beta,\\
\frac{dr_{10}}{d\tau} &= \frac{1}{\varepsilon_1}\left[2r_{20} - r_{10} + \alpha\left(2\frac{L(r_{10}+r_{20})+1}{L+(\beta+1)^2} - 3r_{10} - 2r_{20}\right)\right],\\
\frac{dr_{20}}{d\tau} &= \frac{1}{\varepsilon_1}(\alpha r_{10} - 2r_{20}).
\end{aligned} \tag{B.30}$$

It can easily be verified that the conditions for applying Tihonov's second theorem are met. The reduced model in Eq. (B.30) is an appropriate approximation of the full model in Tab. (B.1) when $q\epsilon \to 0$, $\varepsilon_2 \to 0$ and $\varepsilon \to 0$. In dimensional form these conditions read

$$e^0 \ll K_p, \qquad k_{out} \ll k_{pb}, \qquad k_{out} \ll k_{tb}. \tag{B.31}$$

B.3 Reduced Model

When the Michaelis-Menten constant and the product dissociation constant are of comparable sizes the value of q is of moderate size, and $q\epsilon \to 0$ can only be obtained if $\epsilon \to 0$. As discussed in section B.2.1 $\epsilon \to 0$ implies $\varepsilon_1 \to 0$. Thus, when q is moderate of size the assumption $q\epsilon \to 0$ required for the validity of Eq. (B.30) implies that the Michaelis-Menten reaction is fast equilibrating and the system can be further simplified. When $\epsilon \to 0$ and $\varepsilon_1 \to 0$ the adjoined system of Eq. (B.30) is

$$\begin{aligned} \frac{dr_{10}}{d\tau_1} &= 2r_{20} - r_{10} + \alpha\left(2\frac{L(r_{10}+r_{20})+1}{L+(\beta+1)^2} - 3r_{10} - 2r_{20}\right), \\ \frac{dr_{20}}{d\tau_1} &= \alpha r_{10} - 2r_{20}. \end{aligned} \tag{B.32}$$

The adjoined system is nullified when

$$r_{10} = \frac{\alpha}{L+(\alpha+1)^2(\beta+1)^2}, \qquad r_{20} = \frac{\alpha}{2(L+(\alpha+1)^2(\beta+1)^2)}, \tag{B.33}$$

and it can easily be shown that the singular point is stable and attracts any initial condition. The degenerate system is then

$$\begin{aligned} \frac{d\alpha}{d\tau} &= \nu - \frac{2\sigma\alpha(\alpha+1)(\beta+1)^2}{L+(\alpha+1)^2(\beta+1)^2}, \\ \frac{d\beta}{d\tau} &= \frac{2q\sigma\alpha(\alpha+1)(\beta+1)^2}{L+(\alpha+1)^2(\beta+1)^2} - \beta, \end{aligned} \tag{B.34}$$

The system in Eq. (B.34) is an appropriate approximation of the full system in Tab. (B.1), if q is of moderate value and $\epsilon, \varepsilon_2, \varepsilon \to 0$. The two-dimensional model in Eq. (B.34) may also be derived from Eq. (B.21) or Eq. (B.25) when assuming, respectively, that the ε or ϵ and ε_2 are small. The dimensional conditions for the validity of Eq. (B.34) read

$$e^0 \ll K_m, \quad e^0 \ll K_p, \quad k_{sb} + k_c \ll k_{out}, \quad k_{pb} \ll k_{out}, \quad k_{tb} \ll k_{out}. \tag{B.35}$$

The models in Eq. (B.21) and Eq. (B.25) can be used to investigate the effect of, respectively, a slow allosteric transition and a slow product dissociation reaction. When the Michaelis-Menten constant and the product dissociation constant are of comparable sizes, such that the value of q is moderate, the model in Eq. (B.30) cannot be used to investigate the effect of a slow Michaelis-Menten reaction. The model is based on the assumption $q\epsilon \to 0$ which at finite values of q implies $\epsilon \to 0$. According to Eq. (B.5)

$$\varepsilon_1 \leq \frac{\epsilon}{\sigma} \tag{B.36}$$

and $\epsilon \to 0$ implies $\varepsilon_1 \to 0$ when σ has a moderate value. The substrate α and product β cannot be treated as slow variables without assuming $\epsilon \to 0$ and $q\epsilon \to 0$, respectively, and the full model in Tab. (B.1) cannot be significantly simplified even when $\varepsilon_1 \to 0$ if ϵ is finite and non-zero.

The validity of models simplified using the QSSA relies on the separation of fast and slow variables. In biochemical reactions this requirement manifests through a condition of smallness of the enzyme concentration as compared to the choice of normalization constant for the species that interacts with the enzyme. The elimination of the fast Michaelis-Menten type reactions and product dissociation reaction as employed here require that the total enzyme concentration is, respectively, much less than the Michaelis-Menten constant K_m and the dissociation constant K_p. The problem of non-separable time-scales can be avoided by a variable transformation where the total amount of, for example, substrate, is expressed as the sum of free substrate plus the amount of substrate bound to the enzyme (Borghans *et al.*, 1996). If the new variables

$$\alpha_T = \alpha + \epsilon \sum_{i,j=0}^{2} i r_{ij}, \qquad \beta_T = \beta + \epsilon \sum_{i,j=0}^{2} j r_{ij}, \tag{B.37}$$

are employed instead of α and β in the mass kinetic description in Tab. (B.1), one can obtain simplified models that do not restrain the enzyme concentration and only require fast equilibrating sub-reactions. This would increase the number of cases where the reduced models are applicable. It is, however, not required to derive low dimensional models in order to investigate the effect of high enzyme concentrations. A variable transformation only relates to the chosen reference, for example concentrations of single species, and will not change the dynamic behavior of the system. The effect of high enzyme concentrations may therefore be investigated by numerical investigations of the full set of AODE's given in Tab. (B.1).

APPENDIX C

Suggested Publications

The Failure of the Quasi-steady State Approximation to Reveal Some Nonlinear Properties of Biological Systems

A. Hunding and M. Kærn

Abstract

The quasi-steady state approximation (QSSA) has a central role in the study of nonlinear dynamics as applied to biological control systems. In this paper, we investigate the effect of not assuming a quasi-steady state in a simple model of an auto-catalytic allosteric enzyme reaction showing simple oscillatory behavior through a finite or even slow rate of the allosteric transition of the control enzyme, or finite reaction rates for substrate or product binding.

We report that, even with a prototype biochemical oscillator, the actual behavior may be substantially more complex than the usually recorded dynamics in a corresponding simplified system, obtained from assuming a quasi-steady state. The basic system investigated here has been previously studied in great lengths in the simplified version where QSSA is invoked. Such previous studies of the simplified version have reported only one stable periodic solution and that more complex dynamics rely on more complex multi-enzyme mechanisms. However, we find that birhythmicity may indeed be observed when the truncation induced by assuming quasi steady-state is not invoked. Also, the simplified model may underestimate the system's ability to show simple periodic behavior which might indicate a physiological function of a slow allosteric transition. Finally, we also discuss the mathematical basis of the QSSA and analyze the applicability of the QSSA in general.

(Submitted to J. theor. Biol.)

Complex Dynamic Behavior Require Fast Reactions

M. Kærn and A. Hunding

Abstract

A biochemically plausible mechanism which can introduce complex dynamic behavior such as birhythmicity, bursting and chaos in biological systems is based on two auto-catalytic allosteric enzymes placed in series. The mathematical model for describing this reaction is based on a truncation of mass action kinetic rate equations where the number of independent variables is reduced using the quasi-steady state (QSSA) approximation. In the present paper, only a partial truncation of the mass kinetic rate equations is performed to investigate the effect of a slow allosteric transition in one of the auto-catalytic enzymes. The bifurcation diagram of a critical regulatory parameter reveals that the system shows a wide range of dynamic behaviors such as hard excitation, birhythmicity, quasi-periodicity, period doublings, chaos and bursting, when the allosteric transition is fast. When the rate of the allosteric transition is slowed, the system displays a reduced capacity for showing complex periodic or aperiodic dynamic behavior. It has been reported that the allosteric transition may have a half-time in the order of minutes before the enzyme establishes a quasi-steady state. This suggests that the instability generating mechanism may not be able to explain the emergence of bursting, chaos and quasi-periodicity in biological systems where the allosteric transition cannot be considered fast.

(In preparation)

Extending the Mathematical Basis of the Quasi-state Approximation

M. Kærn and P. G. Sørensen

Abstract

The mathematical foundation of quasi-steady state approximation (QSSA) as applied to chemical and biochemical reaction systems is based on two theorems by A. N. Tihonov. The theorems apply to chemical reactions where the rate equations contain a single small parameter that multiplies the derivative. There are, however, many relevant reactions, such as allosteric regulation, for which the rate equations cannot directly be written in the form required for applying Tihonov's theorems, as each rate equation may contain several small parameters. The standard method used to avoid this problem is to assume that all the small parameters are equal. This approach does not allow for simplification through the QSSA in cases where at least one parameter is not small which reduces the generality of the method.. In the present paper, an extended method for truncation of mass action kinetic equations is presented. The proposed method, which complements Tihonov's theorems, allows for simplification of the mathematical description of systems not meeting the criteria for Tihonov's theorems. The approach is exemplified through the derivation of appropriate models for ligand binding to a Michaelis-Menten enzyme and the effect of assuming quasi-steady state is investigated in a simple oscillatory reaction comprised of auto-catalytic Michaelis-Menten enzymes.

(In preparation)

A Plausible Mechanism for the Regulation of the M-phase Transition in *Xenopus leavis.*

M. Kærn

Abstract

The comprehensive model for the regulation of the early embryonic cell cycle of *Xenopus leavis* proposed recently by Novak and Tyson (the NT-model) is considered. Recent experimental results suggest that kinase Cdk2-cyclin E is required for the rapid divisions during the early development of the *Xenopus* embryos and that Cdk2-cyclin E is a central part of the cell cycle engine. Based on experimental considerations, the activity of Cdk2-cyclin E is incorporated in the NT-model as a positive effector of the phosphatase Cdc25. The extended NT-model can reproduce several recent experimental findings and suggests a plausible mechanism for the regulation of the G2 to M phase transition. A detailed bifurcation analysis reveals that the inclusion of the Cdk2-cyclin E complex leads to the case of an omega explosion where the transition from a uniquely defined cell cycle arrest to repeated divisions occurs through a homoclinic orbit with infinite period. The general properties of an omega explosion can explain the bifurcation as a dynamic mechanism well suited for the regulation of the cell cycle and may suggest a link between G2 checkpoint failure and DNA damage in human cells over-expressing Cdk2.

(In preparation)

Bibliography

ARAGÓN, J. J. & SOLS, A. 'Regulation of Enzyme Activity in the Cell: Effect of Enzyme Concentrations.' *FASEB J.*, **5**: 2945–2950 (1991).

ARKIN, A. & ROSS, J. 'Computational Functions in Biochemical Reaction Networks.' *Biophys. J.*, **67**: 560–578 (1994).

ATKINS, P. W. *Physcial Chemistry.* Oxford University Press, 4th edn. (1992).

BORGHANS, J. A. M., DE BOER, R. J. & SEGEL, L. A. 'Extending the Quasi-steady State Approximation by Changing Variables.' *Bull. Math. Biol.*, **1**: 43–63 (1996).

BRAY, D. 'Protein Molecules as Computational Elements in Living Cells.' *Nature*, **376**: 307–312 (1995).

CHRISTENSEN, U. 'Introduction to Enzyme-chemistry.' Course notes to biophysical chemistry, Chemical Institute, University of Copenhagen (1993).

CORNISH-BOWDEN, A. & CÁRDENES, M. L. 'Co-operativity in Monomeric Enzymes.' *J. theor. Biol.*, **124**: 1–23 (1987).

CREIGHTON, T. E. *Proteins. Structure and Molecular Properties.* W. H. Freeman and Company, 2nd edn. (1993).

DE LA SELVA, S. M. T., PIÑA, E. & GARCÍA-COLÍN, L. S. 'On the simple Michaelis-Menten mechanism for chemical reactions.' *J. Math. Chem.*, **19**: 175–191 (1996).

DECROLY, O. & GOLDBETER, A. 'Birhythmicity, Chaos, and Other Patterns of Temporal Self-organization in a Multiple Regulated Biochemical System.' *Proc. Natl. Acad. Sci. USA*, **76**: 6917–6921 (1982).

DECROLY, O. & GOLDBETER, A. 'Selection Between Multiple Periodic Regimes in a Biochemical System: Dynamical Behaviour Resolved by use of One-dimensional Maps.' *J. theor. Biol*, **113**: 649–671 (1985).

DECROLY, O. & GOLDBETER, A. 'From Simple to Complex Behaviour: Analysis of Bursting in a Multiple Regulated Biochemical System.' *J. theor. Biol*, **124**: 219–250 (1987).

DUPONT, G. & GOLDBETER, A. 'Protein Phoshorylation Driven by Intracellular Calcium Oscillations: A Kinetic Analysis.' *Biophys. Chem.*, **42**: 257–270 (1992).

EIGEN, M. 'New Looks and Outlooks on Physical Enzymology.' *Quart Rev. Biophys.*, **1**: 3–33 (1968).

ELLEDGE, S. J. 'Cell Cycle Checkpoints: Preventing an Identity Crisis.' *Science*, **274**: 1664–1672 (1996).

ERLE, D., MAYER, K. H. & PLESSER, T. 'The Existence of Stable Limit Cycles for Enzyme Catalyzed Reactions with Positive Feedback.' *Math. Biosci.*, **44**: 191–208 (1979).

ERNEUX, T., EDSTROM, R. D. & GOLDBETER, A. 'Enzyme Sharing in Phoshorylation-Dephosphorylation Cascades: The Case where One Protein Kinase (or Phosphatase) Acts on Two Different Substrates.' *J. theor. Biol*, **165**: 43–61 (1993).

ESCHRICH, K., SCHELLENBERGER, W. & HOFMANN, E. '*In Vitro* Demonstration of Alternate Stationary States in an Open Enzyme Reaction Containing Phosphofructokinase.' *Arch. Biochem. Biophys.*, **205**: 114–121 (1980).

ESCHRICH, K., SCHELLENBERGER, W. & HOFMANN, E. 'Sustained Oscillations in a Reconstituted Enzyme Reaction Containing Phosphofructokinase and Fructose 1,6-Bisphosphatase.' *Arch. Biochem. Biophys.*, **222**: 657–660 (1983).

ESPERSON, J. H. *Chemical Kinetics and Reaction Mechanisms.* McGraw-Hill Series in Advanced Chemistry, McGraw-Hill, Inc., 2nd edn. (1995).

FARROW, L. A. & EDELSON, D. 'The Steady-State Approximation: Fact or Fiction?' *International Journal of Chemical Kinetics*, **6**: 787–800 (1974).

FERRELL, J. E. J. 'Tripping the Switch Fantastic: How a Protein Kinase Cascade can Convert Graded Inputs into Switch-like Outputs.' *TIBS*, **21**: 460–466 (1996).

GABRIELLI, B. G., LEE, M. S., WALKER, D. H., PIWNICA-WORMS, H. & MALLER, J. L. 'Cdc25 Regulates the Phosphorylation and Activity of Xenopus Cdk2 Protein Kinase Complex.' *J. Biol. Chem*, **267**: 18040–18046 (1992a).

GABRIELLI, B. G., ROY, L. M., GAUTIER, J., PHILIPPE, M. & MALLER, J. M. 'A Cdc2-related Kinase Oscillates in the Cell Cycle Independently of Cyclins G2/M and Cdc2.' *J. Biol. Chem.*, **267**: 1969–1975 (1992b).

GOLDBETER, A. 'A Minimal Cascade Model for the Mitotic Oscillator involving Cyclin and Cdc2 Kinase.' *Proc. Natl. Acad. Sci. USA*, **88**: 9107–9111 (1991).

GOLDBETER, A. *Biochemical Oscillations and Cellular Rhythms. The Molecular Bases of Periodic and Chaotic Behaviour.* Cambridge University Press (1996).

GOLDBETER, A. & GUILMOT, J. 'Thresholds and Oscillations in Enzymatic Cascades.' *J. Phys. Chem*, **100**: 19174–19181 (1996).

GOLDBETER, A. & KOSHLAND, D. E. J. 'An Amplified Sensitivity Arising from Covalent Modification in Biological Systems.' *Proc. Natl. Acad. Sci. USA*, **78**: 6840–6844 (1981).

GOLDBETER, A. & KOSHLAND, D. E. J. 'Sensitivity Amplification in Biochemical Systems.' *Quart. Rev. Biophys.*, **15**: 555–591 (1982).

GOLDBETER, A. & KOSHLAND, D. E. J. 'Ultrasensitivity in Biochemical Systems Controlled by Covalent Modification.' *J. Biol. Chem.*, **259**: 14441–14447 (1984).

GOLDBETER, A. & WOLPERT, L. 'Covalent Modification of Proteins as a Threshold Mechanism.' *J. theor. Biol*, **142**: 243–250 (1990).

GORYANIN, I. I., SEL'KOV, E. E. & SERDYUK, K. I. 'A Refined Mathematical Model of an Almost Ideal Biochemical Relaxation Oscillator Based on the Covalent Modification of an Enzyme.' *Mol. Biol.*, **26**: 310–322 (1992).

GUADAGNO, T. M. & NEWPORT, J. W. 'Cdk2 Kinase is required for Entry into Mitosis as a Positive Regulator of Cdc2-cyclin B Kinase Activity.' *Cell*, **84**: 73–82 (1996).

GUTFREUND, H. *Enzymes: Physical Principles.* Wiley-Interscience (1972).

HALE, J. & KOCAK, H. *Dynamics and Bifurcations.* Springer Verlag (1991).

Harper, J. W., Adami, G. R., Wei, N., Keyoomarski, K. & Elledge, S. J. 'The p21 Cdk-interacting protein Cip1 is a Potent Inhibitor of G1 Cyclin-dependent Kinases.' *Cell*, **75**: 805–816 (1993).

Hartley, R. S., Rempel, R. E. & Maller, J. L. 'In vivo Regulation of the Early Embryonic Cell Cycle in Xenopus.' *Develop. Biol.*, **173**: 408–419 (1996).

Heineken, F. G., Tsuchiya, H. M. & Aris, R. 'On the Mathematical Status of the Pseudo-steady State Hypothesis of Biochemical Kinetics.' *Math. Biosci.*, **1**: 95–113 (1967).

Heinrich, R. & Schuster, S. *The Regulation of Cellular Systems.* Chapman and Hall (1996).

Hess, B. & Mikhailov, A. 'Microscopic Self-organizations in Living Cells: A Study of Time Matching.' *J. theor. Biol*, **176**: 181–184 (1995).

Hess, B. & Mikhailov, A. 'Transition from Molecular Chaos to Coherent Spiking of Enzymic Reactions in Small Spatial Volumes.' *Available in preprint* (1996).

Higgens, J. *Control of Energy Metabolism*, chap. 1. Academic Press, Inc. (1965).

Hoffman, I., Draetta, G. & Karsenti, E. 'Activation of the Phosphatase Activity of Human Cdc25A by a Cdk2-cyclin E Dependent Phosphorylation a the G-1/S Transition.' *EMBO J.*, **13**: 4302–4310 (1994).

Holden, L. & Erneux, T. 'Understanding Bursting Oscillations as Periodic Slow Passages through Bifurcation and Limit Points.' *J. Math. Biol*, **31**: 351–365 (1993).

Howe, J. A. & Newport, J. W. 'A Developmental Timer Regulates Degradation of Cyclin E1 at the Midblastula Transition during Xenoupus Embryogenesis.' *Proc. Natl. Acad. Sci. USA*, **93**: 2060–2064 (1996).

Huang, C. Y. & Ferrell, J. E. J. 'Ultrasensibility in the Mitogen-activated Protein Cascade.' *Proc. Natl. Acad. Sci. USA*, pp. 10078–10083 (1996).

Hunding, A. & Engelhart, R. 'Early Biological Morphogenesis and Nonlinear Dynamics.' *J. theor. Biol*, **173**: 401–413 (1995).

Hunding, A. & Kærn, M. 'The Failure of the Quasi-steady State to Reveal Some Nonlinear Properties of Biological Systems.' *Submitted to J. theor. Biol.* (1997).

HUNDING, A. & SØRENSEN, P. G. *Physical Chemistry for Biological Systems.* Chemistry Institute, University of Copenhagen (1997). Course notes.

IZUMI, T. & MALLER, J. L. 'Phosphorylation and Activation of the Xenopus Cdc25 Phosphatase in the Absence of Cdc2 and Cdk2 Kinase Activity.' *Mol. Biol. Cell*, **6**: 215–226 (1995).

KÆRN, M. 'Non-liner Dynamics in Coupled Enzymatic Control Systems.' B.Sc. Thesis. University of Copenhagen. (1995).

KAUFFMAN, S. A. *The Origins of Order. Self-regulation and Selection in Evolution.* Oxford University Press, Inc (1993).

KING, R. W., DESHAIES, R. J., PETERS, J. & KIRSCHNER, M. W. 'How Proteolysis Drives the Cell Cycle.' *Science*, **274**: 1652–1659 (1996).

KLONOWSKI, W. 'Simplifying Principles for Chemical and Enzyme Reaction Kinetics.' *Biophysical Journal.*, **18**: 73–87 (1983).

KOSHLAND, D. E. J., NÊMETHY, G. & FILMER, D. 'Comparison of Experimental Binding Data and Theoretical Models in Proteins Containing Subunits.' *Biochemistry*, pp. 365–385 (1966).

KURGANOV, B. I. *Allosteric Enzymes. Kinetic Behaviour.*, chap. 5, pp. 248–343. Wiley (1981).

KURGANOV, B. I., DOROZHKO, A. I., KAGAN, Z. S. & YAKOVLEV, V. A. 'The Theroretical Analysis of Kinetic Behaviour of "Hysteretic" Allosteric Enzymes. III. Dissociating and Associating Enzyme Systems in which the Rate of Installation of Equilibirum between the Oligomeric Forms is Comparable to that of Enzymatic Reaction.' *J. theor. Biol.*, **60**: 287–299 (1976).

LEE & KIRSCHNER. 'An Inhibitor of p34-cdc2/cyclin B that Regulates the G-2/M Transition in Xenopus Extracts.' *Proc. Natl. Acad. Sci. USA*, **93**: 352–356 (1996).

LEES, E. 'Cyclin Dependent Kinase Regulation.' *Curr. Opin. Cell Biol.*, **7**: 773–780 (1995).

MACKEY, M. 'A Unified Hypothesis for the Origin of Aplastic Anemia and Periodic Haemetopoisis.' *Blood*, **51**: 941–956 (1978).

MIKHAILOV, A. & HESS, B. 'Fluctuations in Living Cells and Intracellular Traffic.' *J. theor. Biol*, **176**: 185–192 (1995).

Monod, J., Changeux, J. & Jacob, F. 'Allosteric Proteins and Cellular Control Systems.' *J. Mol. Biol.*, **6**: 306–329 (1963).

Monod, J., Wyman, J. & Changeux, J. 'On the Nature of Allosteric Transitions: A Plausibe Model.' *J. Mol. Biol.*, **12**: 88–118 (1965).

Murray, A. & Hunt, T. *The Cell Cycle: An Introduction.* Oxford University Press (1993).

Murray, A. & Kirschner, M. W. 'Cyclin synthesis Drives the Early Embryonic Cell Cycle.' *Nature*, **339**: 1989 (1989).

Murray, A., Solomon, M. J. & Kirschner, M. W. 'The Role of Cyclin Synthesis and Degradation in the Control of Maturation Promoting Factor Activity.' *Nature*, **339**: 280–286 (1989).

Murray, J. D. *Mathematical Biology.* Springer Verlag, 2nd edn. (1993).

Neet, K. E. 'Cooperativity in Enzyme Function: Equilibirum and Kinetic Aspects.' *Methods in Enzymology*, **249**: 519–567 (1995).

Nielsen, K., Sørensen, P. G. & Hynne, F. 'Chaos in Glycolysis.' *J. theor. Biol*, **186**: 303–306 (1997).

Novak, B. & Tyson, J. J. 'Modelling the Cell Division Cycle: M-phase Trigger, Oscillations and Size Control.' *J. theor. Biol*, **165**: 101–134 (1993a).

Novak, B. & Tyson, J. J. 'Numerical Analysis of a Comphrensive Model of M-phase Control in *Xenopus* Oocyte and Intact Embryos.' *J. Cell Sci.*, **106**: 1153–1168 (1993b).

Novak, B. & Tyson, J. J. 'Quantitative Analysis of a Molecular Model of Mitotic Control in Fission Yeast.' *J. theor. Biol*, **173**: 283–305 (1995).

Obeyesekere, M. N., Herbert, J. R. & Zimmerman, S. O. 'A Model of the G1 Phase of the Cell Cycle Incorporating Cyclin E/cdk2 Complex and Retinoblastoma Protein.' *Oncogene*, **11**: 1199–1205 (1995).

Perko, L. *Differential Equation and Dynamical Systems.* Springer Verlag (1996).

Petrocelli, T., Poon, R., Drucker, D. J., Slingerland, J. M. & Rosen, C. F. 'UVB Radiation Induces p21-Cip1/WAF1 and Mediates G1 and S Phase Checkpoints.' *Oncogene*, **12**: 1387–1396 (1996).

PINES, J. 'Cyclin From Sea Urchins to HeLas: Making the Human Cell Cycle.' *Biochem. Soc. Trans.*, **14**: 15–33 (1996).

REMPEL, R. E., SLEIGHT, S. B. & MALLER, J. L. 'Maternal Xenopus Cdk2-cyclin E Complexes Function during Meiotic and Early Embryonic Cell Cycles that lack a G-1 Phase.' *J. Biol. Chem.*, **270**: 6843–6855 (1995).

ROMOND, P., GUILMOT, J. & GOLDBETER, A. 'The Mitotic Oscillator: Temporal Self-Organization in a Phosphorylation-Dephoshorylation Enzymatic Cascade.' *Ber. Bunsenges. Phys. Chem.*, **98**: 1152–1159 (1994).

SAVAGEAU, M. A. 'Michaelis-Menten Mechanism Reconsidered: Implications of Fractal Kinetics.' *J. theor. Biol*, **176**: 115–124 (1995).

SCHIRMER, T. & EVANS, P. R. 'Structural Basis of the Allosteric Behaviour of Phosphofructokinase.' *Nature*, **343**: 140–145 (1990).

SCOTT, S. K. *Chemical Chaos.* Oxford University Press (1993).

SEGEL, L. & GOLDBETER, A. 'Scaling in Biochemical Kinetics: Dissection of a Relaxation Oscillator.' *J. Math. Biol.*, **21**: 147–160 (1994).

SEGEL, L. A. & SLEMROD, M. 'The quasi-steady state assuption: A case study in perturbation.' *SIAM Rev.*, **31**: 446–477 (1989).

SEYDEL, R. *From Equilibirum to Chaos: Practical Bifurcation and Stability Analysis.* Elsevier Science Publishing Co., Inc. (1988).

SHOU, W. & DUNHPHY, W. G. 'Cell Cycle Control by Xenopus p28-Kix1, a Developmentally Regulated Inhibitor of Cyclin-dependent Kinases.' *Mol. Biol. Cell*, **7**: 457–469 (1996).

SMOLEN, P. 'A Model for Glycolytic Oscillations Based on Skeletal Muscle Phosphofructokinase Kinetics.' *J. theor. Biol.*, **174**: 137–148 (1995).

SPEIGEL, M. R. *Mathematical Handbook of Fourmulas and Tables.* Schaum's Outline Series, McGraw-Hill, Inc (1994).

SRIVASTAVA, D. K. & BERNARD, S. A. 'Biophysical Chemistry of Metabolic Reaction Sequences in Concentrated Enzyme Solution and in the Cell.' *Ann. Rev. Biophys. Biophys. Chem.*, **16**: 175–204 (1987).

TANG, Y. & OTHMER, H. G. 'Frequency encoding in excitable systems with applications to calcium oscillations.' *Proc. Natl. Acad. Sci. USA*, **92**: 7869–7873 (1995).

THOMPSON, J. M. T. & STEWART, H. B. *Nonlinear Dynamics and Chaos.* Wiley Interscience (1986).

THRON, C. D. 'A Model for a Bistable Trigger of Mitosis.' *Biophys. Chem.*, **57**: 239–251 (1996).

TIHONOV, A. N. 'Systems of Differential Equations Containing Small Parameters in The Derivatives.' *Mat. Sb.*, **31**: 575–586 (1952). in Russian.

TYSON, J. J., NOVAK, B., ODELL, G. M., CHEN, K. & THRON, C. D. 'Chemical Kinetic Theory: Understanding Cell-cycle Regulation.' *TIBS*, **21**: 89–96 (1996).

WALKER, D. H., ADAMI, G. R., DOLD, K. M. & BABISS, L. E. 'Misregulated Expression of the Cyclin Dependent Kinase 2 Protein in Human Fibroblasts is Accompanied by the Inability to Maintain a G-2 Arrest Following DNA Damage.' *Cell Growth & Diff.*, **6**: 1053–1061 (1995).

WEINBERG, R. 'How Cancer Arises.' *Scientific American*, **275**: 32–41 (1996).

ZHOU, G., HO, P. S. & VAN HOLDEN, K. E. 'An Analytic Solution to the Monod-Wyman-Changeux Model and all Parameters in this Model.' *Biophys. J.*, **55**: 275–280 (1989).